Alma Mater Studiorum · University of Bologna

School of Science
Department of Physics and Astronomy
Master Degree in Physics

Quantum simulation of abelian and non-abelian gauge theories

Supervisor:
Prof. Elisa Ercolessi

Submitted by:
Luca Marchese

Academic Year 2020/2021

Abstract

Le teorie di gauge sono onnipresenti nella fisica moderna, trovando applicazioni in diversi ambiti, dal modello standard alla fisica della materia condensata. Il recente sviluppo della tecnologia quantistica apre ora le porte a nuove tecniche utili al loro approfondimento, ampliando la nostra conoscenza di questi modelli ed oltrepassando i limiti degli approcci basati sul metodo di Montecarlo, quali il problema del segno e l'impossibilità di studiare la dinamica dei sistemi in tempo reale.
Questa tesi si concentra sull'implementazione di una simulazione per una teoria di Yang-Mills su reticolo con un gruppo di simmetria finito. Abbiamo testato diversi gruppi, sia abeliani ($\mathbb{Z}_2$ e $\mathbb{Z}_4$) che non abeliani (D_4), per i quali abbiamo emulato i risultati di un computer quantistico in un modello a 2+1 dimensioni. Una caratteristica fondamentale di questi modelli è la presenza di vincoli sullo spazio di Hilbert che determinano quali stati possono entrare nella dinamica. Nel caso abeliano siamo in grado di sfruttare la minore dimensione dello spazio degli stati fisici per introdurre una codifica più efficiente nella base computazionale. Nel caso invece di una simmetria data da gruppi non abeliani, questo metodo non può essere direttamente implementato a causa della comparsa di stati più complessi. Usando la misura del valore di aspettazione di vari Wilson loop, abbiamo trovato che tutti i sistemi analizzati presentano due fasi, una confinata e una non confinata. Sfruttando la semplicità dei sistemi abeliani siamo anche riusciti in quei casi a verificare direttamente la legge del perimetro e la legge dell'area, che descrivono il comportamento dei Wilson loop nelle due differenti fasi.

Abstract

Gauge theories are ubiquitous in modern physics, finding applications from the standard model to condensed matter. While they have been studied in the past, the recent development of quantum technology opens the door to new techniques, expanding our knowledge of these models and overcoming the limits of classical Montecarlo approaches, mainly the sign problem and the lack of real time dynamic.
This thesis focuses on the implementation of a simulation for a lattice Yang-Mills theory with a finite group gauge symmetry. We test different groups, both abelian ($\mathbb{Z}_2$ and $\mathbb{Z}_4$) and non-abelian(D_4), and emulate the results of a quantum computer on a 2+1 dimensional lattice. A key feature of these models is the presence of constraints on the Hilbert space, dictating which states can enter the dynamic of the system. In the abelian case, we are able to take advantage of the smaller dimension of the constrained space, producing a more efficient encoding into the computational basis. In the case of a non-abelian group symmetry, this method cannot be directly implemented due to the emergence of more complex excitations. Using the measurement of the expectation values of various Wilson loops we found all the different systems to exhibit two phases, a confined and a deconfined one. Due to the small complexity of the abelian systems we were able in those cases to directly verify the perimeter and area law, which dictates the behavior of the Wilson loops in the two phases.

Contents

Introduction

Gauge theories are a class of field theories which, under a set of local transformations called gauge transformations, remain invariant[42]. The term gauge refers to the mathematical apparatus needed to describe systems with redundant degrees of freedom. The invariance under a gauge transformation is therefore connected to the different ways in which the same physical state can be described. Historically the first known gauge theory has been classical electromagnetism, describing the behavior of the electric and magnetic phenomena.
With the advent of quantum field theory gauge theories have seen incredible success due to their ability to describe three of the four fundamental interactions[42]. The quantum field theory of these interactions describes both how matter interacts with the gauge fields and the dynamics of the fields themselves.
Quantum electrodynamics (QED), the quantum field theory generalization of classical electrodynamics, can be obtained by imposing invariance under a local $U(1)$ transformation. This simple invariance condition provides a set of constraints on the form of the theory and on the coupling between the fermionic field, describing charged matter, and the vector field which describes the particles that mediate electromagnetic interaction.
The gauge fields connected to the other two fundamental interactions were found to be described by Yang-Mills theories[54]. These theories were first introduced in order to understand the forces between nucleons, and were based on a generalization of the electromagnetic theory obtained by requiring invariance under a more general group $SU(N)$.
Quantum chromodynamics (QCD), the quantum field theory connected to the strong interaction, can be described by a $SU(3)$ Yang-Mills theory coupled with matter.
Similarly quantum flavourdynamics (QFD), related to the weak interaction, is described by a $SU(2)$ Yang-Mills theory coupled with matter. However, the term QFD is rarely used, because the weak force is better understood by electroweak theory, which describes both the weak and the electromagnetic interactions.

The application of gauge theories is not limited to high energy physics. Condensed matter physics has provided a different field where gauge theories have been implemented with great success [17], leading to important results in the description of particularly difficult phenomena such as fractional quantum Hall effect, which finds its theoretical

framework in Chern-Simons theory[53], and superconductivity. In this field the constant interplay between the theoretical models and easily accessible physical systems has pushed toward new developments in both directions. While at first condensed systems were considered "toy models" in which to try new techniques of field theory, the direct observations have provided the phenomenology on which it was possible to investigate many fundamental conceptual problems in quantum field theory.

The first framework which has been used in the study of gauge theories on a continuum spacetime is perturbation theory, in which an expansion is performed in terms of the coupling parameter. However the coupling parameter itself depends on the energy scale of the analyzed process, due to renormalization. This leads to widely different behaviors between gauge theories with different gauge groups. For example in QED the coupling parameter becomes larger as the energy scale of the system increases, showing that perturbation theory can be applied only in the low energy regime. The point at which perturbation theory becomes unreliable is nevertheless at an extremely high energy[42], where other effects are already expected to produce deviations for the model. In QCD, the coupling parameter is instead observed to decrease as the energy of the system increases[42]. This allows the possibility to obtain precise results in the high energy limit using perturbation theory. At lower energies it is instead impossible to apply perturbation methods, due to the diverging value of the coupling parameter. This widely different behavior is connected to the non-abelian nature of the symmetry group $SU(3)$. In order to study this limit an extremely successful scheme has been the introduction of lattice gauge theories[52]. In this method the continuous spacetime is substituted by a discrete lattice, which introduces a high energy cut-off. The fields and Lagrangian are then redefined on this lattice, using the euclidean path-integral approach. The action and observables are then calculated numerically via Montecarlo methods[19]. This technique has achieved a number of successes, the most important of which is the reproduction of confinement[5], where the large coupling constants at low energies forbids the existence of free quarks, which are instead found only clumped together in small color-neutral groups.
However, there are two limits to the use of Montecarlo methods. The first appears when we try to introduce fermions at a finite chemical potential. In that case the partition function becomes a sum of highly oscillating terms, making it difficult to compute. This is known as the sign problem[1, 20] and it limits the regions of the phase diagrams where it is possible to obtain results. The second limit is that the computation can be preformed only in the euclidean theory, where the path integral is positive. This means that we cannot obtain results for dynamical processes, and out of equilibrium phenomena.

The presence of these difficulties has encouraged researchers to try different kinds of simulations. A new approach, which was made possible by the recent development in quantum technologies[50], is to use quantum simulations for lattice gauge sys-

tems. The idea of using quantum systems to simulate other quantum systems has seen R.Feynman[16] as one of its first proponents. Many high energy and condensed matter phenomena owe their non trivial behavior to their inherent quantum mechanical properties. While classical computing allows us to approximate this behavior, it can do so only at a high computational cost. On the other hand a quantum simulator is intrinsically equipped to work efficiently. In the past, the required technology to control a quantum down to its single components was a significant limiting factor. A great push has been performed to cross this barrier, and at the present day many architectures capable of performing quantum simulations are in development, varying from ultra-cold atoms, to trapped ions, photons and superconducting circuits[50].
The common effort in the development of quantum technologies has also seen the birth of new devices, called quantum computers[38], which directly harness the properties of quantum mechanical systems in order to perform certain calculations. This devices allowed the introduction of a universal language for quantum computations, separating the algorithms from the specific implementations.

In the case of the lattice gauge theory, quantum simulations have been shown to be intrinsically free of the sign problem[3] and, since they are formulated in the Hamiltonian formalism, it is possible to study the real dynamic of the system.
There are two challenges we need to solve in order to produce a quantum simulation for a gauge theory. The first is the description of the system in the Hamiltonian formalism, which is required to implement quantum computing methods. The solution to this problem has been addressed by Kogut and Susskind [26]. The second issue is that even on a finite lattice the degrees of freedom are infinite. Quantum simulations are instead limited to the finite number of degrees of freedom that the experimental apparatus can control. The way in which the number of degrees of freedom are reduced to a finite number may vary. The works that give the foundations for the models in this thesis solve this problem by substituting the gauge group with a finite group[32, 40], producing a set of models with the desired characteristics for the implementation.

The model we will study describes a lattice Yang-Mills theory with a finite group gauge symmetry. The representation of this system is a quantum link model, which consists in a lattice where a quantum state lives on each link. Gauge theories represent a special case of quantum link models, since the redundant degrees of freedom are translated into constraints for the physical states of the systems. The techniques necessary for the analysis of constrained system are of great interest for quantum simulations algorithms, either because it is necessary to devise a way to maintain the system in a physical state, or because the smaller space can be exploited to work only with the physical degrees of freedom, greatly reducing the computational costs of the simulations. More generally, quantum link models have been object of recent interest. In particular the toric code has been shown to be the simplest example of a system with topological

order[55]. This model has also been studied since the high resistance of its ground states against decoherence has been considered as a strategy for protecting quantum computers from decoherence errors[55]. The group based generalization of the toric model, known as Quantum Double model[7] is strictly connected to lattice Yang-Mills theory. This connection allows many results of one system to be related to the other, providing a new interesting point of view.

The study of finite groups Yang-Mills theories is the crossroad of many interest. From a gauge theory perspective we are interested in probing new regions of the phase diagram, where classical computation fails. From a quantum computing perspective, gauge theories prove to be an important testing grounds for the implementation and confrontation of different quantum algorithms. From a quantum information perspective we are interested in the features of the model, and its connections to important topological properties.
Since the implementation of simulations of Yang-Mills theories with $\mathbb{Z}_2$ gauge symmetry has already been performed[8, 30], in this thesis we aim at extending these results to more general groups, in particular non-abelian groups, where more complex phenomena are expected.

The first chapter of the thesis focuses on the general aspects of the model. We start through a description of the derivation of the model, showcasing the connection between continuous Yang-Mills theory with a continuous symmetry group and the lattice model with a finite group gauge symmetry. This connection allows us to define and interpret many different observables encountered in the following parts of the thesis.
We then focus on the Hilbert space of the theory, studying its structure for a general finite group. Borrowing the notation from Quantum Double Models we introduce the plaquette and vertex operators, from which we are able to define the one-plaquette character states, which form the simplest examples of gauge invariant states. Generalizing the one-plaquette states to arbitrary loops allows also the description of many different gauge invariant states. The development of this notation allows also to show the connection between Yang-Mills lattice gauge theories and Quantum Double Models. The magnetic ground state of the Yang-Mills theory is easily calculated trough this relation, showing the topological nature of the state.
The closing part of the chapter investigates the phase structure, providing a guide for where and what to look for in the numerical analysis. In particular it introduces the area and perimeter laws, which are able to identify the confined and deconfined phase of the system.

The second chapter is devoted to the implementation of the theory for abelian groups. Exploiting the simplicity of these theories we show that the one-plaquette states gives a complete description of the gauge invariant subspace, allowing a more efficient implemen-

tation of the simulation algorithms. We discuss various schemes for the implementation of the algorithm, focusing on the advantages and disadvantages of each. Our choice settles on the adiabatic algorithm, which takes the greatest advantage of the pseudo quantum simulation we are able to implement. These simulations emulate the behavior of a quantum computer utilizing classical hardware and are crucial in verifying the correct behavior of the implementation methods, in wait for more advanced quantum computers to be developed.
We end the chapter with an explanation of the implementation of the circuit for $\mathbb{Z}_2$ and $\mathbb{Z}_4$, and the analysis of the numerical results. A direct investigation of the area and perimeter law is used to identify the confined and deconfined phase.

The third chapter focuses on non-abelian theories. A series of examples with a small number of plaquettes in the D_4 model is used to underline the non-trivial behaviors. Although a complete description of the Hilbert space is no longer available, it is still possible to perform the adiabatic simulation.
We show the quantum circuit implementation for the simulation of the D_4 group, focusing on the more complex combination of gates needed to implement the needed operations. In the last section of the chapter the results of a simulation on a 2x2 periodic lattice are analyzed, showcasing the transition from a confined to a deconfined phase.

Chapter 1

Quantum Links models and Lattice gauge theory

The aim of this chapter is to introduce the physical system that will be the focus of study of this thesis. The first section will show how a lattice Hamiltonian with a finite group gauge symmetry can be derived from the continuous gauge theory. Then we will give a description of the Hilbert space of such system, showcasing important conventions for all states. We will then calculate some general results, using also the comparison between the Yang-Mills model we study and another similar quantum link model: the Quantum Double Model. In the end we will use the conventions previously defined to figure out what are the main observables of the theory.

1.1 Gauge Hamiltonian with finite group gauge symmetry

A gauge Hamiltonian with finite group gauge symmetry describes a constrained lattice system. In order to understand its main features and nomenclatures we will briefly show how it is derived, focusing on the key steps of its derivation. We will not go into too many details since a more extensive derivation has already been performed by Mariani [32] and Lumia [30], where more insight is given into each step.
We will also focus only on the gauge fields leaving out of our analysis the fermionic matter part, which won't be studied in this thesis.

The starting point for our analysis will be Yang-Mills theories. This class of theories was firstly introduced as a generalization of electrodynamics, and has its most important applications in the description of strong and weak nuclear forces. It describes a set of N fermionic fields $\psi(x)$, when their $SU(N)$ symmetry becomes local. Preserving the local symmetry requires the introduction of a set of vector field. Since the group SU(N) has

N^2-1 generators τ_a there are N^2-1 vector fields A_a^μ, each corresponding to one boson. The generators of the $su(2)$ Lie algebras are chosen such that

$$[\tau_a, \tau_b] = f_{abc}\tau_c \tag{1.1}$$
$$tr(\tau_a\tau_b) = 2\delta_{ab} \tag{1.2}$$

where f_{abc} are the structure constants of the Lie algebra.
The theory is then described by the Yang-Mills Lagrangian:

$$\mathcal{L} = \bar{\psi}(i\not{D} - m)\psi - \frac{1}{2g^2}tr\left(F^{\mu\nu}F_{\mu\nu}\right) \tag{1.3}$$

We use some typical conventional notations:

- $A_\mu = \sum_a A_a^\mu \tau_a$ represents the sets of gauge fields
- We use the Dirac slashed notation $\not{D} = \gamma^\mu D_\mu$, where the Clifford's algebra's operators acts on the components of the Dirac spinors, in the same way on each of the N fermionic fields.
- The covariant derivative is $D_\mu = \partial_\mu - iA_\mu$. where the gauge part A_μ introduces non trivial couplings between the various fermionic fields.
- The field strength tensor (aka curvature tensor) $F_{\mu\nu} = i[D_\mu, D_\nu] = d_\mu A_\nu - d_\nu A_\mu - i[A_\mu, A_\nu]$
- The coupling constant in the denominator of the second term is g. Sometimes a different convention is used for the electromagnetic potential $\tilde{A}_\mu = gA_\mu(x)$, which leads to equivalent results.

From the Lagrangian we can calculate the action of the system:

$$S[\psi, \bar{\psi}, A_\mu] = \int dx^d \mathcal{L}[\psi(x), \bar{\psi}(x), A_\mu(x)] \tag{1.4}$$

This theory contains N spinor matter fields and N^2-1 gauge fields. The coupling between spinors and gauge fields is through the minimal coupling given by the covariant derivative D_μ. Moreover there is a non-trivial coupling between the gauge fields themselves, whenever the gauge group is not abelian (e.g. $SU(N)$ for $N \geq 2$).
Any gauge transformation on this Lagrangian is described by a function $g : \mathcal{M} \to SU(N)$ from the spacetime $\mathcal{M}$ to the group. Under such transformation the spinor and vector fields transform as:

$$\begin{cases} A'_\mu(x) = g(x)A_\mu(x)g(x)^{-1} + g(x)\partial_\mu g(x)^{-1} \\ \psi'(x) = g(x)\psi(x) \end{cases} \tag{1.5}$$

Substituting such transformations in the action leaves it invariant, showing the symmetry of the system.
This Lagrangian is usually studied in the Minkowski $3+1$ dimensional spacetime, but can be generalized also to other dimensions. For the $SU(3)$ model in $3+1$ dimensions the antisymmetric tensor $F_{\mu\nu}$ can be divided into 2 parts with specific names: the chromoelectric field $E_i = F_{0i}$, which correspond to mixed time and spatial indices, and the chromomagnetic part $B_i = \frac{1}{2}\epsilon_{ijk}F_{jk}$, which correspond to a double spatial index. In the more general cases we will keep a similar nomenclature, distinguishing the electric and magnetic parts of the field strength tensor.

The process by which we obtain the finite group Hamiltonian corresponding to the previously described Lagrangian can be broken down into three steps. The first is reducing the system from the continuous spacetime to a discrete lattice. This step has been historically important because it produces a class of theories known as lattice gauge theories, and has been the base for many classical computational results. Many of the observables that we will look at in the following sections are described in these formulation. These first two steps can be taken independently in any order. We will then combine them to obtain a lattice Hamiltonian, known in the literature as the Kogut-Susskind Hamiltonian [26]. In this combination we will have an important difference: while the lattice Lagrangian is usually defined on a spacetime lattice, the lattice Hamiltonian is defined on a space lattice, while the time coordinate is kept continuous. Although it should be possible to obtain a lattice Lagrangian with continuous time and a space lattice, it is never done in literature, because the completely discretized version is better suited for classical computations. The final step will be changing the gauge symmetry group from continuous (as $SU(N)$ is) to a finite group.

1.1.1 Lagrangian lattice gauge theory

The first step we have to perform in order to change the spacetime of the theory from continuous to discrete is to substitute the Minkowski spacetime $\mathcal{M}$ with a directed spacetime hyper-cubic lattice Λ of spacing a:

$$\Lambda = \left\{ x \in \mathbb{R}^d \; s.t \; x = \sum_{\mu=1}^{d} n_\mu a\hat{\mu}, \; n_\mu \in \mathbb{Z} \right\} \tag{1.6}$$

where d is the dimension of the system and $\hat{\mu}$ is the unit vector in the $\mu = 1, ..., d$ spacetime dimension.

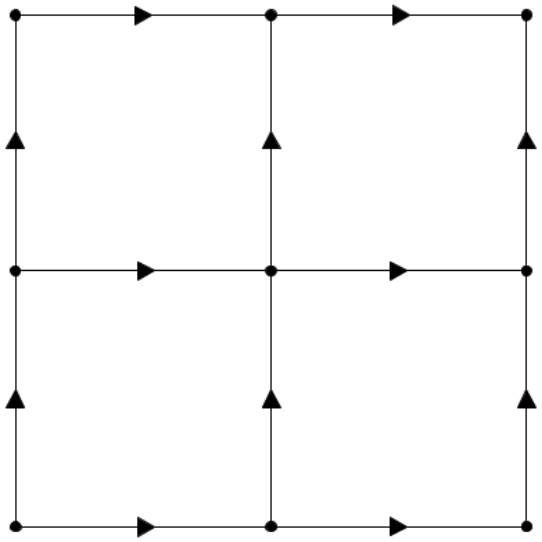

Figure 1.1: Piece of an ordered lattice Λ in $d = 2$ dimensions. Each link is identified by a vertex x and a versor $\hat{\mu}$. We say that the link is traversed in the positive direction if the versor is aligned with the lattice orientation, and negative otherwise. The size of the lattice can be infinite in theoretical models, but is usually restricted to a finite lattice for numerical simulations.

In this lattice each vertex is identified by its position x. To refer to a given link instead, we use a couple $(x, \pm\mu)$, where x is the position of the vertex to which the link is connected, μ identify one of the d Cartesian axis, and the sign identify one of the two possible directions along that axis. Each vertex is connected to $2d$ links. In return each link is connected to 2 vertices. We can see that it is possible to describe each vertex in two different ways: (x, μ) and $(x + a\hat{\mu}, -\mu)$. This double description allow us also to know if the link is traversed in the positive or negative direction (which can be chosen arbitrarily). An example of this notation is given in figure 1.1, in the case of a $2d$ lattice. The clear simplification of working on a lattice is that where in the continuous case the action is an integral of the Lagrangian, in the lattice case it is reduced to a sum on the lattice sites:

$$\int dx^d \to a^d \sum_{x \in \Lambda} \tag{1.7}$$

thus obtaining a finite sum which can be computed directly in numerical simulations.
Another feature introduced by the lattice, common in condensed matter systems, is the existence of a Brillouin zone, to which the momenta of the theory are confined. In this sense the lattice acts as a high-energy regularization of the system. From another point of view we can see that a lattice makes the low wavelengths/high frequency states im-

possible, imposing a high energy cut-off [36].

We now face the challenge to understand how to represent the fields, which make up the Lagrangian. The guiding principle in this section will be the correspondence between the continuous theory and the lattice theory in the limit for the spacing $a \to 0$.
The fermionic part $\psi(x)$ can be conveniently approximated by simply requiring the positions x to be in the lattice. The derivatives reduce to finite differences and the action can be calculated out of finite sums. Nevertheless this process is not trivial due to the emergence of unexpected poles in the Brillouin zone, leading to the so called fermion doubling [37, 46]. Such problem can be solved with different methods [14].
The gauge fields are described instead as living on the links, which means that we will have a quantity that describes $A_\mu(x)$ at each link of the model.
One heuristic argument we can give to justify this description goes as follows. The minimal coupling between spinors and gauge fields is given by the covariant derivative $D_\mu = \partial_\mu - iA_\mu$. In the lattice the partial derivative is substituted by the finite increment $\partial_\mu f(x) \approx \frac{f(x+a\hat{\mu})-f(x)}{a}$, which contains two vertices. Accordingly the other term in the sum will connect the two vertices, as the link does.
The quantity used to describe the value of a field $A_\mu(x)$ on a link (x, μ) is the comparator:

$$U_\mu(x) = \exp(iaA_\mu(x)) \tag{1.8}$$

This quantity is used whenever the link is traversed in the positive direction. Instead when the link is traversed in the negative direction we use the adjoint $U_\mu(x)^\dagger$. Since $A_\mu(x)$ is an element of the Lie algebra the comparators belong to the Lie group $SU(N)$.
The question we still have to answer is how the gauge fields appear in the Lagrangian. In order to do so we define the plaquette Wilson loop:

$$\operatorname{tr} W_\square = \operatorname{tr} U_\mu(x) U_\nu(x + a\mu) U_\mu(x + a\nu)^\dagger U_\nu(x)^\dagger \tag{1.9}$$

This quantity is the product of four comparators along the four links surrounding an elementary plaquette, identified by a starting vertex x and two directions μ and ν. We can expand the comparators for small a. For example for the first comparator in the previous equation we have:

$$U_\mu(x) = 1 + iaA_\mu(x) - \frac{a^2}{2} A_\mu^2(x) + ... \tag{1.10}$$

Substituting this and similar expansions in equation (1.9) we find:

$$\operatorname{tr} W_\square = N + \frac{a^4}{2} F^{\mu\nu} F_{\mu\nu} + \mathcal{O}(a^6) \tag{1.11}$$

where we don't sum over the indices μ and ν.
Fixing the constants we find that the pure gauge action can be rewritten as:

$$S = -\frac{1}{g^2 a^{3-d}} \sum_\square \operatorname{tr}\Big(W_\square + W_\square^\dagger\Big) \tag{1.12}$$

where the sum over all plaquettes also restores the sum over the Minkowski indices.

In this formalism the general gauge transformation is defined by an element $g(x)$ on each vertex of the lattice. Under such transformation the comparator transform as:

$$U_\mu(x) \to g(x)U_\mu(x)g(x+a\hat{\mu})^\dagger \tag{1.13}$$

If we expand such transformation for small a, at the first non-trivial order, we recover the condition:

$$A_\mu(x) \to g(x)A_\mu(x)g(x)^{-1} + ig(x)\partial_\mu g(x)^{-1} + \mathcal{O}(a) \tag{1.14}$$

which is compatible with the continuum case.
From the expression of the gauge transformation on the comparators it can be seen that, in the products present in the plaquettes Wilson loop, the gauge element on each vertex cancels and the plaquette Wilson loop remains unchanged. This implies that the action, which is a sum of gauge invariant quantities, remains gauge invariant even in the lattice model.
This cancellation of the transformation in two adjacent comparators can be used to define more general gauge invariant objects, which are known as Wilson loops. Take a closed path γ of consecutive links $\{(x_i, \mu_i)\}$. Then we can define the Wilson loop:

$$W_\Gamma = \mathrm{tr} \prod_{i\in\gamma} U_{\mu_i}^{|\mu_i|}(x_i) \tag{1.15}$$

where $|\mu_i| = \pm 1$ depending whether the link is traversed in the positive or negative direction.

Classical lattice simulations use the lattice action to calculate average observables, often after applying a Wick rotation in order to work in the euclidean formalism [4].

$$\langle O \rangle = \frac{1}{Z} \int \mathcal{D}U O(U) e^{-S[U]} \tag{1.16}$$

These quantities can be calculated through numerical methods and can be used to find the structure of the phase space.

1.1.2 Hamiltonian formalism

While the euclidean formalism allows simpler classical computations, the Hamiltonian formalism takes a different path, enforcing the difference between time and space coordinates. This choice allows the study of the time evolution of the system and is better suited for quantum simulations, where we can directly implement the Hamiltonian in the simulator. This approach has been pursued as a way to overcame the sign problem,

which prevents the application of Monte Carlo algorithms in regions of the phase space with non-zero chemical potential [20]. We will focus from now on only on pure gauge theories.
The first step to obtain the Hamiltonian is to calculate the conjugate momenta:

$$\Pi_a = \frac{\delta \mathcal{L}[\phi_a, \partial_\mu \phi_a]}{\delta \partial_0 \phi_a} \tag{1.17}$$

Then we perform a Legendre transformation to obtain the Hamiltonian density:

$$\mathcal{H} = \sum_a \Pi_a \partial_0 \phi_a - \mathcal{L}[\phi_a, \partial_\mu \phi_a] \tag{1.18}$$

which, after some substitutions, depends only on the fields, their spatial derivative and the conjugate momenta.

The first issue we have in applying this methodology is that for any given gauge field A^a_μ the time derivative of the time component $\partial_0 A^a_0$ is not present in the pure gauge Lagrangian $\mathcal{L}_g$. Therefore we have

$$\Pi^0_a = \frac{\delta \mathcal{L}_g}{\delta \partial_0 A^a_0} = 0 \tag{1.19}$$

and it is impossible to define a conjugate momentum.
In order to circumvent this problem we can exploit the gauge invariance to fix the temporal gauge $A^0 = 0$ (also know with other names [28, 29, 40, 45]), which allows us to perform the Legendre transform without issues. The price to pay is that the Hamiltonian obtained is no longer gauge independent. Moreover we only used a part of the total gauge invariance, and we will have some leftover invariance to take care of, as we will see later.
In the temporal gauge we find the conjugated momenta to be

$$\Pi^i_a = \frac{E^i_a}{g^2} \tag{1.20}$$

Once substituted in the Legendre transform we obtain the Hamiltonian density:

$$\mathscr{H} = \operatorname{tr}\left(g^2 \mathbf{\Pi}^2 + \frac{1}{g^2} \mathbf{B}^2 \right) \tag{1.21}$$

where we used bold symbols to denote spatial components of the fields. Expanding the trace and the spatial indices, and using the normalization of the generators τ_a, we find

$$\operatorname{tr} \mathbf{B}^2 = \frac{1}{2} \sum_{a,i} B^i_a B^i_a \tag{1.22}$$

and a similar result for $\operatorname{tr} \mathbf{\Pi}^2$.
Following canonical quantization the gauge field and the canonical momenta are promoted to operators which follow the commutation relations:

$$[\hat{A}_i^a(x), \hat{\Pi}_b^j(y)] = i\delta_{ab}\delta_{ij}\delta^3(\mathbf{x}-\mathbf{y}) \tag{1.23}$$

In order to better understand the operatorial nature of $\hat{A}_i$ and $\hat{\Pi}^j$ we need to find a description of the Hilbert space of the system. It turns out that such space is the set of complex valued functionals $\psi[\mathbf{A}]$. The reason is that similarly to the $|x\rangle$ basis in canonical quantization, we can introduce a position basis $|\mathbf{A}\rangle$. Any given state is a linear superposition $|\psi\rangle = \psi[\mathbf{A}]\,|\mathbf{A}\rangle$. The functionals can then be understood as the coordinate representation of a given state with respect to the position basis.
In the position basis the operators act as

$$\hat{A}_i^a(x)\psi[\mathbf{A}] = A_i^a(x)\psi[\mathbf{A}] \tag{1.24}$$

$$\hat{\Pi}_a^i(x)\psi[\mathbf{A}] = -i\frac{\delta}{\delta A_i^a(x)}\psi[\mathbf{A}] \tag{1.25}$$

With this expression we can prove the previous commutation relations, and also calculate other commutations relation between all the important fields, like A^i, E^i and B^i. We can also notice that the momenta act as generator of the translations on the Hilbert space. This fact will be useful later.

As previously stated, we used a part of the gauge invariance to be able to go in the Hamiltonian formalism. Nevertheless, there is still some invariance in the system. This fact lead to the presence of many non-physical states in the Hilbert space. In order to extract the physical subspace we must impose some conditions to ensure the invariance of the states under the remaining symmetry. It is found the generators of the transformation can be written as $D_i\hat{E}_i$. Therefore to ensure the physicality of the states the gauge invariance is expressed through the conditions [14, 29]:

$$D_i\hat{E}_i\,|phys\rangle = 0 \tag{1.26}$$

This condition is referred as Gauss' law, since it implies the conservation of charges of the theory.

1.1.3 Kogut-Susskind Hamiltonian

If we combine the previous two step we obtain an Hamiltonian for a lattice gauge theory, known as the Kogut-Susskind Hamiltonian [26]. The starting point is the continuous Hamiltonian:

$$H = \int d\mathbf{x} \operatorname{tr}\left(g^2\hat{\mathbf{\Pi}}(x)^2 + \frac{1}{g^2}\hat{\mathbf{B}}(x)^2\right) \tag{1.27}$$

We then try to introduce a lattice. The first difference from the previous case is that since the Hamiltonian is the generator of the temporal translations we need to keep the time dimension continuous and substitute the lattice only for the spatial dimensions.
This constraint imposes a stark difference between spatial and time dimensions. It is then useful to divide the Hamiltonian into two parts: the electric part H_E which contains temporal related quantities, and the magnetic part H_B which only contains spatial quantities.
Starting form the magnetic part we notice that $\mathbf{B}(x)^2 = \frac{1}{2}F^{ij}F_{ij}$ and we already shown that the corresponding quantity in lattice formalism is the Wilson plaquette loop $\operatorname{tr} W_\square \simeq \frac{a^4}{2}F^{ij}F_{ij}$, where we used the fact that all plaquette are doubly spatial, since there is no temporal lattice. Nevertheless since the magnetic fields are now operators we must find an Hilbert space based description of the Wilson loop quantity.
As in the continuous Hamiltonian case we want to use a position basis to describe the Hilbert space, but by introducing the lattice we substitute the gauge field $A(x)$ with the comparators $U(x,\mu)$, therefore the basis of the Hilbert space will be given by one $|U\rangle$ for each link in the model:

$$\bigotimes_{\#links} |U\rangle \qquad U \in SU(N) \tag{1.28}$$

Any general state is a square integrable superposition of these states, so that the total Hilbert space can be expressed as

$$\mathcal{H} = \bigotimes_{\#links} L_2(SU(N)) \tag{1.29}$$

On any given link two elements of the continuous basis follow the orthogonality condition:

$$\langle U|V\rangle = \delta(U,V) \tag{1.30}$$

and a general state con be decomposed as

$$|\psi\rangle = \int dU \psi(U)\,|U\rangle \tag{1.31}$$

where dU is the Haar measure [2].
It is important to notice that while in the Lagrangian lattice we have also comparators representing the state in the time direction it is not so in the Hamiltonian case, since we don't have time directed links. Luckily it is not a problem since by working in the temporal gauge we have $A_0 = 0$ so that we don't need any more information on the temporal configuration of the gauge field.
On the Hilbert space we can introduce a set of position operators $\hat{u}_{mn}$, defined by their action

$$\hat{u}_{mn}\,|U\rangle = U_{mn}\,|U\rangle \tag{1.32}$$

These operators form a $N \times N$ matrix, which will be denoted by $\hat{u}$. We can also define the adjoint operator:

$$(\hat{u}^\dagger)_{mn} |U\rangle = (U^\dagger)_{mn} |U\rangle \tag{1.33}$$

These operators can be used to define the Hamiltonian version of the Wilson loop.
For any closed loop on the lattice we give one matrix of operators for each link in the loop $\hat{u}(e_l)$, where e_l identifies the links in the loop. Such matrix is $\hat{u}$ whenever the link is traversed in the positive direction, and $\hat{u}^\dagger$ when it is traversed in the opposite direction. In the plaquette case we obtain

$$\operatorname{tr} \hat{W}_\square = \operatorname{tr} \prod_{l \in \square} \hat{u}(e_l) \tag{1.34}$$

where the order of the operators follow the path around the plaquette, as can be seen in figure 1.2. The starting vertex can be chosen arbitrarily, due to the cyclic property of the trace.

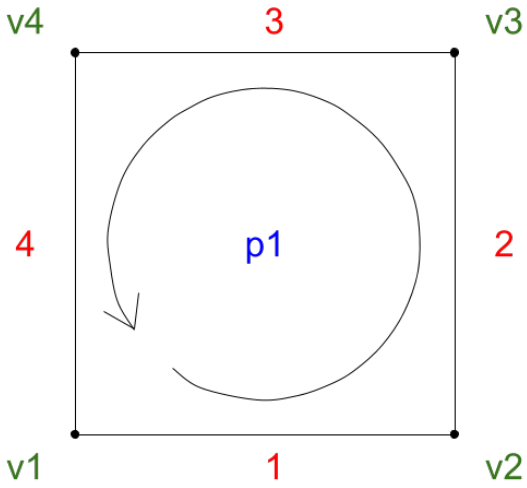

Figure 1.2: Disposition for ordered links around a plaquette $2d$ plaquette, with the plaquette index in blue, link index in red and vertex index in green. With this ordering we traverse first the two positive links and later the two negative links.

In a more general Wilson loop we similarly have

$$\operatorname{tr} \hat{W}_\gamma = \operatorname{tr} \prod_{l \in \gamma} \hat{u}(e_l) \tag{1.35}$$

where γ is a closed path in the system.
The action of any Wilson loop operator on the Hilbert space is diagonal on the position

basis, with each eigenvalue equal to the value of the Wilson loop on the field configuration defined by the quantum state.
Extending this to the whole lattice we find that the magnetic part of the Hamiltonian can be written as

$$H_B = -\frac{1}{g^2 a^{4-d}} \sum_{\square} \mathrm{tr}\left(\hat{W}_{\square} + \hat{W}_{\square}^{\dagger}\right) \tag{1.36}$$

where the sum is now only on the plaquettes of the spatial lattice.
Since there are no plaquettes whose sides lie in the temporal direction, which is not discretized, we cannot use a similar procedure for the electric portion of the Hamiltonian. We can overcome this difficulty by noticing that the canonical momenta, which constitute the electric term, act as generators of the translations on the position basis. In the case of lattice Hamiltonian theory the position basis is $|U\rangle$, and finite translations are described by the regular representation [18]:

$$L_U |V\rangle = |UV\rangle \tag{1.37}$$

For each Lie group representation π it is possible to obtain a Lie algebra representation $\tilde{\pi}$ which describes its infinitesimal action [18, 21]. Therefore it is possible to define the regular Lie algebra representation $\tilde{L}$. The representations of the generators of $\mathfrak{su}(N)$ are the quantities we are looking for:

$$\hat{l}_a = \tilde{L}(\tau_a) \qquad \tilde{L} : \mathfrak{su}(N) \to \mathrm{End}(L_2(SU(N))) \tag{1.38}$$

Using these operators the electric Hamiltonian becomes

$$H_E = \frac{g^2}{2a^{d-2}} \sum_{e \in links} \sum_{a} \hat{l}_a^2(e) \tag{1.39}$$

Regarding gauge invariance we want to find the new expression for the constraint on the physical states. We start by looking at the effect of a gauge transformation on the system. Such a transformation is defined by by an element $g(x)$ at each vertex. On any given link the transformation becomes

$$|U\rangle \to |g(x_1) U g(x_2)^{\dagger}\rangle = L_{g(x_1)} R_{g(x_2)} |U\rangle \tag{1.40}$$

where $g(x_1)$ is the transformation at the starting vertex and $g(x_2)$ at the arriving one, and we used the left and right regular representations L and R to describe the action in term of operators on the Hilbert space. This operators are defined uniquely for each vertex, it is therefore possible to describe the single vertex transformation. For vertex v and gauge element g we have

$$G_v(g) = \otimes_{e+} L_g(e+) \otimes_{e-} R_g(e-) \tag{1.41}$$

where $e+$ are the outgoing links and $e-$ the incoming ones. An example in the 2-dimensional case is given in figure 1.3.

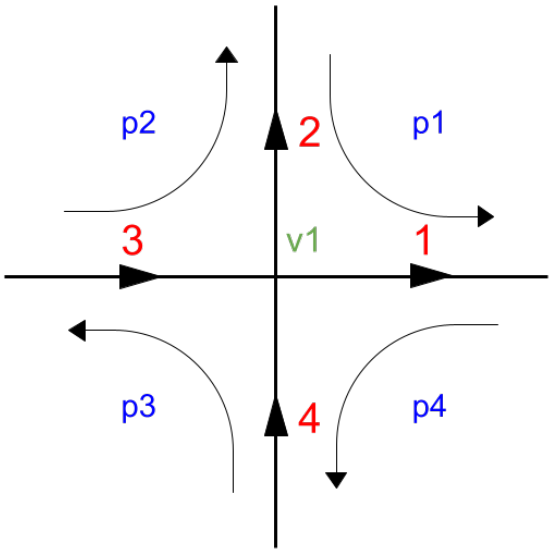

Figure 1.3: Disposition for the links around a vertex in the 2-dimensional case. We number the links going counterclockwise from the link in the positive x direction, so that links 1 and 2 are outgoing and links 3 and 4 go into the vertex.

The general condition for gauge invariance becomes

$$G_v(g)\,|phys\rangle = |phys\rangle \quad \forall g \in SU(N), v \in \Lambda \tag{1.42}$$

As can be expected, the Hamiltonian is gauge invariant, since it is a physical quantity.

1.1.4 Finite group gauge Hamiltonian

The final step of our discussion will be to introduce the finite group Hamiltonian, which allows the system to have a finite number of degrees of freedom. The main difference between finite groups and Lie groups is that the latter have an infinitesimal description given by the Lie algebra, which is not present anymore.
Regarding the Hilbert space this problem is already circumvented by working with the comparators $U(x,\mu)$, which are elements of the group, instead of the gauge fields $A_\mu(x)$, which are elements of the algebra. This fact allow the introduction of the Hilbert space

$$\mathcal{H} = \bigotimes_{\#links} L_2(G) \tag{1.43}$$

Looking closely at the single link space we can see that $L_2(G)$ is the group algebra, which is a finite complex vector field of dimension equal to the group order $|G|$. This algebra has many useful structures and properties which are analyzed in appendix A.
Adopting this space it easy to define the positions operator

$$\hat{u}_{mn} |g\rangle = \rho_{mn}(g) |g\rangle \tag{1.44}$$

where we have chosen an arbitrary representation of the group ρ as a substitute to the defining representations in the $SU(N)$ case. This representation is denoted as π_F, in analogy with the fundamental representation for $SU(N)$ groups, and choosing different representations produces different results.
From the position operators it is possible to define the single plaquette Wilson loop and therefore the magnetic Hamiltonian in the same way as in the continuous case.

$$H_B = -\lambda_B \sum_{\square} \mathrm{tr}\left(\hat{W}_{\square} + \hat{W}_{\square}^{\dagger}\right) \tag{1.45}$$

More problems arise with the description of the electric parts, where the operators $\hat{l_a}$, which are element of a Lie algebra representation, have no analog in the finite group systems. We need to find another way to describe the electric Hamiltonian.
The term that we should focus on is the single link electric Hamiltonian

$$\sum_a \hat{l_a}^2 \tag{1.46}$$

To find a new expression for this quantity we need to take a step back. In the $SU(N)$ case we introduced the position basis for a single link $|U\rangle$. As for many system in the canonical quantization there is another basis, connected to the momenta which should be better suited to describe the electric term. Such a basis is called the representation basis. This basis consist in the matrix elements of all irreducible representations π^j_{mn}. Using Haar measure these functions can be interpreted as orthonormal states [48], if we adjust the normalization:

$$|j_{mn}\rangle = \sqrt{\frac{d_j}{Vol(G)}} \int dU \pi^j_{mn}(\tau_a) |U\rangle \tag{1.47}$$

In this basis the left regular representation takes the form

$$L_U = \bigoplus_j \pi^{*j}(U) \otimes \mathbb{1} \tag{1.48}$$

where the direct sum is performed over all irreducible representations.
In the $SU(N)$ case $\hat{l_a}$ was defined from the regular representation of L_U, using the

derivative at the identity. In the same way we can obtain the regular representation of the Lie Algebra as

$$\hat{l}_a = \bigoplus_j \tilde{\pi}^{*j}(U) \otimes \mathbb{1} \tag{1.49}$$

Substituting this identity in equation (1.46) we obtain

$$\sum_a \hat{l_a}^2 = \bigoplus_j \sum_a \tilde{\pi}^{Tj}(\tau_a)\tilde{\pi}^{Tj}(\tau_a) \otimes \mathbb{1} = \bigoplus_j \tilde{\pi}^j(\Omega) \otimes \mathbb{1} \tag{1.50}$$

where Ω is the Casimir element. This quadratic operator is constant on all representations, therefore the electric term can be expressed by the Casimir eigenvalues $C(j)$:

$$\sum_a \hat{l_a}^2 = \sum C(j)\mathbb{P}_j \qquad \mathbb{P}_j = \sum_{m,n=1}^{d_j} |j_{mn}\rangle \langle j_{mn}| \tag{1.51}$$

The last expression does not depends on the representation of the Lie algebra generators and we are free to use it in the finite case as well.
As shown in appendix A the properties of the finite groups algebras are similar: we still have a representation basis $|j_{mn}\rangle$ on which the left and right representations take the form

$$L_g = \bigoplus_j \pi^{*j}(g) \otimes \mathbb{1}_{d_j} \qquad R_g = \bigoplus_j \mathbb{1}_{d_j} \otimes \pi^j(g) \tag{1.52}$$

The electric term on a link is written as

$$h_E = \lambda_E \sum_j f(j)\mathbb{P}_j \tag{1.53}$$

where the general function $f(j)$ takes the place of the Casimir eigenvalues, since we no longer have an analog of the Casimir operator in finite groups.
The choice of the function $f(j)$ can be performed in various ways. For example in $\mathbb{Z}_N$ theories it can be obtained as a truncation of the $U(1)$ group infinite representations. As explained in [32], another possibility is to use graph theory and construct a discrete laplacian operator, giving an expression for $f(j)$:

$$f(j) = |\Gamma| - \frac{1}{d_j} \sum_{g \in \Gamma} \chi_j(g) \tag{1.54}$$

where χ_j is the character of representation j, while Γ is a generating set closed under conjugation and inversion.

After describing the two parts of the Hamiltonian we are left with one last object to define: the gauge conditions. Similarly to the continuous case it is possible to impose invariance under any gauge transformation on the Hilbert space through a set of conditions:

$$G_v(g)\,|phys\rangle = |phys\rangle \quad \forall g \in G, v \in \Lambda \tag{1.55}$$

$$G_v(g) = \otimes_{e+} L_g(e+) \otimes_{e-} R_g(e-) \tag{1.56}$$

which restrict the Hilbert space into a smaller physical space.
For finite groups it is possible to rapidly reduce this constraints, by asking the states to be invariant under the generators only, instead of under all the elements of the group.

1.2 Structures in the Hilbert space

Since the aim of this thesis is to study the properties of the previously described Hamiltonian it is useful to introduce some convenient descriptions of the Hilbert space, in order to allow a better mapping to a quantum device and an easier description of the theoretical properties of any given state .
Our analysis will focus on two dimensional systems. In this case we can write the total Hamiltonian as

$$H = \lambda_E H_E + \lambda_B H_B \tag{1.57}$$

$$= \lambda_E \sum_l h_E^l - \lambda_B \,\mathrm{tr} \sum_\square \hat{W}_\square + \hat{W}_\square^\dagger \tag{1.58}$$

with

$$h_E^l = \sum_j f(j)\mathbb{P}_j(e_l) \qquad \mathrm{tr}\,\hat{W}_\square = \mathrm{tr} \prod_{l\in\square} \hat{u}(e_l) \tag{1.59}$$

The two dimensional gauge conditions become

$$G_v(g) = L_g(e_1) \otimes L_g(e_2) \otimes R_g(e_3) \otimes R_g(e_4) \tag{1.60}$$

with e_1, e_2 outgoing and e_3,e_4 going into the vertex.
In order to be able to perform numerical simulations we will work with a finite lattice with periodic boundary conditions (PBC).

1.2.1 The Hilbert space

The Hilbert space is constituted by the tensor product of L copies of the group algebra, one for each link in the system. We can introduce a basis, called the group basis, composed by the elements:

$$|g_1 ... g_L\rangle \tag{1.61}$$

where the subscript identify which link it is referred to. One convention for the numbering of links is given in figure 1.4.

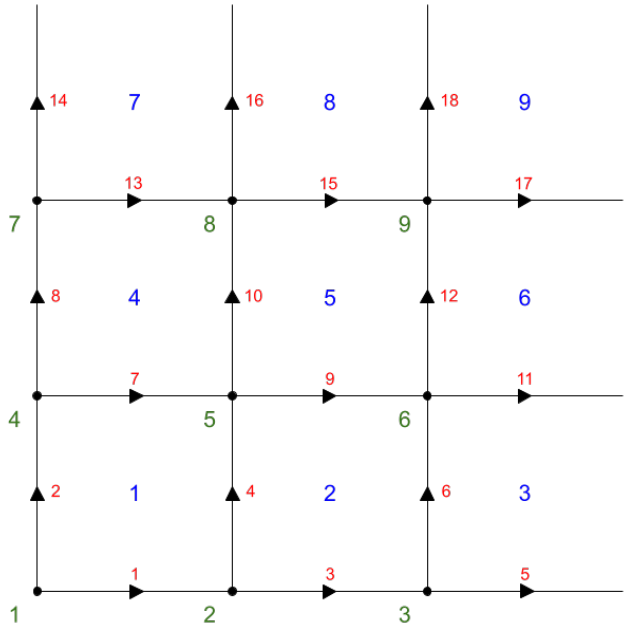

Figure 1.4: 3x3 configuration for the lattice in 2 dimensions. The right and top links are left empty due to periodic boundary conditions. The vertices and plaquettes are numbered from the bottom left, and are colored in green and blue respectively. The links follow the vertex order; since we have 2 links for each vertex we number the horizontal one first.

There is another useful basis, dual to the previous one, called the representation basis. The elements of these basis are written as

$$|\bar{\jmath}_1 \dots \bar{\jmath}_L\rangle \tag{1.62}$$

In this case we used a compact notation $\bar{\jmath}_l$ to describe the set of three indices (j_l, m_l, n_l) which identify an element of the representation basis on the link l, as in equation (1.47). On each link the group basis $|g\rangle$ is connected to the representation basis $|\bar{\jmath}\rangle$ by the transformation:

$$|\bar{\jmath}\rangle = \sqrt{\frac{d_j}{|G|}} \sum_{g \in G} \pi^j_{mn}(g)\, |g\rangle \tag{1.63}$$

which is known as the group Fourier transform (GFT).
The two bases for the total system are therefore connected by the product of L group Fourier transforms:

$$|\bar{j}_1...\bar{j}_L\rangle = \sqrt{\frac{d_1...d_L}{|G|^L}} \sum_{g_1,...,g_L} \pi^{j_1}_{m_1 n_1}(g_1)....\pi^{j_L}_{m_L n_L}(g_L)\,|g_1...g_L\rangle \tag{1.64}$$

The representation basis is useful due to the fact that it diagonalizes the electric portion of the Hamiltonian. For any link we have:

$$h^l_E\,|\bar{j}_1...\bar{j}_L\rangle = f(j_l)\,|\bar{j}_1...\bar{j}_L\rangle \tag{1.65}$$

For any finite group there is always a 1-dimensional irreducible representation, called the trivial representation, defined as $\pi^0(g) = 1\ \forall g \in G$.

The magnetic part is diagonal on the group basis as can be seen by the action of the Wilson loop:

$$\mathrm{tr}\,\hat{W}_\square\,|g_1...g_L\rangle = \mathrm{tr}\,\rho(\prod_{l\in\square} g(e_l))\,|g_1...g_L\rangle = \chi_F(\prod_{l\in\square} g(e_l))\,|g_1...g_L\rangle \tag{1.66}$$

Here $g(e_l)$ is g_l if the link is traversed in the positive direction, and g_l^{-1} otherwise, while χ_F is the character of the chosen representation π_F. The starting element of the loop doesn't matter due to the cyclic property of the trace, but it matters the succession between the links.
There is a better way to describe this action, using quantities related to each plaquettes as we will see in the next section.

1.2.2 Plaquette and Vertex operators

The single plaquette Wilson loop acts on four continuously connected links, while the gauge conditions acts on four links connected to a vertex. This action can be formalized in vertex and plaquette operators [24], on the footprints of another quantum link model: the toric code.
The vertex operators are defined in terms of left and right regular representations as a generalization of the vertex operators of the toric model [25]. Their explicit expression is found to be equal to the action of the gauge constraints:

$$A^g_v = G_v(g) \tag{1.67}$$

These operators commute whenever they are applied on different vertices, since they have at most one link in common and in that case they act once with the left and once

with the right regular representation. If instead they act on the same vertex they follow the relation:

$$A_v^g A_v^h = A_v^{gh} \tag{1.68}$$

So they commute only if g and h commute.
Since in a finite group any element g has finite order, that we denote by $|g|$, we have:

$$(A_v^g)^{|g|} = \mathbb{1} \tag{1.69}$$

The eigenvalues of the vertex operators are therefore complex roots of unity.
From the action of the single element g it is possible to obtain a total vertex operator:

$$A_v = \frac{1}{|G|} \sum_{g \in G} A_v^g \tag{1.70}$$

This operator is a projector, which means that $A_v^2 = A_v$, therefore it can have only eigenvalue 1 or 0. The states with eigenvalue 1 are the gauge invariant states, because we have $|G|$ terms in the sum, each of which is a root of unity. Since we divide by $|G|$ in front, each of them must be one, which implies the invariance under gauge transformation.

For the plaquette operator we want to associate a group element to the given loop. We start by considering a plaquette p, then choose one vertex v, and enumerate from 1 to 4 the links on the boundary. The operator is defined as

$$B_{p,v}^h = \sum_{g_1,\dots,g_4} \delta(h, g(e_1)g(e_2)g(e_3)g(e_4)) \mathbb{P}_{g_1} \mathbb{P}_{g_2} \mathbb{P}_{g_3} \mathbb{P}_{g_4} \tag{1.71}$$

where $g(e_l)$ is again g_l or g_l^{-1} depending on the orientation of the link and $\mathbb{P}_{g_l} = |g_l\rangle \langle g_l|$ is a projector over the state $|g_l\rangle$ in the Hilbert space of the link l. The action is assumed to be the identity on all other links of the system.
Again we have $(B_{p,v}^h)^2 = B_{p,v}^h$, which means that the plaquette operators are projectors, with eigenvalues always 1 or 0.
The vertex choice is important, since it leads to different operators. To understand why we can confront for example the case in which we start at the bottom left of a plaquette and the case in which we start at the bottom right. In one case we have:

$$B_{p,v}^h = \sum_{g_1,\dots,g_4} \delta(h, g_1 g_2 g_3^{-1} g_4^{-1}) \mathbb{P}_{g_1} \mathbb{P}_{g_2} \mathbb{P}_{g_3} \mathbb{P}_{g_4} \tag{1.72}$$

while in the other we have:

$$B_{p,v'}^h = \sum_{g_1,\dots,g_4} \delta(h, g_2 g_3^{-1} g_4^{-1} g_1) \mathbb{P}_{g_1} \mathbb{P}_{g_2} \mathbb{P}_{g_3} \mathbb{P}_{g_4} = \sum_{g_1,\dots,g_4} \delta(g_1 h g_1^{-1}, g_1 g_2 g_3^{-1} g_4^{-1}) \mathbb{P}_{g_1} \mathbb{P}_{g_2} \mathbb{P}_{g_3} \mathbb{P}_{g_4} \tag{1.73}$$

When we try to confront the two states on the same vertex the path between the two vertices (in this case the link e_1) act as a conjugation on the group element representing the state. The support of the two operators overlap only in part, having some states in common while others not.
We have already shown some commuting properties, but it is useful to look at all of them to better understand their interaction. We will look at all possible configurations on the lattice for all combination of vertex and plaquette operators. Obviously if the operators act on different links they commute, so we can restrict ourself to a smaller set of non trivial cases. We will not go through the algebra, which can be found in [24].
There are two non-trivial cases for vertex-vertex configuration:

- One link in common. In this case: $[A_v^g, A_{v'}^h] = 0$
- On the same vertex. In this case: $A_v^g A_v^h = A_v^{gh}$, so they commute only if g and h commute

We have three cases for plaquette-plaquette configurations:

- One link in common. In this case: $[B_{p,v}^g, B_{p',v'}^h] = 0$
- Same plaquette but different vertices. In this case: $[B_{p,v}^g, B_{p,v'}^h] = 0$
- Same plaquette and same vertex. In this case: $B_{p,v}^g B_{p,v}^h = \delta(g,h) B_{p,v}^g$, so they commute again.

We have two non trivial case for plaquette-vertex configuration

- The starting vertex of the plaquette operator is different from the vertex of the vertex operator. In this case the operators commute: $[A_v^g, B_{p,v'}^h] = 0$
- The starting vertex of the plaquette operator is the same as that of the vertex operator. In this case $A_v^g B_{p,v}^h = B_{p,v}^{g^{-1}hg} A_v^g$. They commute only if h is invariant under commutation by g. This is true for example if $h = e$.

From these relations it is possible to obtain also the commutation relations for the total vertex operator A_v.

We saw that vertex operators are connected to the gauge invariant conditions. The plaquettes operators can instead be used to obtain a convenient expression of the magnetic Hamiltonian. Using equation (1.66) on a single plaquette described by the conventions in figure 1.2, we can write the action of the plaquette Wilson loop operator as:

$$\operatorname{tr} \hat{W}_\square \left| g_1 g_2 g_3 g_4 \right\rangle = \chi_F(g_1 g_2 g_3^{-1} g_4^{-1}) \left| g_1 g_2 g_3 g_4 \right\rangle \tag{1.74}$$

From which we can see that:

$$\operatorname{tr} \hat{W}_{\square} = \sum_{g_1,g_2,g_3,g_4 \in G} \chi_F(g_1 g_2 g_3^{-1} g_4^{-1}) \mathbb{P}_{g_1} \mathbb{P}_{g_2} \mathbb{P}_{g_3} \mathbb{P}_{g_4} \tag{1.75}$$

We can then expand this expression as

$$\operatorname{tr} \hat{W}_{\square} = \sum_{g \in G} \sum_{g_1,g_2,g_3,g_4 \in G} \chi_F(g) \delta(g, g_1 g_2 g_3^{-1} g_4^{-1}) \mathbb{P}_{g_1} \mathbb{P}_{g_2} \mathbb{P}_{g_3} \mathbb{P}_{g_4} \tag{1.76}$$

where we can recognize the expression for the plaquette operators. The final result is:

$$\operatorname{tr} \hat{W}_{\square} = \sum_{g \in G} \chi_F(g) B^g_{v,p} \tag{1.77}$$

From these expression for the Wilson loops the magnetic Hamiltonian can be written in the equivalent form:

$$H_B = \sum_p \sum_{h \in G} (\chi_F(h) + \chi_F^*(h)) B^h_{v,p} \tag{1.78}$$

1.2.3 The electric ground state

Since we want to study the properties of the Hamiltonian as a function of the parameters λ_E and λ_B we can start by considering the extreme cases where the Hamiltonian is totally dominated by the electric or magnetic part.
In the electric case we can see that on a single link the function $f(j)$ has always a minimum on the trivial representation. In fact we have $f(j = 0) = 0$ for any group and choice of the generators. This means that the ground state of the system in the representation basis is:

$$|0_E\rangle = |0\rangle^{\otimes L} \tag{1.79}$$

where we omitted the mn indices since the trivial representation is always one-dimensional. Since in this basis the left and right regular representations act trivially, this state is always gauge invariant.
Another interesting property comes from expressing the electric vacuum in the group basis, where it turns out that the electric vacuum is an equal weight superposition of all group states:

$$|0_E\rangle = \frac{1}{\sqrt{|G|^L}} \sum_{g_1 \dots g_L \in G} |g_1, \dots g_L\rangle \tag{1.80}$$

This state can be extremely useful because it can be defined universally for any finite group theory, and can be used as a starting point to generate other important states in the theory, in a structure similar to the creation and annihilation operators in second quantization.

1.2.4 The one-plaquette states

The simplest case of states obtainable from the electric vacuum are the one-plaquette group states, in which we can assign one group element to each plaquette in the system, through the action of a plaquette operator. On a lattice with M plaquettes we obtain the state:

$$|\tilde{g_1}...\tilde{g_M}\rangle = c_n B^{g_1}_{p_1,v_1}...B^{g_M}_{p_M,v_M}|0_E\rangle \tag{1.81}$$

where the tilde indicates that they refer to a plaquette, while c_n is the normalization constant of the state. In general we would expect that each plaquette operator $B^g_{p,v}$ selects a fraction $1/|G|$ of the states. Therefore in order to keep the normalization we should just need to introduce a factor $\sqrt{|G|}$ for each plaquette operator. This reasoning fails in the case of a PBC lattice, where the plaquette projectors combine in more convoluted ways. In that case it is also possible for a set of projectors to have only the 0-norm state as common support. This state is not normalizable and cannot be interpreted as a physical wave function. It is therefore important to understand that describing a state through the previous definition is not enough to warrant its existence. We will show an example of such effects in the case of the group D_4, when we will analyze the non-abelian theory. The one-plaquette group states depend on the vertices we chose for each plaquette. Conventionally, if nothing else is specified, we can take them to be the bottom left corner.
These states are not a basis of the Hilbert space, since generally there are always more links than plaquettes. Moreover they are not gauge invariant, as can be calculated from the commuting relations on a single plaquette:

$$A^h_v|\tilde{g}\rangle = |G|^{\frac{1}{2}}A^h_v B^g_{p,v}|0_E\rangle = |G|^{\frac{1}{2}}B^{h^{-1}gh}_{p,v}A^h_v|0_E\rangle = |(\tilde{h^{-1}gh})\rangle \tag{1.82}$$

We can nonetheless use these states as a starting point to obtain gauge invariant states. There are in fact two ways to do so. The first is to perform a linear combination of all group elements belonging to a given conjugacy class, in which case the gauge transformation leads only to a reshuffling of terms, leaving the state invariant. For the single plaquette we write those as

$$|C\rangle = \frac{1}{\sqrt{|C|}}\sum_{g\in C}|\tilde{g}\rangle \tag{1.83}$$

where C is a conjugacy class of G.
The other way is to introduce the character states, defined as

$$|\chi_j\rangle = \frac{1}{\sqrt{|G|}}\sum_{g\in G}\chi_j(g)|\tilde{g}\rangle \tag{1.84}$$

which remain unchanged under a gauge transformation since the characters are class functions [47].

Sometimes it is useful to describe these states through the action of an operator. In order to do so we define:

$$\hat{C}_p = \sum_{g \in C} B^g_{p,v} \tag{1.85}$$

$$\hat{\chi}_j(p) = \sum_{g \in G} \chi_j(g) B^g_{p,v} \tag{1.86}$$

The two sets of states are related by the transformation:

$$|\chi_j\rangle = \sum_{C \in \tilde{G}} \sqrt{\frac{|C|}{|G|}} \chi_j(C) \, |C\rangle \tag{1.87}$$

which can be calculated easily from the group Fourier transform. In this case $\tilde{G}$ is the set of conjugacy classes, and $\chi_j(C)$ is the value of the character on any element of the conjugacy class.
Another remarkable property of the conjugacy and character sets of states is that they no longer depend on the vertex choice. This is again because when we change the starting vertex we change the group state by a conjugation, which is canceled by reshuffling in the conjugacy case and characters being class functions in the other.

We can generalize the one-plaquette states to the whole lattice as

$$|\chi_{j_1} \cdots \chi_{j_M}\rangle = \frac{1}{\sqrt{|G|^M}} \sum_{g_1,\ldots,g_M \in G} \chi_{j_1}(g_1) \cdots \chi_{j_M}(g_M) \, |\tilde{g_1} \ldots \tilde{g_M}\rangle \tag{1.88}$$

$$|C_1 \ldots C_M\rangle = \frac{1}{\sqrt{|C_1| \ldots |C_M|}} \sum_{g_1,\ldots,g_M \in C_1,\ldots,C_M} |\tilde{g_1} \ldots \tilde{g_M}\rangle \tag{1.89}$$

The character states can also be represented as

$$|\chi_{j_1} \cdots \chi_{j_M}\rangle = \frac{1}{\sqrt{|G|^M}} \sum_{g_1,\ldots,g_L \in G} \chi_{j_1}(g_{\gamma 1}) \cdots \chi_{j_M}(g_{\gamma M}) \, |g_1, \ldots, g_L\rangle \tag{1.90}$$

where $g_{\gamma p}$ is the product of the four group elements on the links around plaquette p taken directly or inverted based on the orientation in which the link is traversed.
It is useful to notice that states in these two sets are orthonormal. This is obvious in the conjugacy case, since two group states with different conjugacy class are orthogonal. In the representation case it is instead due to the orthogonality of characters: $\sum_{g \in G} \chi_i^*(g) \chi_j(g) = |G| \delta_{i,j}$ [56].

1.2.5 General results on one-plaquette states

The one-plaquette states can be useful to calculate matrix elements of the Hamiltonian. Starting from the magnetic part the group plaquette states can be used to easily calculate the matrix elements, since the action of the Wilson loops becomes trivial:

$$\langle \tilde{g_1}...\tilde{g_M}| \, H_B \, |\tilde{h_1}...\tilde{h_M}\rangle = -2\delta_{g_1,h_1}...\delta_{g_M,h_M} \sum_{p=1}^{M} Re(\chi_F(g_p)) \tag{1.91}$$

A similar relation also holds for the conjugacy class states:

$$\langle C_1...C_M| \, H_B \, |C_1'....C_M'\rangle = -2\delta(C_1,'C_1)...\delta(C_M,C_M') \sum_{p=1}^{M} Re(\chi_F(C_p)) \tag{1.92}$$

The situation for the electric term is more complicated. We can start by calculating the value for a single link operator h_E^l. If we have only one plaquette than

$$|\chi_j\rangle = \frac{1}{\sqrt{|G|^4}} \sum_{g_1,g_2,g_3,g_4 \in G} \chi_j(g_1 g_2 g_3^{-1} g_4^{-1}) \, |g_1 g_2 g_3 g_4\rangle \tag{1.93}$$

In this case the character of four elements can be made explicit as the product of the representations, which in turn can be understood as elements of the representation basis:

$$|\chi_j\rangle = \frac{1}{\sqrt{|G|^4}} \sum_{\substack{m_1,m_2,m_3,m_4 \\ g_1,g_2,g_3,g_4}} \pi^j_{m_1 m_2}(g_1)\pi^j_{m_2 m_3}(g_2)\pi^{j*}_{m_4 m_3}(g_3)\pi^{j*}_{m_1 m_4}(g_4) \, |g_1 g_2 g_3 g_4\rangle \tag{1.94}$$

$$= \frac{1}{\sqrt{d_j^4}} \sum_{m_1,m_2,m_3,m_4=1}^{d_j} |j_{m_1 m_2} j_{m_2 m_3} {j^*}_{m_4 m_3} {j^*}_{m_1 m_4}\rangle \tag{1.95}$$

where we used the conjugate representation j^*. Since the single link electric term is constant for all states with the same j it is easy to see that on any of the four links

$$h_E^l \, |\chi_j\rangle = f(j) \, |\chi_j\rangle \tag{1.96}$$

since $f(j^*) = f(j)$ for a symmetric set of generators Γ.
In case we have more than one plaquette we notice that the state of a link can be influenced only by the state of the two nearest plaquettes. To solve the general case we can then reduce ourself to a two-plaquette system, and calculate the value of h_E^l on the shared link.

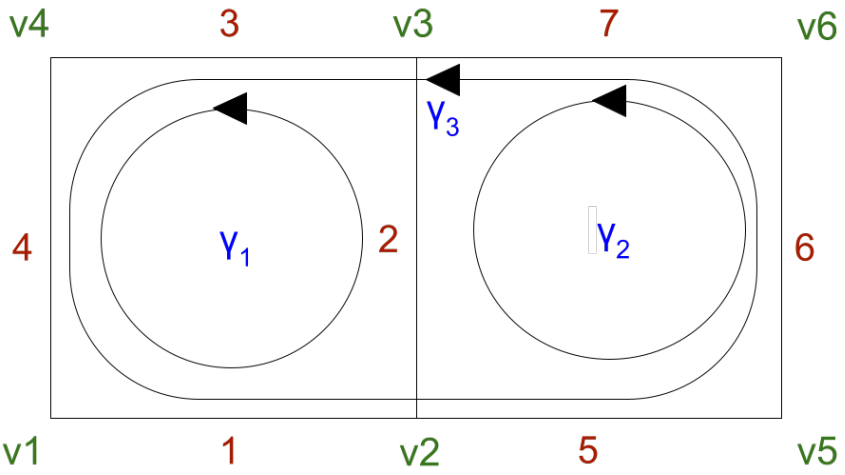

Figure 1.5: Conventions for a 2 plaquette system. In this case γ_1 is the loop around plaquette 1, γ_2 the loop around plaquette 2 and γ_3 the loop around both plaquettes.

Using the conventions in figure 1.5, the only non-trivial single link electric component is related to link 2. Therefore we calculate:

$$\langle \chi_{i_1}\chi_{i_2}| \, h_E^2 \, |\chi_{j_1}\chi_{j_2}\rangle = \frac{1}{|G|^2} \sum_{g_a g_b h_a h_b} \chi^*_{i_1}(h_a)\chi^*_{i_2}(h_b)\chi_{j_1}(g_a)\chi_{j_2}(g_b) \, \langle \tilde{h}_a\tilde{h}_b| \, h_E^2 \, |\tilde{g}_a\tilde{g}_b\rangle \tag{1.97}$$

The last term can be expanded on the group basis:

$$\langle \tilde{h}_a\tilde{h}_b| \, h_E^2 \, |\tilde{g}_a\tilde{g}_b\rangle = \frac{1}{|G|^5} \sum_{\substack{h_1,\dots,h_7 \\ g_1,\dots g_7}} \delta(h_a, h_{\gamma_1})\delta(h_b, h_{\gamma_2})\delta(g_a, g_{\gamma_1})\delta(g_b, g_{\gamma_2}) \, \langle h_1 \dots h_7| \, h_E^2 \, |g_1 \dots g_7\rangle \tag{1.98}$$

where $h_{\gamma_i} = \prod_{l\in\gamma_i} h(e_l)$ and $g_{\gamma_i} = \prod_{l\in\gamma_i} g(e_l)$.
We notice that h_E^2 acts only on the subspace of link 2, therefore the scalar products on

all the other links can be resolved as $\langle h_l g_l \rangle = \delta(h_l, g_l)$. On link 2 we have instead:

$$\begin{aligned}
\langle h_2 h_E^2 g_2 \rangle &= \sum_j f(j) \langle h_2 \mathbb{P}_j g_2 \rangle && (1.99)\\
&= \sum_{j,m,n} f(j) \langle h_2 j_{mn} \rangle \langle j_{mn} g_2 \rangle && (1.100)\\
&= \sum_{j,m,n} \frac{d_j}{|G|} f(j) \pi^j_{mn}(h_2) \pi^{j*}_{mn}(g_2) && (1.101)\\
&= \sum_{j,m,n} \frac{d_j}{|G|} f(j) \pi^j_{mn}(h_2) \pi^j_{nm}(g_2^{-1}) && (1.102)\\
&= \sum_j \frac{d_j}{|G|} f(j) \chi_j(h_2 g_2^{-1}) && (1.103)\\
& && (1.104)
\end{aligned}$$

Substituting this relation, and simplifying the 6 simplest deltas we get

$$\begin{aligned}
\langle \tilde{h}_a \tilde{h}_b | \, h_E^2 \, | \tilde{g}_a \tilde{g}_b \rangle = \quad & \textstyle\sum_j \sum_{g_1,\dots g_7, h_2} \delta(h_a, g_1 h_2 g_3^{-1} g_4^{-1}) \delta(h_b, g_5 g_6 g_7^{-1} h_2^{-1}) && (1.105)\\
& \delta(g_a, g_1 g_2 g_3^{-1} g_4^{-1}) \delta(g_b, g_5 g_6 g_7^{-1} g_2^{-1}) \tfrac{d_j}{|G|^6} f(j) \chi_j(h_2 g_2^{-1}) && (1.106)
\end{aligned}$$

In order to simplify this expression we use the first and third term to solve the sum over h_2 and g_2. In the character term all group elements cancel thanks to the cyclic property. We are left with

$$\begin{aligned}
\langle \tilde{h}_a \tilde{h}_b | \, h_E^2 \, | \tilde{g}_a \tilde{g}_b \rangle = \quad & \textstyle\sum_j \sum_{g_1, g_3, \dots g_7} \delta(h_b, g_5 g_6 g_7^{-1} g_3^{-1} g_4^{-1} h_a^{-1} g_1) && (1.107)\\
& \delta(g_b, g_5 g_6 g_7^{-1} g_3^{-1} g_4^{-1} g_a^{-1} g_1) \tfrac{d_j}{|G|^6} f(j) \chi_j(h_a g_a^{-1}) && (1.108)
\end{aligned}$$

The product $g_5 g_6 g_7^{-1} g_3^{-1} g_4^{-1}$ is the same in the two deltas. From the second delta it is equal to $g_b g_1^{-1} h_a$, which can be substituted in the first one so that we can also write

$$\begin{aligned}
\langle \tilde{h}_a \tilde{h}_b | \, h_E^2 \, | \tilde{g}_a \tilde{g}_b \rangle = \quad & \textstyle\sum_{j, g_1} \tfrac{d_j}{|G|^6} f(j) \chi_j(h_a g_a^{-1}) \delta(h_b^{-1} g_b, g_1^{-1} h_a g_a^{-1} g_1) && (1.109)\\
& \textstyle\sum_{g_3, \dots g_7} \delta(h_b, g_5 g_6 g_7^{-1} g_3^{-1} g_4^{-1} h_a^{-1} g_1) && (1.110)
\end{aligned}$$

The last five sums are trivial, and give as a result a factor $|G|^4$. To solve the sum in g_1 instead we notice that

$$\sum_{k \in G} \delta(g, k^{-1} h k) \tag{1.111}$$

is always zero if g and k are in different conjugacy classes. If they are in the same then the result of such sum is $\frac{|G|}{|C(g)|}$. Thanks to the orthogonality relations of characters we can write it as

$$\sum_{k \in G} \delta(g, k^{-1} h k) = \sum_j \chi_j^*(g) \chi_j(h) \tag{1.112}$$

Using this expression in the previous equation we find:

$$\langle \tilde{h}_a \tilde{h}_b |\, h_E^2 \,| \tilde{g}_a \tilde{g}_b \rangle = \sum_{l,m} \tfrac{d_l}{|G|^2} f(l) \chi_l(h_a g_a^{-1}) \chi_m^*(h_b^{-1} g_b) \chi_m(h_a g_a^{-1}) \tag{1.113}$$

If we substitute this expression in equation (1.97) we obtain:

$$\langle \chi_{i_1} \chi_{i_2} |\, h_E^2 \,| \chi_{j_1} \chi_{j_2} \rangle = \frac{1}{|G|^4} \sum_{l,m} \sum_{g_a g_b h_a h_b} f(l) d(l) \chi_{i_1}^*(h_a) \chi_{i_2}^*(h_b) \chi_{j_1}(g_a) \chi_{j_2}(g_b) \tag{1.114}$$

$$\chi_l(h_a g_a^{-1}) \chi_m^*(h_b^{-1} g_b) \chi_m(h_a g_a^{-1}) \tag{1.115}$$

In this formula we can change variable from g_a to $k = h_a g_a^{-1}$. We can then recognize two convolutions and one orthogonality relations, given by the sums over g_b, h_a and h_b. The end result is:

$$\langle \chi_{i_1} \chi_{i_2} |\, h_E^2 \,| \chi_{j_1} \chi_{j_2} \rangle = \delta_{i_1,j_1} \delta_{i_2,j_2} \frac{1}{d_{i_1} d_{i_2} |G|} \sum_{l,k} f(l) d_l \chi_{i_1}^*(k) \chi_l(k) \chi_{i_2}(k) \tag{1.116}$$

If we make the electric eigenvalues $f(l)$ explicit, according to equation (1.54), it is possible to simplify this expression further:

$$\langle \chi_{i_1} \chi_{i_2} |\, h_E^2 \,| \chi_{j_1} \chi_{j_2} \rangle = \delta_{i_1,j_1} \delta_{i_2,j_2} \frac{1}{d_{i_1} d_{i_2} |G|} \quad \Big(\sum_{l,k \in G} d_l |\Gamma| \chi_{i_1}^*(k) \chi_l(k) \chi_{i_2}(k) - \tag{1.117}$$

$$\sum_{l,k \in G, g \in \Gamma} \chi_l(g) \chi_{i_1}^*(k) \chi_l(k) \chi_{i_2}(k) \Big) \tag{1.118}$$

In the first term we can substitute d_l with $\chi_l^*(e)$, and perform the sum over l. This gives a term $\delta_{k,e}$ which can be used to calculate the sum in k:

$$\sum_{l,k \in G} d_l |\Gamma| \chi_{i_1}^*(k) \chi_l(k) \chi_{i_2}(k) = d_i d_j |G| |\Gamma| \tag{1.119}$$

In the second term instead we perform the sum over l, which restricts k to give non zero results only on the conjugacy classes of the elements in Γ. Since the latter group is closed under conjugation the result is:

$$\sum_{l,k \in G, g \in \Gamma} \chi_l(g) \chi_{i_1}^*(k) \chi_l(k) \chi_{i_2}(k) = |G| \sum_{g \in \Gamma} \chi_{i_1}^*(g) \chi_{i_2}(g) \tag{1.120}$$

Putting together the two results we find

$$\langle \chi_{i_1} \chi_{i_2} |\, h_E^2 \,| \chi_{j_1} \chi_{j_2} \rangle = \delta_{i_1,j_1} \delta_{i_2,j_2} \bar{f}(i_1, i_2) \tag{1.121}$$

where we defined

$$\bar{f}(i,j) = |\Gamma| - \frac{1}{d_i d_j} \sum_{g \in \Gamma} \chi_i^*(g) \chi_j(g) \tag{1.122}$$

This function can be seen as a generalization for the average electric energy on a link, when two plaquettes interact to give the state of the link. From this simple relation it is possible to see that the matrix elements between character one-plaquette basis states for an arbitrary lattice can be written as

$$\langle \chi_{i_1} ... \chi_{i_M} H_E \chi_{j_1} ... \chi_{j_M} \rangle = \delta(i_1, j_1) ... \delta(i_M, j_M) \sum_{<i_m, i_n>} \bar{f}(i_m, i_n) \tag{1.123}$$

where the sum is performed over nearest neighbor plaquettes.

While this relations can be useful to calculate matrix values and average energies, it is important to notice that the electric part is not diagonal on the one-plaquette states. This is due to the fact that those states don't form a basis of the Hilbert space. Although the electric Hamiltonian has matrix element zero between two one-plaquette character states, there could be other states for which it is not so.
Since the Hamiltonian is gauge invariant these other states must be in the gauge invariant sector. A key example of this fact will be shown when we will treat the non-abelian theory.

1.2.6 Multiple plaquette states

If we want to work with more general gauge invariant states and operators we need to consider closed paths which surround more than one plaquette. If we call one of those paths γ we can define the operator that associates it to a group element as

$$B_v^g(\gamma) = \sum_{h_1, ..., h_{l_{max}}} \delta\left(g, h_\gamma\right) \bigotimes_{l \in \gamma} \mathbb{P}_{h_l}(e_l) \tag{1.124}$$

where $h_\gamma = \prod_{l \in \gamma} h(e_l)$.
We can use this operator to construct projectors to the character and conjugacy class states as

$$\hat{\chi}_j(\gamma) = \sum_{g \in G} \chi_j(g) B_v^g(\gamma) \tag{1.125}$$

$$\hat{C}(\gamma) = \sum_{g \in C} B_v^g(\gamma) \tag{1.126}$$

These operators can be used on the electric vacuum to obtain gauge invariant states, written as $|\chi_j(\gamma)\rangle$ or $|C(\gamma)\rangle$, and no longer depend on the starting vertex v due to the same reasons as for the one-plaquette case.
They can also be combined to create more complex states, such as

$$|\chi_{j_1}(\gamma_1)\chi_{j_2}(\gamma_2)...\rangle = c_n \hat{\chi}_{j_1}(\gamma_1)\hat{\chi}_{j_2}(\gamma_2)... \left|0_E\right\rangle \tag{1.127}$$

The main issue of these states is that if we use all possible paths we obtain many redundant descriptions of the same state, leading to an over-complete sets of states for the description of the gauge invariant subspace.
This is a known problem [26], particularly hard to solve in the case of non-abelian theories, as we will show later.

1.3 Related models

Now that we have introduced the plaquette and vertex operators it is interesting to look at another class of quantum link models, collectively known as Quantum Double Model (QDM) [10, 11, 13, 31]. They were first developed as group based generalization of the toric model.
QDM are defined on a ordered lattice as the previous models and base their structure on a finite group G. The total Hilbert space is the same: a copy of the group algebra for each link in the model. From the group structure it is possible to construct the same plaquette and vertex operators, from which we can write the Hamiltonian as

$$H = -\sum_p B_p - \sum_v A_v \tag{1.128}$$

where $B_p = B^e_{p,v}$ and we can omit the vertex index, since on a plaquette operator connected to the identity element e all starting points are equivalent. This can be seen from the special case $h = e$ in equation (1.73).
In the QDM all addends of the Hamiltonian commute with each other. This means that it is possible to diagonalize both on the same basis. We can then look at the spectrum of each individual part separately and then combine the results to obtain the spectrum of the whole theory.
In the case of gauge group theories we have instead the electric term, which does not commute with the magnetic term, giving a non-trivial behavior.
Looking at the vertex part first, in order to reconstruct the spectrum of the whole theory, we can start by noticing that the operators A_v are projectors, therefore they can only have eigenvalues equal to 0 or 1. Since each vertex operator enters the Hamiltonian with a minus sign the lower energy states correspond to states on which the eigenvalue of each vertex operator is 1. In principle we cannot know if there is only one ground state or if it is a degenerate eigenspace. Nevertheless we know that on any state in the ground eigenspace of the vertex part $|\psi^0_v\rangle$ all vertex operators act with eigenvalue 1, which means that we can write:

$$A_v |\psi^0_v\rangle = |\psi^0_v\rangle \tag{1.129}$$

The energy of such states is $E_v = -N_v$, where all N_v vertices contribute with an energy -1.

This condition is the gauge invariant condition of the finite group Yang-Mills models. Therefore the vector space of physical states in the gauge theory corresponds to the eigenspace of ground states of the QDM.

Also the operators B_p are projectors, and enter the Hamiltonian with a minus sign. Therefore, we have a minimum of the plaquette term when all plaquettes correspond to the eigenvalue 1, giving a total contribute to the energy equal to $E_p = -N_p$, where N_p is the number of plaquettes. These states satisfy the condition

$$B_p \left|\psi_p^0\right\rangle = \left|\psi_p^0\right\rangle \tag{1.130}$$

In order to understand the relation between QDM and the Yang-Mills model we can look at a single plaquette in the group plaquette basis, which is defined by a state $|\tilde{g}\rangle$, and compare the action of one operator B_p with the one plaquette Wilson loop operator. In this case we have:

$$B_p \left|\tilde{g}\right\rangle = \delta_{e,g} \left|\tilde{g}\right\rangle \tag{1.131}$$

$$W_p \left|\tilde{g}\right\rangle = \chi_F(g) \left|\tilde{g}\right\rangle \tag{1.132}$$

where χ_F is again the character of the arbitrary representation π_F. This relation allows us to draw a parallel between the plaquette part of the QDM Hamiltonian with the magnetic part of the Yang-Mills Hamiltonian. In the magnetic Hamiltonian we have also to consider the action of the adjoint Wilson loop, which, summed to the other, leads to real eigenvalues $2\,\mathrm{Re}\,\chi_F(g)$. Since the value of any character χ_j is a sum of d_j complex roots of unity [23], where d_j is the dimension of representation π_j, the maximum value of $\mathrm{Re}\,\chi_F(g)$ is attained when all addends are equal to 1. The sum becomes $\mathrm{Re}\,\chi_F(g) = d_F$ which is always true for $g = e$. In this case the single plaquette contribute assumes the value $2d_F$. But such state correspond also to the greatest possible eigenvalue on the double model, which is 1. Therefore, a state that minimizes the plaquette part also minimizes the magnetic Hamiltonian.
If we look instead at one-plaquette states with $g \neq e$ we have eigenvalue zero in the QDM case, while we have different values in the gauge case, which depend on the group G and the chosen representation π_F. This means that the magnetic excitations of the Yang-Mills model are more complex than in the QDM.

Putting together the considerations on both the plaquette and the vertex part we can see that the ground states of the QDM minimizes the magnetic energy and are gauge invariant. Therefore they can be useful to describe the ground state of the Yang-Mills Hamiltonian in the case it is totally dominated by the magnetic part.

1.3.1 The toric model

The simplest and most studied double model is the toric model, which corresponds to the choice of $\mathbb{Z}_2$ as the defining group.
For this group we have 2 elements: e and r. Since each of them form a conjugacy class we have 2 conjugacy classes and therefore 2 irreducible representations. We denote the trivial as π_0, with $\pi_0(g) = 1\ \forall g$, and the non trivial as π_1, which has values $\pi_1(e) = 1$ and $\pi_1(r) = -1$.
We can then define the 2-dimensional single link Hilbert space in the position basis as $|e\rangle$ and $|r\rangle$, or equivalently in the representation basis as $|0\rangle$ and $|1\rangle$. The two bases are connected by the group Fourier transform:

$$\langle g|j\rangle = \frac{1}{\sqrt{2}}\pi_j(g) \tag{1.133}$$

This change of basis can be represented as a 2 by 2 matrix:

$$\langle g|j\rangle = \frac{1}{\sqrt{2}}\begin{pmatrix}1 & 1\\ 1 & -1\end{pmatrix} \tag{1.134}$$

The left and right regular representations are 2-dimensional representations, since $|G| = 2$. The representations of element e are $L_e = R_e = \mathbb{1}_2$ in all bases, while the regular representations of element r are diagonal in the representation basis:

$$L_r\,|0\rangle = R_r\,|0\rangle = +1\,|0\rangle \tag{1.135}$$
$$L_r\,|1\rangle = R_r\,|1\rangle = -1\,|1\rangle \tag{1.136}$$

which means that we can write $L_r = R_r = \sigma_z$ in the representation basis, using the Pauli matrix $\sigma_z = \begin{pmatrix}1 & 0\\ 0 & -1\end{pmatrix}$.
This allows us to write the vertex operators as

$$A_v^e = \mathbb{1} \tag{1.137}$$
$$A_v^r = \sigma_z^{(1)}\sigma_z^{(2)}\sigma_z^{(3)}\sigma_z^{(4)} \tag{1.138}$$
$$A_v = \frac{1}{2}(\mathbb{1} + \sigma_z^{(1)}\sigma_z^{(2)}\sigma_z^{(3)}\sigma_z^{(4)}) \tag{1.139}$$

The position operators $\hat{u}$ are 1×1 matrices since the chosen representation $\pi_F = \pi_1$ is one dimensional. They are diagonal on the position basis and have eigenvalue $+1$ on $|e\rangle$ and eigenvalue -1 on $|r\rangle$. Using the relation between position basis and representation basis we can see that on the latter they take the form $\hat{u} = \sigma_x$. We can then rewrite the eigenstates as $|e\rangle = |+\rangle$ and $|r\rangle = |-\rangle$, in accordance to classical conventions for 2-dimensional Hilbert spaces.

We have two plaquette operators $B^e_{p,v}$ and $B^r_{p,v}$. If we look at the product of four σ_x along the boundary of a plaquette acting on a state in the position base we can see that they have eigenvalue 1 when the group product of the links is e and -1 when it is r. We can then write:

$$B^e_{p,v} = \frac{1}{2}(\mathbb{1} + \sigma_x^{(1)}\sigma_x^{(2)}\sigma_x^{(3)}\sigma_x^{(4)}) \tag{1.140}$$

$$B^r_{p,v} = \frac{1}{2}(\mathbb{1} - \sigma_x^{(1)}\sigma_x^{(2)}\sigma_x^{(3)}\sigma_x^{(4)}) \tag{1.141}$$

From these we can define also the single plaquette Wilson loop operator:

$$\hat{W} = \chi_1(e)B^e_{p,v} + \chi_1(r)B^r_{p,v} = \sigma_x^{(1)}\sigma_x^{(2)}\sigma_x^{(3)}\sigma_x^{(4)} = \hat{u}(e_1)\hat{u}(e_2)\hat{u}(e_3)\hat{u}(e_4) \tag{1.142}$$

where $\hat{W} = \operatorname{tr}\hat{W}$, since the chosen representation is one-dimensional. We can use these operators to write the Hamiltonian

$$H_{toric} = -\sum_p B_p - \sum_v A_v \tag{1.143}$$

Before moving forward it is useful to comment about conventions. In many standard textbooks [55, 8] the Hamiltonian is given as

$$H'_{toric} = -\sum_p B'_p - \sum_v A'_v \tag{1.144}$$

$$B'_p = \prod_{l\in p}\sigma_x^{(l)} \quad A'_p = \prod_{l\in v}\sigma_z^{(l)} \tag{1.145}$$

Since the two Hamiltonians (1.143) and (1.144) differ only by a constant (equal to $N_v + N_p$) they have the same structure of the spectrum.
Another common difference in conventions is that the Pauli matrices are often inverted, using σ_x for the vertex operators and σ_z for the plaquette operators. This can be interpreted as working in position basis instead of representation basis, where $\hat{u} = \sigma_z$ and $L_r = R_r = \sigma_x$.

Using the plaquette operators it is possible to define the ground state of the system as

$$|\psi^0_B\rangle = \prod_p B_p\,|0_E\rangle \tag{1.146}$$

To prove that this is indeed the ground state of the system we can see that all A_v operators commute with the plaquette operators and act trivially on the electric ground state. The plaquette operators B_p combine with the plaquette operator in the definition as $B_pB_p = B_p$, leaving the state invariant.

In order to visualize this ground state we can work in the representation basis and indicate the states in the $|0\rangle$ state as turned off, while the states in the $|1\rangle$ state as turned on. The σ_x operator act as a toggle, changing the state on a link from off to on and vice versa. The Wilson plaquette loop operator $\hat{W}$ is a product of σ_x operators, and therefore simultaneously toggles all states around a given plaquette. The action of the B_p operator can be divided in two parts: the first acts trivially, leaving the state unchanged, while the second is proportional to the plaquette toggle $\hat{W}$.
Moreover when two adjacent plaquettes are turned on the link in between is acted upon twice, leaving it unchanged. This produces active loops which wrap around more than one plaquette.
Putting all this together we can see that the magnetic ground state is a superposition of all possible combinations of on and off plaquettes. It also contains all loops that can be represented as a union of 2 or more plaquettes. Such a state is called a *loop gas* [24].

Not all the possible loops are found in such state. Due to the PBC the topology of the space is a torus and there are two non contractible loops which cannot be represented as a product of plaquettes as can be seen in figure 1.6.

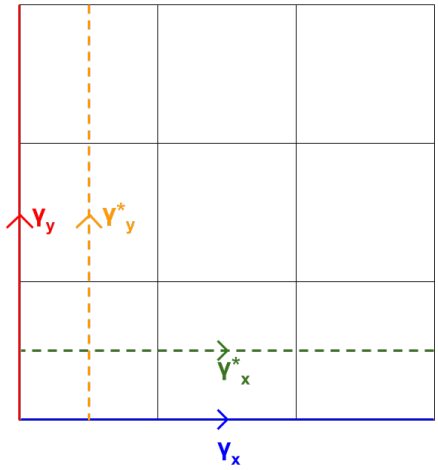

Figure 1.6: Non-contractible loops in a 3x3 2-dimensional periodic lattice. In red and blue are shown the two possible loops in the direct lattice, while γ_x^* and γ_y^* are the loops in the dual lattice.

We can access states which contains non contractible loops turned on through the action of the Wilson loop operators $\hat{W}(\gamma_x) = \prod_{l\in\gamma_x} \hat{u}(e_l)$ and $\hat{W}(\gamma_y) = \prod_{l\in\gamma_y} \hat{u}(e_l)$. Since these two operators commute with all B_p and A_v they don't change the value of

the Hamiltonian. We can then define:

$$|\psi^0_{B,x}\rangle = \hat{W}(\gamma_x)\,|\psi^0_B\rangle \quad |\psi^0_{B,y}\rangle = \hat{W}(\gamma_y)\,|\psi^0_B\rangle \quad |\psi^0_{B,xy}\rangle = \hat{W}(\gamma_x)\hat{W}(\gamma_y)\,|\psi^0_B\rangle \tag{1.147}$$

These three states, together with the starting state $|\psi^0_B\rangle$ are all ground states of the toric model, and therefore are also ground states of the $\mathbb{Z}_2$ gauge theory, when dominated by the magnetic term.
This states cannot be easily perturbed from one to the other and have been used to prove that the Hamiltonian is topological [51] and play a fundamental role in the study of quantum error correcting codes [55].
In general all states that can be obtained by local transformation on these four states are said to belong to the same topological sector. Therefore we can say that the toric model has four topological sectors.
In order to understand if a state is in a certain topological sector we can use the t'Hooft loop operators, defined as

$$Z(\gamma^*) = \prod_{l\in\gamma*} \sigma_z^{(l)} \tag{1.148}$$

where γ^* is a closed loop in the dual lattice, as seen in figure 1.6. In this case the t'Hooft loops around the non contractible dual loops γ^*_x and γ^*_y have eigenvalues ± 1 and can be used to categorize states into the four sectors: "++", "−+", "+−","−−".
It is simple to see that $|\psi^0_B\rangle$ is in the first sector, $|\psi^0_{B,x}\rangle$ is in the second, $|\psi^0_{B,y}\rangle$ is in the third, and $|\psi^0_{B,x,y}\rangle$ in the fourth.

1.3.2 The magnetic ground state

Using the toric model as a guideline we would like to find an explicit description of the ground state of double models with a different gauge group, which corresponds to the various magnetic ground states of the related Yang-Mills theories.
We can start by defining the simple state

$$|\psi^0_B\rangle = c_n \prod_p B_p\,|0_E\rangle \tag{1.149}$$

From the commutation rules between B_p and A_v, the action of A_v on $|0_E\rangle$ and the composition of B_p and $B_{p'}$ we can see that this is indeed a ground state for the QDM.
Before moving forward we must verify that this state indeed exist. In order to do so we can calculate the normalization constant:

$$\frac{1}{|c_n|^2} = \langle 0_E| \prod_{p,p'} B_{p'}B_p\,|0_E\rangle \tag{1.150}$$

We can use the projector relations between the plaquette operators to simplify the expression, expand the electric vacuum in the group basis and obtain:

$$\langle 0_E| \prod_{p,p'} B_{p'} B_p \, |0_E\rangle = \langle 0_E| \prod_{p} B_p \, |0_E\rangle \tag{1.151}$$

$$= \frac{1}{|G|^L} \sum_{g_1,\dots,g_L} \prod_{p} \delta(e, g(\gamma_p)) \tag{1.152}$$

Here $g(\gamma_p)$ is the product of the group elements along the path which wraps around the p plaquette. Using the conventions for the states on the 3x3 lattice, as can be seen in figure 1.7, we can show that the deltas combine nicely. For example for plaquette 1 and 2 we have

$$\delta(e, g(\gamma_{p_1}))\delta(e, g(\gamma_{p_2})) = \delta(e, g_1 g_4 g_7^{-1} g_2^{-1})\delta(e, g_3 g_6 g_9^{-1} g_4^{-1}) = \tag{1.153}$$

$$= \delta(e, g_1 g_4 g_7^{-1} g_2^{-1})\delta(g_4, g_3 g_6 g_9^{-1}) = \delta(e, g_1 g_3 g_6 g_9^{-1} g_7^{-1} g_2^{-1})\delta(g_4, g_3 g_6 g_9^{-1}) \tag{1.154}$$

This is due to the fact that taken any two vertex on a plaquette, the delta on that plaquette produces an identification between the two possible paths between the two vertices, which can be substituted on other plaquettes to obtain any contractible loop. After the substitution there is only one dependence on g_4 and therefore we can sum over it, solving one of the deltas in the sum.
Extending this reasoning on the whole lattice we can put all loops into one, eliminating the other $M - 1$ deltas. The choice of merging is arbitrary. We use the comb shape in figure 1.7, which can be easily generalized to larger lattices. The result is:

$$\frac{1}{|c_n|^2} = \frac{1}{|G|^L} \sum_{g_i} \delta(e, g(\gamma_{comb})) \tag{1.155}$$

where the g_i summed over are the one appearing in γ_{comb}.

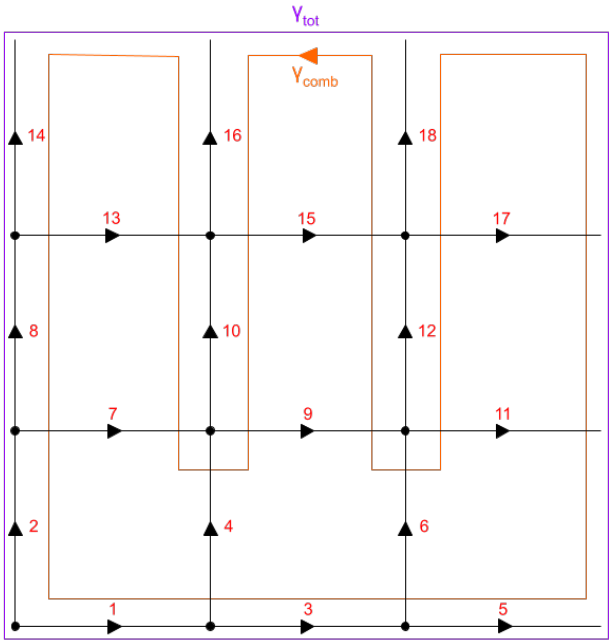

Figure 1.7: 3x3 periodic lattice, with two useful paths γ_{comb} and γ_{tot} shown.

The group elements between the comb teeth are taken once in a direction and once in the opposite, canceling each other out. We can then sum over those states, obtaining a factor $|G|$ for each. We are left with a loop γ_{tot} which wraps around the whole lattice. Due to the PBC these loop contains the lower border and the left border twice, traveled in opposite direction. Instead of summing over each link in the lower border we can substitute their product with a new element g_x, and do the same for the vertical border g_y. The sum depends only on these products, and we are free to sum over the remaining elements to obtain a factor $|G|$ for each. We are left with

$$\frac{1}{|c_n|^2} = |G|^{-M-1} \sum_{g_x, g_y} \delta(e, g_x g_y g_x^{-1} g_y^{-1}) \tag{1.156}$$

The last sum can be calculated as

$$\sum_{g_x, g_y} \delta(g_y, g_x g_y g_x^{-1}) = \sum_{g_y} \frac{|G|}{C(g_y)} = |G||\hat{G}| \tag{1.157}$$

where $|\hat{G}|$ is the number of irreducible representations. We can then write the normalization constant as

$$c_n = \sqrt{\frac{|G|^M}{|\hat{G}|}} \tag{1.158}$$

which proves that the state $|\psi_0^B\rangle$ exists for any group G.
We can also interpret such a state as a *loop gas*. In fact, using the orthogonality relations one finds:

$$B_p = \sum_{g_i} \delta(e, g_1 g_2 g_3^{-1} g_4^{-1}) \mathbb{P}_{g_1} \mathbb{P}_{g_2} \mathbb{P}_{g_3} \mathbb{P}_{g_4} \tag{1.159}$$

$$= \sum_{j,g_i} \frac{\chi_j^*(e)}{|G|} \chi_j(g_1 g_2 g_3^{-1} g_4^{-1}) \mathbb{P}_{g_1} \mathbb{P}_{g_2} \mathbb{P}_{g_3} \mathbb{P}_{g_4} \tag{1.160}$$

$$= \sum_j \frac{d_j}{|G|} \hat{\chi}_j(p) \tag{1.161}$$

Therefore each plaquette operator projects over the superposition of all possible character states on that plaquette. The product of all plaquette operators therefore projects on all possible combinations of one-plaquette character states.

We can also introduce the concept of topological sectors in the following way. We define the operators $\hat{\chi}_{j_x}(\gamma_x)$ and $\hat{\chi}_{j_y}(\gamma_y)$ and apply them on the magnetic vacuum. We obtain

$$|\psi_0^B(j_x, j_y)\rangle = \hat{\chi}_{j_x} \hat{\chi}_{j_y}(\gamma_y) \, |\psi_0^B\rangle \tag{1.162}$$

These states have the same energy of the ground state, but exhibit an excitation along a non contractible loop, which makes them topologically different. Therefore the eigenspace with minimum energy of the QDM is $|\hat{G}|^2$ dimensional.
It is interesting to notice that the choice of the two non-contractible loops is irrelevant, since given two operators $\hat{\chi}_j$ along the loop γ_x and another loop γ_x' parallel to the first, acting on the state $|\psi_0^B\rangle$, it is possible to use the identities on each plaquette to deform a loop into the other.

Comparing the toric case with the more general quantum double model we can see that in both cases it is possible to describe explicitly the ground states through the action of certain operators. Such state can be interpreted as a *loop gas*, although only states that can be described as products of one-plaquette states are present.
Nevertheless there are some important differences. In the toric case the $\hat{W}(\gamma)$ operators act as toggles. This is due to the fact that the operator $\hat{W}(\gamma)$ can be interpreted as $\hat{\chi}_1(\gamma)$, where χ_1 is the character of the non-trivial representation π_1, and that $\chi_1^2 = \chi_0$. Therefore applying two times the operators is equal to applying the trivial operator $\hat{\chi}_0$ which leaves the state invariant. In more general quantum double models applying two times any operator can lead to more general results. An example will be studied later.
Another difference is that in the toric case we were able to define the 't'Hooft loop operator $Z(\gamma^*)$ which allowed us to distinguish between states of different topological sectors. This operator is a product of the left(or right) regular representations of the

elements r along the dual path γ^*. This description does not allow us to easily generalize to different gauge groups. Since it is not needed for the numerical analysis, the search of an explicit expression of t'Hooft loop operators for finite group gauge theories is left to further development.

1.4 Phases and observables

The main aim of the study of gauge theories with a finite symmetry group is to understand the structure of its phase diagram, which determines the macroscopic behavior at different energy scales. In this sections we will show which are the interesting phases of the system and which are the observables that allow us to identify such phases. Before moving forward we need first to clarify which are the coordinates of the phase diagram, which correspond to the parameters of the Hamiltonian.

1.4.1 Parameterization of the Hamiltonian

The Hamiltonian of Yang-Mills theories assumes the form:

$$H = \lambda_E H_E + \lambda_B H_B \tag{1.163}$$

Since we are not interested in the absolute values of the energies, but only on the structure of the Hamiltonian it is useful to study the Hamiltonian

$$H = H_E + \lambda H_B \tag{1.164}$$

which differs from the previous only by a trivial multiplicative constant. This convention will be useful in the numerical calculations that we will perform later. In this case we study the Hamiltonian for $\lambda \in [0, +\infty)$. This substitution shows that we have only one meaningful parameter on which we need to study the system. It is possible to work with more complex models, with more parameters, for example by introducing the chemical potential μ.
An equivalent choice of parameterization, widely used in literature [17] is

$$H = gH_E + H_B \tag{1.165}$$

In this case the constant g multiplies the electric part. It is through this convention that the nomenclatures "strong-coupling phase" and "weak-coupling phase" are defined: the first corresponding to the case in which the electric term is stronger then the magnetic, while the latter to the opposite case.
Another convention that we will use is the compactified version:

$$H = (1 - \lambda_c)H_E + \lambda_c H_B \tag{1.166}$$

which has the nice property that it reduces to the purely electric Hamiltonian for $\lambda_c = 0$ and to the purely magnetic Hamiltonian for $\lambda_c = 1$, allowing us to describe all possible relative weights of the two parts with a single parameter on a finite interval $\lambda_c \in [0, 1]$.

1.4.2 Confinement

Now that we have defined where we are looking, we need to understand what we are looking for. The characteristic that differentiates the various phases of Yang-Mills theories is a property called confinement. Confinement is the phenomenon, typical in chromodynamics, in which particles cannot be isolated, and therefore cannot be directly observed in normal conditions. This happens when the attraction between particles doesn't decrease with the distance between them, requiring infinite energy to keep them apart.
In order to describe confinement in our theory we must introduce particles. We can do so by introducing the operators

$$\hat{\pi}^j_{mn}(\gamma) = \sum_{g_i \in G} \pi^j_{mn}(g_\gamma) \bigotimes_i \mathbb{P}_{g_i} \tag{1.167}$$

where γ is an open path, and the index i runs over all links in path γ. This operator can be applied on the electric vacuum to obtain states that violates the gauge invariant conditions at the two extreme points v_1, v_2 of the path γ. This loss of symmetry can be recovered if we recall that the gauge invariant condition serve to enforce charge conservation, therefore the state can be understood as the case in which two charged static particle from the matter field live on the two vertices. We can then calculate the energy of the interaction as the difference between the energy of the ground state vacuum and the energy of the ground state when the gauge conditions are violated at two points of the lattice. This energy, which is given as a function of the distance R between the two points is usually known as the static quark potential $V(R)$. If the system is confined it increases continuously at large values of R, while it stops growing if the system is not confined.

It is simple to see that in the electric dominated phase the difference in energy between the vacuum ground state and the static quark ground state is exactly $\Delta E(R) = Rf(j)$, since the lowest energy state in the latter case is the one in which the path γ connects the two points through the shortest path, giving a contribute $f(j)$ for each link traversed. This potential increases linearly with R, showing that in the strong-coupling regime the system is confined. The proportionality constant is called the string tension σ.
In the magnetic case the ground state with two static quarks is a superposition of all possible path between the two points, combined with all possible loops on the lattice. The energy of the magnetic Hamiltonian on such state is the same as the energy on the magnetic vacuum. Therefore the static quark potential $V(r)$ is always zero, and the

weak coupling phase is not confined.

Although it is possible to identify the phases through the calculations of the static quark potential there is a better alternative, through the study of an order parameter, which corresponds to the average value of a certain observable on the ground state. Due to Elitzur's theorem [15] the observable must be gauge invariant, otherwise it would have a vanishing expectation value, therefore a good candidate is the Wilson loop:

$$\langle \operatorname{tr} \hat{W}_\gamma \rangle_g = \langle 0_g | \operatorname{tr} \hat{W}_\gamma | 0_g \rangle \tag{1.168}$$

where $|0_g\rangle$ is the ground state for parameter g. It has been shown [17] that indeed the Wilson loop gives a good order parameter, which is able to feel the global changes of the system due to its non-local nature.

It is found that in the confined phase the expectation value follows the area law

$$\langle \operatorname{tr} \hat{W}_\gamma \rangle_g = constant \times e^{-\mu(g) A[\gamma]} \tag{1.169}$$

where $A[\gamma]$ is the area enclosed in the closed loop γ and μ is a function of g. If the Hamiltonian is purely electric the expectation value is zero, which means that if $g \to \infty$ than $\mu \to \infty$. At the transition point both the parameter μ and the string tension σ goes to zero, allowing us to identify the transition.

Instead in the deconfined phase the Wilson loop follows the perimeter law

$$\langle \operatorname{tr} \hat{W}_\gamma \rangle_g = constant \times e^{-\rho(g) P[\gamma]} \tag{1.170}$$

where $P[\gamma]$ is the length of the closed loop γ. In the extreme case, where $g = 0$, we have $\langle \operatorname{tr} \hat{W}_\gamma \rangle_{g=0} = \chi_F(e) = d_F$, showing that $\rho(g) \to 0$ for $g \to 0$.

Chapter 2

Abelian field theory

In this chapter we will focus on a subset of Yang-Mills theories where the gauge group is a finite abelian group on a periodic 2-dimensional lattice. These theories feature a number of simplifications, which can be used to create a more efficient quantum algorithm.
We will start the chapter by describing these features, and how they can be derived from the theoretical context described in the previous chapter. Then we will use these models to discuss the different ways in which this system can be implemented on a quantum device. In the last sections we will give a precise description of the implementation in two cases, the $\mathbb{Z}_2$ and $\mathbb{Z}_4$ models, and show the results.

2.1 Simplifications in the abelian case

2.1.1 Finite abelian groups

Finite abelian groups are remarkably easy to describe. Thanks to the fundamental theorem of finite abelian groups [27] every finite abelian group G can be expressed as the direct sum of cyclic subgroups of prime-power order, up to an isomorphism. A cyclic group of order n is always isomorphic to the additive group $\mathbb{Z}_n$ of integers modulo n. Therefore any finite abelian group can be written as

$$G \simeq \mathbb{Z}_{{p_1}^{m_1}} \times ... \times \mathbb{Z}_{{p_N}^{m_N}} \tag{2.1}$$

where p_j are primes and m_j are positive integers. The number of terms in this decomposition and the order of each group is uniquely determined by the group G.
Due to this decomposition we will focus mostly on cyclic groups in the following sections, keeping in mind that it is possible to generalize to all possible abelian groups by combining them appropriately.
All irreducible representations of any abelian group is 1-dimensional. Since for a finite group $\sum_j d_j^2 = |G|$ (as is shown in equation (A.5)), there are exactly $|G|$ irreducible representations for any group G. There is a single matrix element for each representation,

which can be denoted simply as $\pi^j(g)$, and it corresponds to the value of the irreducible character $\chi_j(g)$.
The unitarity of the representations requires that $\pi^{j*}(g) = \pi^j(g^{-1})$.

2.1.2 Lattice structures

Since the irreducible representations are one dimensional we can write each single link state in the representation basis as $|j\rangle = |j_{mn}\rangle$, where mn are both always 1. The group basis is still denoted with $|g\rangle$.

The vertex operators, which correspond to the gauge conditions defined in equation (1.60), are defined in terms of the left and right regular representations. Since all irreducible representations are one dimensional the regular representations are diagonal in the representation basis:

$$L_g = \bigoplus_j \pi^{j*}(g) \qquad R_g = \bigoplus_j \pi^j(g) \tag{2.2}$$

Therefore the representation basis diagonalizes all gauge conditions, and is the best basis to use in order to find the gauge invariant subspace.
Whenever two vertex operators defined with the same group element A_v^g and $A_{v'}^g$ are applied to two neighboring vertices the action on the link between is given by the product of the action of a left and right regular representation. Therefore we have:

$$L_g R_g \,|j\rangle = \pi^{j*}(g)\pi^j(g)\,|j\rangle = |j\rangle \tag{2.3}$$

which always leaves the state invariant. This fact can be easily seen also in the group basis:

$$L_g R_g \,|h\rangle = |ghg^{-1}\rangle = |h\rangle \tag{2.4}$$

due to the abelian nature of the group. Extending this property to the whole lattice we find that

$$\prod_v A_v^g = \mathbb{1} \tag{2.5}$$

since each link in a periodic lattice is acted upon twice from the two vertices it is connected to. This means that the gauge condition on one of the vertices is always trivial, since it can be expressed through the action of the other vertex operators.

Regarding character loop operators we can make two interesting considerations. The first one is that since all irreducible representations are one dimensional we can separate

the action on each link. For example for the one-plaquette states we have:

$$\hat{\chi}_j \left|0000\right\rangle = \frac{1}{|G|^2} \sum_{g_1 g_2 g_3 g_4} \chi_j(g_1 g_2 g_3^{-1} g_4^{-1}) \left|g_1 g_2 g_3 g_4\right\rangle \tag{2.6}$$

$$= \frac{1}{|G|^2} \sum_{g_1 g_2 g_3 g_4} \pi_j(g_1)\pi_j(g_2)\pi_j(g_3^{-1})\pi_j(g_4^{-1}) \left|g_1 g_2 g_3 g_4\right\rangle = \left|jjj^*j^*\right\rangle \tag{2.7}$$

where j^* is the state corresponding to the conjugate representation π^{j^*}.
The second is that when acting on two neighboring plaquettes the action on the central link is trivial. This can be seen using the conventions in figure 1.5:

$$\hat{\chi}_j(\gamma_1)\hat{\chi}_j(\gamma_2) \left|0_E\right\rangle = \frac{1}{\sqrt{|G|^7}} \sum_{\{g_i\}} \chi_j(g_1 g_2 g_3^{-1} g_4^{-1}) \chi_j(g_5 g_6 g_7^{-1} g_2^{-1}) \left|g_1 g_2 g_3 g_4 g_5 g_6 g_7\right\rangle \tag{2.8}$$

$$= \frac{1}{\sqrt{|G|^7}} \sum_{\{g_i\}} \pi_j(g_1)\pi_j(g_2)\pi_j(g_2^{-1})\pi_j(g_3^{-1})... \left|g_1 g_2 g_3 g_4 g_5 g_6 g_7\right\rangle \tag{2.9}$$

$$= \hat{\chi}_j(\gamma_3) \left|0_E\right\rangle \tag{2.10}$$

This means that each character operator described by contractible loop can be expressed as a product of one-plaquette operators.
If we apply a single plaquette character operator on each plaquette of a lattice with periodic boundary conditions we can see that on each link the action of the two adjacent plaquette cancels out, therefore we have

$$\prod_p \hat{\chi}_j(\gamma_p) = \mathbb{1} \tag{2.11}$$

where γ_p is the path along the p-th plaquette.

2.2 $\mathbb{Z}_N$ Yang-Mills theories

Since all other abelian groups are a direct sum of cyclic groups it is useful the develop explicitly the theory for $\mathbb{Z}_N$ groups.
Any cyclic group will be defined as

$$\mathbb{Z}_N := \{g | g = r^k \text{ and } k = 0, ..., N-1\} \tag{2.12}$$

where r is the generator of the group. The group basis can be written simply as $|k\rangle = |r^k\rangle$ on a single link, with $k = 0, ..., N-1$.
In this case the N irreducible representations are

$$\pi_j(r^k) = (\omega_N^j)^k = \omega_N^{jk} \qquad j = 0, ..., N-1 \tag{2.13}$$

where $\omega_N = \exp\{2\pi i/N\}$.
In particular we can see that for $j = 0$ we obtain the trivial representation $\pi^0(g) = 1\ \forall g$. The arbitrary representation π_F is usually chosen as π_1, which is always faithful for all N. The $\hat{u}$ operators used in the definition of the Wilson loop act on the group basis as

$$\hat{u}\,|k\rangle = \pi_1(r^k)\,|k\rangle = \omega_N^k\,|k\rangle \tag{2.14}$$

The group Fourier transform which allow us to change from the group basis to the representation basis is given by

$$|j\rangle = \sum_{k=0}^{N-1} \langle k|j\rangle\,|k\rangle = \frac{1}{\sqrt{N}} \sum_{k=0}^{N-1} \omega_N^{kj}\,|k\rangle \tag{2.15}$$

which is the well-known quantum Fourier transform.

2.2.1 Gauge invariant subspace

The remarkable feature of $\mathbb{Z}_N$ models is that it is possible to completely describe the gauge-invariant subspace of the theory. To prove this fact we will start by calculating the dimension of the gauge-invariant subspace, and then we will provide a base which contains all the possible states.
Since the $\mathbb{Z}_N$ group has only one generator, denoted r, the gauge conditions reduce to

$$A_v^r\,|\psi\rangle = |\psi\rangle \qquad \forall v \tag{2.16}$$

since all other restrictions can be traced back to it. Working in the representation basis, we can see the action on a single vertex becomes:

$$A_v^r\,|j_1 j_2 j_3 j_4\rangle = \omega_n^{j_1+j_2-j_3-j_4}\,|j_1 j_2 j_3 j_4\rangle \tag{2.17}$$

Therefore a state is gauge invariant if $j_1 + j_2 - j_3 - j_4 = (0 \mod N)$. This means that on any vertex we can choose three links arbitrarily, while the fourth link is forced by the invariance condition. Each condition reduces the space of states by a factor of $|G|$. This is true for all vertices except the last one. In this case we can use equation (2.5) to show that the action of the last operator is trivial, and doesn't add any constraints to the system. Since the dimension of the total Hilbert space is $|G|^L$ and we impose $V - 1$ constraints, where L is the number of links and V the number of vertices, the dimension of the gauge invariant Hilbert space is $|G|^{L-V+1}$.

In order to describe the gauge invariant subspace we can start by looking at a single plaquette. The character one-plaquette states are best suited since they can be easily

described in the representation basis. On a single plaquette there are N gauge invariant states, which we can write as

$$|\chi_j\rangle = \hat{\chi}_j(p)\,|0_E\rangle \tag{2.18}$$

Since on any element of the group we have that

$$\chi_{j_1}(r^k)\chi_{j_2}(r^k) = \omega_n^{(j_1+j_2)k} = \chi_{j_1+j_2}(r^k) \tag{2.19}$$

applying plaquette operators repeatedly leads to the useful identity

$$\hat{\chi}_{j_1}(p_1)\hat{\chi}_{j_2}(p_1)\,|0_E\rangle = \hat{\chi}_{j_1+j_2}(p_1)\,|0_E\rangle \tag{2.20}$$

The Wilson loop operator, which corresponds to $\hat{\chi}_1$, cycles through all the possible invariant states. We can then use its action multiple times to obtain all the one-plaquette invariant states:

$$|\chi_j\rangle = \hat{W}_\square^j\,|0_E\rangle \tag{2.21}$$

Another consequence of equation (2.20) is that we can easily find that the inverse of any $\hat{\chi}_j$ is $\hat{\chi}_{N-j}$, if we consider the sum as modulo N.
On the full lattice we can use these properties to write the set of one-plaquette states as

$$|\chi_{j_1}\cdots\chi_{j_M}\rangle = \prod_{p=1}^{M}\hat{W}^{j_p}(p)\,|0_E\rangle \tag{2.22}$$

There is an important issue with these states. If we write equation (2.11) in the case for $j = 1$ we find that the operators $\hat{W}(p)$ are not independent:

$$\prod_p \hat{\chi}_1(p) = \prod_p \hat{W}(p) = \mathbb{1} \tag{2.23}$$

We can then solve for one of the plaquette Wilson loop operator, as a function of all the others. Conventionally we choose the operator on plaquette M, which we call the M-th operator:

$$\hat{W}(M) = \prod_{p\neq M}\hat{W}^{-1}(p) \tag{2.24}$$

Substituting this identity in equation (2.22) gives us the identities:

$$|\chi_{j_1}\cdots\chi_{j_M}\rangle = |\chi_{j_1-j_M}\cdots\chi_{j_{M-1}-j_M}\chi_0\rangle \tag{2.25}$$

which show that some states in the previous description are described in multiple different ways. To remove this redundancy we can simply take the M-th plaquette to be in the

state of the trivial representation. Therefore, if we want to uniquely describe all one-plaquette states, we can use the set of states

$$|\chi_{j_1}\cdots\chi_{j_{M-1}}\rangle = \prod_{p=1}^{M-1} \hat{W}^{j_p}(p)\,|0_E\rangle \tag{2.26}$$

Due to the combinations between one-plaquette states in the abelian theory all combinations of contractible loops are also present in this set of states. We can just add the two non contractible loops to obtain all possible loops, which means introducing the Wilson loop operators along the two non contractible loops γ_x and γ_y, and obtain the following states:

$$|\chi_{j_1}\cdots\chi_{j_{M-1}};\chi_{j_x}\chi_{j_y}\rangle = \hat{W}^{j_x}(\gamma_x)\hat{W}^{j_y}(\gamma_y)\prod_{p=1}^{M-1} \hat{W}^{j_p}(p)\,|0_E\rangle \tag{2.27}$$

This set of states contains $|G|^{M+1}$ states. Since on a periodic lattice $M = V = L/2$ this is exactly the dimension of the gauge invariant subspace previously calculated. Therefore this is a basis of the gauge invariant subspace.
The values of j_x and j_y cannot change under an evolution of the system, since the Hamiltonian only contains local terms. Therefore we can identify different sectors, called topological sectors, that are not connected to each other, and simulate in only one of them at a time. The simplest case is $j_x = j_y = 0$, which is called the trivial sector.

2.2.2 Energy eigenvalues in the gauge invariant basis

It is useful to write the energy eigenvalues in the basis defined in (2.27).
The state on a single link is given by the two adjacent plaquettes and one of the non-contractible loops, if they pass through that link. The result is:

$$|j_l\rangle = |j_{p1} - j_{p2} + j_{x/y}\rangle \tag{2.28}$$

where $p1$ is the plaquette for which the loop passes through link l in the positive direction, $p2$ is the plaquette for which the link is traversed in the negative direction, and $j_{x/y}$ is the state of the non-contractible loop, if present. Recalling equation 1.54 we can calculate the single link electric eigenvalues as

$$h_E\,|j\rangle = f(j)\,|j\rangle = 4\sin^2\left(\frac{\pi j}{N}\right)|j\rangle \tag{2.29}$$

where we used $\Gamma = \{r, r^{-1}\}$, which is the smallest generating set closed under conjugation and inversion.
In $\mathbb{Z}_N$ groups the function f, which gives the single link electric eigenvalues, has two useful properties: it is symmetric ($f(j) = f(-j)$) and periodic $f(j+N) = f(j)$.

The electric eigenvalues on the total system can be obtained as the sum of the electric eigenvalues on each link. The result is:

$$H_E \left|\chi_{j_1}...\chi_{j_{M-1}}; \chi_{j_x}\chi_{j_y}\right\rangle = \sum_{<j_{p1},j_{p2}>} f(j_{p1} - j_{p2} + j_{x/y}) \left|\chi_{j_1}...\chi_{j_{M-1}}; \chi_{j_x}\chi_{j_y}\right\rangle \tag{2.30}$$

where the sum is over all neighboring plaquettes, except for links around the M plaquette, for which we have only one-plaquette contribute.

For the magnetic part of the Hamiltonian we notice that on a plaquette

$$\hat{W} \left|\chi_j\right\rangle = \hat{W}^{j+1} \left|0_E\right\rangle = \left|\chi_{j+1}\right\rangle \tag{2.31}$$

so that the one plaquette Wilson loop operator cycles through all the character states. We can take an Inverse Quantum Fourier transform on the first $M-1$ plaquettes in order to obtain a dual basis:

$$\left|q_1,...q_{M-1}; \chi_{j_x}\chi_{j_y}\right\rangle = \frac{1}{\sqrt{|G|^{M-1}}} \sum_{j_1,...j_{M-1}} \omega_N^{-i(j_1 q_1 + ... + j_{M-1} q_{M-1})} \left|\chi_{j_1}...\chi_{j_{M-1}}; \chi_{j_x}\chi_{j_y}\right\rangle \tag{2.32}$$

On this base the fist $M-1$ Wilson loops operators are diagonal and simple to calculate:

$$\hat{W}(p) \left|q_1,...q_{M-1}; \chi_{j_x}\chi_{j_y}\right\rangle = \omega_N^{q_p} \left|q_1,...q_{M-1}; \chi_{j_x}\chi_{j_y}\right\rangle \tag{2.33}$$

On plaquette M we need to use identity (2.24) first, which gives us the following eigenvalues:

$$\hat{W}(M) \left|q_1,...q_{M-1}; \chi_{j_x}\chi_{j_y}\right\rangle = \omega_N^{-\sum_{p\neq M} q_p} \left|q_1,...q_{M-1}; \chi_{j_x}\chi_{j_y}\right\rangle \tag{2.34}$$

In the Hamiltonian the contribution form any single plaquette is proportional to

$$-(\hat{W}(p) + \hat{W}^\dagger(p)) \tag{2.35}$$

The eigenvalues of such expression can be easily calculated for each plaquette as

$$-(\omega_N^{q_p} + \omega_N^{q_p *}) = -2\cos\left(\frac{2\pi q_p}{N}\right) = 4\sin^2(\frac{\pi q_p}{N}) - 2 \tag{2.36}$$

which is only a constant away from the form of the electric single link eigenvalues in (2.29). This symmetry between the electric and magnetic part is peculiar in $\mathbb{Z}_N$ theories, and can be used to simplify the implementation of the system, as we will see shortly.

2.3 Quantum simulations

The recent interest in the Hamiltonian formalism of quantum gauge theories has been caused by the advancement in quantum technologies, which promise a more efficient way to perform simulations.

Due to their simplicity $\mathbb{Z}_n$ models are an ideal testing ground for quantum computing implementations. This section will offer a general overview of quantum simulations, in order to understand how they can be used, their techniques and limitations.

2.3.1 Analog and digital quantum simulations

The scale of quantum systems grows exponentially with their size, therefore it becomes increasingly difficult to use them to gain insight in a reasonable amount of time. Therefore it has been proposed to use quantum systems to simulate other quantum systems [16], in a way that the resources needed for the simulations grow at the same rate of the complexity of the system.
The most direct way to perform this task is to create a similar system in the controlled environment of a laboratory. This can be done for example with ultracold quantum gasses, photons, and trapped ions [50, 35]. In all these cases the simulator is a quantum system where many different parameters can be tuned precisely, which can be used to manipulate the interactions between the components and other physical properties. This method is called analog simulation, and can be used to great results. The limit is that only certain systems lend themselves to be simulated this way, and for each of them the required architecture of the simulator can vary greatly.
Another way to perform quantum simulations is to use quantum computers, which consist of a general programmable quantum device. It is usually constructed out of a set of 2-level quantum systems, called qubits. The original system is mapped onto the quantum computer and all possible operations, such as the unitary evolution, are encoded into gates [38]. This sort of simulations is called digital. Using a quantum computer in order to program simulations has the advantage that any possible system can be simulated. It also allows the development of an universal language which can be used regardless of the specific construction of the computer.
Quantum computers can be used also for different applications, such as integer factorization, or search algorithms [38]. At the present time we are in the Noisy Intermediate-Scale Quantum(NISQ) era [43], which means that quantum computers are confined by their size and by the noise of each gate, which limits the number of subsequent calculations that can be performed reliably. In working with present day computers it is of interest to develop algorithms that work well even on NISQ devices.
Digital simulation is a powerful tool that can be used on many different systems, while keeping the overall architecture similar; in contrast analog simulation is a narrower tool, which requires a different implementation on a case by case basis, but is also more robust against noise and imperfections.
In the case of lattice gauge theories, there have recently been many proposals for the analog implementation of lattice gauge theories [9, 22, 39, 49], using ultra-cold atoms or trapped ions in a lattice to reproduce the interactions of the model. These schemes mostly focus on 1+1 dimensional systems, in the presence of fermionic matter. At the same time digital simulation has started to give its first results [33], using a four qubit quantum computer.
The focus of this thesis will be on digital simulations, which allows us to obtain more general results.

2.3.2 Simulating on a quantum computer

The procedure to develop any digital quantum simulation can be divided into three main steps: how to encode the system into the set of qubits, how to evolve the state, and how to connect the measures on the quantum computer to the observables of the system.
Since each qubit corresponds to a Hilbert space of dimension 2, a collection of n qubits, called the quantum register, can be used to describe a quantum system with dimension up to 2^n. Larger systems require a larger number of qubits, in order for their states to be mapped into the quantum register. Systems with a Hilbert space dimension equal to a power of 2 can be implemented more efficiently, since it is possible to map them one to one.
On each qubit it is possible to use the standard notations for two levels systems. The computational basis is $\{|0\rangle, |1\rangle\}$ and a tensor product can be used to obtain a basis for all states of the quantum computer.

The evolution of the system is performed through a series of gates. The simplest gates act on a single qubit and can be described as rotations:

$$R_j(\theta) = \exp\left(-i\frac{\theta}{2}\sigma_j\right) \tag{2.37}$$

where σ_j are the Pauli matrices. In general any unitary operation can be broken down to arbitrary accuracy through the action of the three rotations on all qubits and the $CNOT$ gate [55].
A key step in encoding complex evolutions in a series of gates can be obtained from the de Trotter formula[55]:

$$e^{i(A+B)t} = \lim_{n\to\infty}(e^{iAt/n}e^{iBt/n})^n \tag{2.38}$$

which allows to approximate the evolution of any system by breaking down the evolution of an Hamiltonian made of different non-commuting terms into the evolution of each term separately. Each of these terms can then be given a gate implementation separately, which is simpler than the one for the total Hamiltonian.
The most direct version of this decomposition is given by:

$$e^{i(A+B)\Delta t} = e^{iA\Delta t}e^{iB\Delta t} + \mathscr{O}(\Delta t^2) \tag{2.39}$$

An alternative expansion, which leads to more accurate results at a low computational cost, is the symmetrized version:

$$e^{i(A+B)\Delta t} = e^{iA\Delta t/2}e^{iB\Delta t}e^{iA\Delta t/2} + \mathscr{O}(\Delta t^3) \tag{2.40}$$

In order to perform a quantum measurement of any observable O, we need to first perform an unitary operation such that the eigenstates of operator O are mapped into

the computational basis. We can then perform a projective measurement on each qubit, in order to identify which eigenstate of the operator the state is in. The corresponding eigenvalue gives us the result of the measurement. Multiple measurements can be used in order to compute the average value $\langle O \rangle$ of an observable on a given state.

2.3.3 Simulating lattice gauge theories

There are different algorithms which can be used to obtain useful results for any physical system. In the case of pure lattice gauge theories we want to find the ground state for the Hamiltonian as the relative importance of the electric and magnetic Hamiltonian part changes.
The first algorithm we will look at is based on adiabatic evolution. This method allows us to find the ground state of a parametric Hamiltonian as the parameters change. We start by initializing the system in a ground state for one configuration of the parameters, then we evolve it while slowing changing the parameters and, if the change is slow enough, the final state is a ground state for the Hamiltonian at the final parameter configuration. We can then perform measurements to obtain any interesting observable on the system. Using the conventions in equation (1.164), in which

$$H = H_E + \lambda H_B \tag{2.41}$$

We can see that we can initialize the system in the electric ground state, which corresponds to parameter $\lambda = 0$, and is easy to implement. Then we can evolve it up to a certain value λ_{max} before taking measurements for the Wilson loops and other quantities. The main issue of this method is that the number of gates which needs to be implemented grows with the value of λ_{max}, which means that we need a high fidelity device, in order to obtain meaningful results for higher values of λ_{max}. Although such devices don't exist at the present day, it is still interesting to develop the theory behind this simulations.

An alternative, which has been developed to work on NISQ hardware, is the Variational Quantum Eigensolver (VQE), which consists of an hybrid quantum and classical algorithm [34, 41]. In the VQE a quantum algorithm is used to calculate the average value of an Hamiltonian on any state. This results are used by a classical algorithm in order to improve an ansatz for the ground state. The procedure is repeated multiple times in order to obtain a good enough approximation of the ground state.

2.3.4 Real quantum computers and their simulations

Although there are already some openly available quantum computers, they are still limited by performance, number of qubits and infrastructure, since on many public quantum computers not all qubits are connected directly, which greatly hinders how they can be

used. Nevertheless programs have been developed in order to reproduce the results of quantum computers with classical computations. An example is the qiskit language [6], developed as a python extension, which we will use in the following part of the thesis. Using these languages allows us to test the algorithms and prepares us for applications with real quantum computers in the future.
There are some important differences between a real quantum computer and their classical simulations. Recognizing these differences allows us to be more efficient with our computations and produce better results.
The first difference is that since the Hilbert space grows exponentially with the number of qubits any classical simulation is exponentially hard. Consequently we can only use classical simulations for relatively small systems.
Another main difference is that while quantum measurements are destructive, their classical counterpart is not. This can be used extremely well in the simulation of the adiabatic algorithm where, instead of starting over after each measurement of the system at λ_{max}, we can instead save the wave function, take the measurement and then move on to the next chosen value.
Although in the long run the hope is for quantum algorithms to assert their dominance and produce efficient results on larger and more interesting systems, we can start to probe the quantum computing techniques for lattice gauge theories, and understand how they work.

2.4 Implementation for $\mathbb{Z}_N$ theories

It is now time to show how to implement a simulation of a $\mathbb{Z}_N$ theory on a quantum computer. We will work directly in the gauge invariant subspace, and in a fixed topological sector, using the bases:

$$|\chi_{j_1}\cdots\chi_{j_{M-1}};\chi_{j_x}\chi_{j_y}\rangle \tag{2.42}$$

$$|q_1,\ldots q_{M-1};\chi_{j_x}\chi_{j_y}\rangle \tag{2.43}$$

We will focus on cyclic groups with order N equal to a power of 2, which allows us to achieve an efficient simulation and simpler implementation in gates.
Each of the $M-1$ plaquettes corresponds to a N dimensional Hilbert space, while the total invariant subspace can be represented as a tensor product, of dimension N^{M-1}. We can map each plaquette into a set of n qubits, such that $N=2^n$.
Working in the character basis, on each plaquette the N states are identified by $j_p = [0, N-1]$, and can be mapped into n qubits. This map is simply the base 2 representation of j_p:

$$|j_p\rangle = |(j_p)_2\rangle \tag{2.44}$$

In particular the state associated with the trivial representation $j_p = 0$ is mapped into the state $|0\rangle^{\otimes n}$. Which means that the electric ground state is:

$$|0_E\rangle = |0\rangle^{\otimes N_q} \tag{2.45}$$

where $N_q = n(M-1)$ is the total number of qubits necessary for the simulation. This is the state in which we initialize our system for the adiabatic algorithm.

For the evolution we notice that the Hamiltonian is composed of two non-commuting parts: the electric Hamiltonian H_E and the magnetic Hamiltonian H_B. We can then use the symmetric Trotter formula to decompose the evolution as:

$$U(\Delta t) \approx \prod_{t_i} e^{-iH_E \frac{\Delta t}{2}} e^{+i\lambda(t_i) H_B \Delta t} e^{-iH_E \frac{\Delta t}{2}} \tag{2.46}$$

where t_i is the initial time at each step and Δt is the time interval of each step. In principle there is no difference in placing the electric or the magnetic as the external term in this approximation. Nevertheless, since in our case the electric part does not depend on the parameter λ, it is convenient to put it as the outside term. This allows us to combine the last term of each step with the first term of the next step, using a single set of gates with parameter Δt instead of 2 sets with parameter $\Delta t/2$, greatly reducing the depth of the algorithm.
We are now left to describe the evolution of the two separate parts. In both cases such evolution is simpler if we can work in a basis in which they are diagonal. In the case of the electric part the correct basis is the character basis, described in equation (2.42), while for the magnetic part it is better to use the group plaquette basis, described in equation (2.43). The connection between the 2 basis can be implemented by a quantum Fourier transform on each set of qubits representing the $M-1$ plaquettes.

For the electric part the contribution of each link to the evolution can be determined by the configuration of the two adjacent plaquettes. The single link eigenvalues are:

$$h_E \, |\chi_{j_1} \chi_{j_2}\rangle = f(j_1 - j_2) \, |\chi_{j_1} \chi_{j_2}\rangle \tag{2.47}$$

The states are encoded in the quantum register as binary numbers:

$$|\chi_{j_1} \chi_{j_2}\rangle = |j_1, j_2\rangle \tag{2.48}$$

Therefore we can encode the evolution starting with a gate that makes the difference between the two states

$$M_{12} \, |j_1, j_2\rangle = |j_1, j_2 - j_1\rangle \tag{2.49}$$

Then we can use a single plaquette gate U_1, which depends on the group we wish to simulate, to evolve the state:

$$U_1(\Delta t) \, |j\rangle = e^{-if(j)\Delta t} \, |j\rangle \tag{2.50}$$

which, if applied to the plaquette in state $|j_2 - j_1\rangle$, gives the correct evolution.
In the end we use a summing gate S_{12}, defined as:

$$S_{12} |j_1, j_2\rangle = |j_1, j_2 + j_1\rangle \tag{2.51}$$

Applying these gates in succession allows us to reconstruct the correct phase attained by evolution on the original state, as can be seen by the composition:

$$S_{12} U_1(\Delta t) M_{12} |j_1, j_2\rangle = e^{-if(j_1 - j_2)\Delta t} |j_1, j_2\rangle \tag{2.52}$$

These 3 operations can be collected into a single gate, which represents the single link evolution. We call this gate U_{ab}, where a and b are the two plaquettes it act on.
Applying this evolution on all couples of plaquettes allows us to reconstruct the total electric evolution. We need to take care that for the four links adjacent to the M-th plaquette, the state is defined by only one of the plaquettes. We can therefore implement their evolution directly with the U_1 gate, without the need of the summing or subtracting gates.
For the implementation of the magnetic evolution we start by using a set of unitary gates that bring us in the basis in equation (2.43), where the magnetic part is diagonal. We can then implement directly the evolution on each of the $M - 1$ plaquettes using the U_1 gates:

$$U_1(\Delta t) |q\rangle = e^{-if(q)\Delta t} |q\rangle \tag{2.53}$$

taking advantage of the symmetry between single link electric eigenvalues and single plaquette magnetic eigenvalues. For the last plaquette we can reconstruct evolution using a total sum circuit:

$$S_{TOT} |q_1, ..., q_{M-1}\rangle = |q_1, ..., \sum_{p=1}^{M-1} q_p\rangle \tag{2.54}$$

and then apply the inverse U_1 gate to the qubits representing $M - 1$ plaquette.

After completing the evolution the only step left to perform is the measurements. We take 3 types of measurements: electric Hamiltonian, magnetic Hamiltonian, and Wilson loops of varying length.
For the electric Hamiltonian we can work in the plaquette character basis directly. If the ground state, obtained at time t_m through the adiabatic evolution, is $|\psi(t_m)\rangle$ we can decompose it on the computational base as

$$|\psi(t_m)\rangle = \sum_{j_1,...,j_{M-1}} c_{j_1,...,j_{M-1}} |\chi_{j_1} \cdots \chi_{j_{M-1}}; \chi_0 \chi_0\rangle \tag{2.55}$$

We can calculate the expected value as:

$$\langle H_E \rangle = \sum_{j_1,\ldots,j_{M-1}} H_{Ej_1,\ldots,j_{M-1}} |c_{j_1,\ldots,j_{M-1}}|^2 \qquad H_{Ej_1,\ldots,j_{M-1}} = \sum_{<j_{p1},j_{p2}>} f(j_{p1} - j_{p2}) \quad (2.56)$$

The other two measurements are better performed in the dual basis, in which the wave function can be decomposed as:

$$|\psi(t_m)\rangle = \sum_{q_1,\ldots,q_{M-1}} c_{q_1,\ldots,q_{M-1}} |q_1, \ldots q_{M-1}; \chi_0\chi_0\rangle \quad (2.57)$$

The expectation value of the magnetic energy is

$$\langle H_B \rangle = \sum_{q_1,\ldots,q_{M-1}} H_{Bq_1,\ldots,q_{M-1}} |c_{q_1,\ldots,q_{M-1}}|^2 \quad (2.58)$$

$$H_{Bq_1,\ldots,q_{M-1}} = \left(\sum_{p=1}^{M-1} 4\sin^2\left(\frac{\pi q_p}{N}\right) - 2 \right) + 4\sin^2\left(-\frac{\pi \sum_{p=1}^{M-1} q_p}{N} \right) - 2 \quad (2.59)$$

The expectation value for any Wilson loop on a closed loop γ is:

$$\left\langle \hat{W}(\gamma) \right\rangle = \sum_{q_1,\ldots,q_{M-1}} \left(\sum_{p\in\gamma} \omega_N^{q_p} \right) |c_{q_1,\ldots,q_{M-1}}|^2 \quad (2.60)$$

where the sum is over the plaquettes inside the closed loop γ.

2.4.1 Example: 2x2 lattice for $\mathbb{Z}_2$ and $\mathbb{Z}_4$

In this section we will show the circuitry for the two cases on which we will perform simulations. The main difference between the two is the U_1 gate, and the fact that for $\mathbb{Z}_2$ we have one qubit for each plaquette, while for $\mathbb{Z}_4$ we have 2.
We show the case for a 2x2 lattice, since it can be displayed in a smaller space, while using comments to explain how it can be generalized, whenever it is not intuitive.
In this case we will need to describe 3 plaquettes, while the state of the fourth will be given implicitly from the states of other plaquettes. We use the conventions in figure 2.1

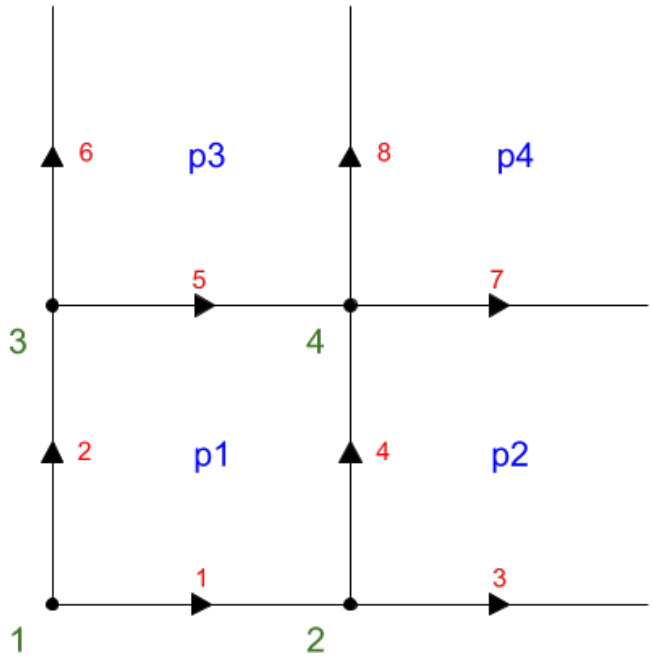

Figure 2.1: Conventions for the 2x2 lattice used in the examples of the quantum circuit. Plaquette $p4$ is chosen as the M-th plaquette, which is not mapped in any set of qubits.

We evolve the state from $\lambda_0 = 0$ at time τ_0 to λ_{max} at time τ_{max} taking N_s steps. For each step the evolution $U(\tau_1, \tau_2)$ is divided in N_Δ substeps. At the end of each step we save the wave function and calculate the measurements.
Using the previous notions we know that we can combine the last electric evolution of each substep with the first of the next. This is true except for the first and last substep. The evolution of each step U_s can be broken down as

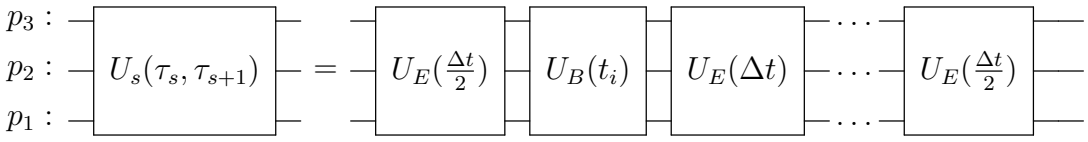

where we repeat the couple of gates $U_B(t_i)$ and $U_E(\Delta t)$ for N_Δ times, with t_i starting from τ_s and increasing at each step. Each line in this circuit represents the set of qubits which describes one of the $M-1$ plaquettes.
For $U_E(\Delta t)$ we notice that in a 2x2 periodic lattice we have four links around the $M-th$ plaquette for which the state is described by only one of the plaquettes, while for the other four links we need to create operators which act on couples of plaquettes. Each $U_E(\Delta t)$ can be represented as

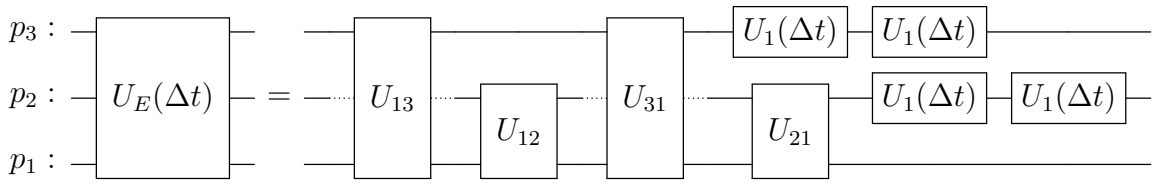

where each 2-plaquette operator U_{ab} can be broken down further as

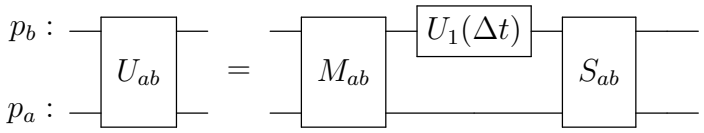

The implementation of the sum and difference gates is described in a general way in [12], while the explicit form they take in the case of the $\mathbb{Z}_2$ and $\mathbb{Z}_4$ algorithms is found in appendix B.

In a larger lattice we would still have 4 links around the M-th plaquette, whose evolution can be implemented directly by a U_1 gate. The other $L-4$ links are instead implemented through U_{ab} gates.
In a 2x2 lattice we have a particular circumstance, in which two U_{ab} gates representing different links act on the same couple of plaquettes. For example link 2 and 4 are both described by the couple of plaquettes p_1 and p_2. Since the action of U_{ab} is symmetric on the plaquettes it acts upon, we can combine the two gates into one, reducing the number of gates required for the simulation. Nevertheless this is only a special case; it can be easily seen that for larger lattices each link is described by a different couple of plaquettes, requiring one gate for each link.

For the magnetic evolution we instead use the following circuit:

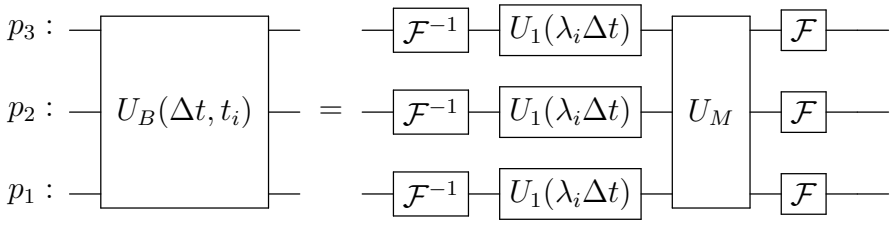

where we start by taking an inverse Fourier transform on each plaquette, followed by the evolution of each plaquette. The value λ_i is the value of λ at time t_i. We then perform the evolution on the M-th plaquette U_M, followed by a set of Fourier transform gates which bring us back to the character plaquette basis. The gate U_M can be expanded

further as:

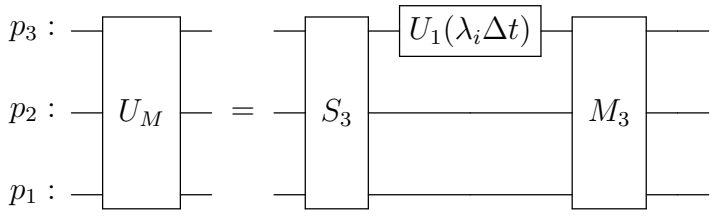

The gate U_1 needs to encode the evolution on a single link, or equivalently on a single plaquette. In the $\mathbb{Z}_2$ case the electric eigenvalues are

$$f(j) = 4\sin^2\left(\frac{\pi j}{2}\right) \tag{2.61}$$

As previously stated it is useful to use a new set of eigenvalues, shifted by a constant. This new set of eigenvalues translates to a global phase in the evolution, which doesn't affect the final measurements. We call these new eigenvalues $\tilde{f}$ defined as:

$$\tilde{f}(j) = f(j) - 2 \tag{2.62}$$

which take the values

$$\tilde{f}(0) = -2, \tilde{f}(1) = 2 \tag{2.63}$$

The single link electric Hamiltonian becomes proportional to the Pauli matrix σ_z, and the evolution is encoded by a rotation around the $z - axis$:

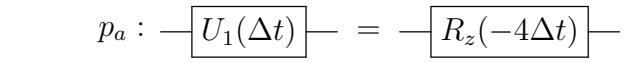

where $R_z(\theta) = \exp\left(-i\sigma_z \frac{\theta}{2}\right)$ is a fundamental gate.

j	0	1	2	3
$\|j\rangle$	$\|00\rangle$	$\|01\rangle$	$\|10\rangle$	$\|11\rangle$
$\tilde{f}(j)$	-2	0	2	0

Table 2.1: Conventions for encoding states into the computational basis for a $\mathbb{Z}_4$ model, and eigenvalues connected to each state.

In the case of the $\mathbb{Z}_4$ groups the shifted eigenvalues are given by

$$\tilde{f}(j) = f(j) - 2 = 4\sin^2\left(\frac{\pi j}{4}\right) - 2 \tag{2.64}$$

These values are shown in table 2.1. In the same table we also show that the four states are encoded in a binary base $|j\rangle = |q_1 q_0\rangle$. On this base it is possible to construct the Hamiltonian with the correct eigenvalues using Pauli matrices:

$$h_E = -\sigma_z^1 - \sigma_z^1 \sigma_z^0 \tag{2.65}$$

where the superscript identify on which qubit it acts. The first term can be performed simply by a rotation on qubit 1, while for the second we need to use a couple of $CNOT$ gates, whose description is found in appendix B. The circuit of the U_1 gate becomes

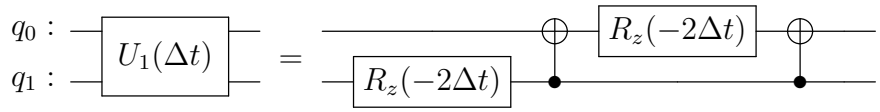

2.5 Results

In order to perform the simulation we use a $PYTHON$ code, taking advantage of the qiskit package in order to encode the various operations. The important parameters of the simulations are the size of the system, described by the number of plaquettes M, the time increment Δt and the total number of substeps N_{tot}. Finding the correct balance between the last two is the key to obtain an efficient code. If we use a smaller Δt we reduce the error in the Trotterization; nevertheless by reducing it we also give less time for the system to evolve, and lose the adiabatic hypothesis. The solution is to increase the number of steps, which allows the system enough time to fully evolve into the new ground state. The cost of this process is an increase in the length of the simulation.
Using instead larger Δt and less steps improves the speed of the simulations, but introduces larger errors in the Trotterization, which can hinder the quality of the results.
It is possible to recognize if the parameters are wrong by analyzing the value of the ground state energy in the simulation, by looking for pathological behaviors or by confronting it with the theoretical results we have for the extreme cases of a system dominated by the electric or magnetic term. In case a diverging behavior is found we can use these observations to distinguish if the problem is the adiabatic evolution, which can be corrected with larger Δt or more steps, or if it is a Trotterization problem, which can be resolved with smaller Δt.
In the first case the state doesn't evolve fully, therefore the ground state energy in the magnetic limit tends to be different from its correct value. In the second case we have the excitation of non ground states, causing a rapid oscillation in the energies.

We analyze the system with λ going from 0 to λ_{max}. The latter needs to be high enough to approach the magnetic dominated regime. Nevertheless we cannot raise it too much otherwise the simulations become too long. The compromise leads us to chose $\lambda_{max} = 5$.
In order to get a better representation, all final results are mapped such that they are in accordance to the conventions in the compactified version of the Hamiltonian (1.166). We can confront the two:

$$H_1 = H_E + \lambda H_B \tag{2.66}$$

$$H_2 = (1 - \lambda_c) H_E + \lambda_c H_B \tag{2.67}$$

and find that we can transform from one to the other by setting

$$H_2 = (1 - \lambda_c) H_1 \tag{2.68}$$

$$\lambda = \frac{\lambda_c}{1 - \lambda_c} \Rightarrow \lambda_c = \frac{\lambda}{1 + \lambda} \in [0, 1] \tag{2.69}$$

2.5.1 Results for $\mathbb{Z}_2$

In the $\mathbb{Z}_2$ model each of the $M - 1$ plaquettes used to describe the system is mapped into a single qubit. The first parameter that we need to fix is the size of the system, which we try to make as large as possible in order to better represent the adiabatic limit. The limiting factor is the computational power required to perform the calculation in a reasonable time, and the *RAM* space required to work on the results. Using a computer equipped with an Intel(R) Core(TM) i7(2.80GHz) and 16 GB RAM, we find that the maximum size we can achieve is a 4x4 lattice, which requires $M - 1 = 15$ qubits, and takes around 10 minutes per run. The next step, a 5x5 lattice, would require $M - 1 = 24$ qubits. This implies that the Hilbert space grows by a factor $2^9 = 512$. Since the number of operations grows at least linearly with the dimension of the Hilbert space each run would take at least 1 week. Larger lattices cannot be simulated using a qiskit code since the software is limited to simulate up to 24 qubits.

We now need to find the parameters for the evolution of the system. We first chose the interval $\lambda \in [0, \lambda_{max}]$ which we want to analyze. Our choice, allowing us to probe an interesting region, is $\lambda_{max} = 5$. It corresponds to a value of the compactified parameter $\lambda_c \in [0, 0.83]$. We then choose the number of measurements that we want to take, which we set to $N_s = 50$. We are left with the need to fix the number of substeps N_{tot} and the time Δt by which the system is evolved after each substep. Since we need to take at least N_s stops we can start by setting $N_{tot} = N_s$. We then work on Δt, starting from a low value, for which the system doesn't evolve, and increase it until changes are visible. The result at this stage is a noisy behavior around the expected outcome, due to large errors in the Trotterization with a small number of substeps. We can then increase N_{tot} until this effect becomes negligible. We can double check that we obtained the best parameters by varying them around the final point.
For the 4x4 system we find $N_{tot} = 1000$ and $\Delta t = 0.05$.

The first quantity we look at is the expected value for the total electric energy $\langle (1 - \lambda_c) H_E \rangle$, the total magnetic energy $\langle \lambda_c H_B \rangle$, and the total energy $\langle H \rangle$, which can be obtained as the sum of the two parts. In order to make these results independent on the size of the system we divide all values by the number of plaquettes M. The results are shown in figure 2.2.

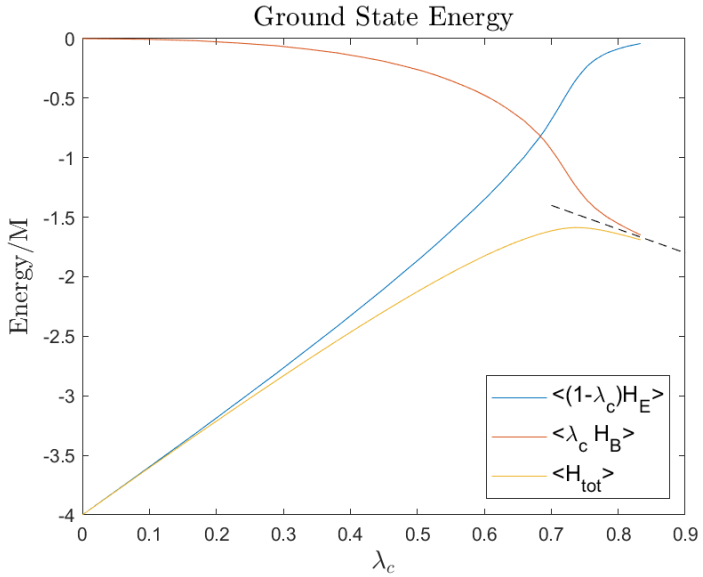

Figure 2.2: Energy measurements in a $\mathbb{Z}_2$ simulation on a 4x4 lattice, with electric and magnetic part separated. All measures are normalized by the size $M = 16$ of the system. The dashed line shows the expected behavior near the magnetic limit.

As expected at $\lambda_c = 0$ the system is in the electric ground state. The total energy is the sum of the single links electric energy, which with our convention is -2 for each link. The total energy is $-2L = -64$, while the energy per plaquette is $-2L/M = -4$. In the magnetic limit the total energy corresponds to the magnetic energy on the magnetic ground state, which is -2 for each plaquette, for a total of $-2M = -32$. Since we cannot reach the magnetic limit, which would require an evolution up to $\lambda = +\infty$, we cannot compare the values we obtained directly. We need to confront them with the behavior near the limit instead. In order to so we notice that near the magnetic limit the total energy is $\langle H_{tot} \rangle \approx -\lambda_c \langle H_B \rangle$, and the magnetic energy is $\langle H_B \rangle \approx -2M$. The behavior for the total energy per plaquette is therefore $\langle H_{tot} \rangle / M \approx -2\lambda_c$, which is represented as a dashed line in the previous graph. The results we obtained are in accordance with this model as can be seen in the picture. This fact, combined with the absence of undulating behaviors, verifies that the choice of parameters for the simulation is sufficient for obtaining correct results.
By looking at the energies we find that in the region with λ_c small the total energy is mostly determined by the electric contribution, while for λ_c large it is mostly determined by the magnetic part. There is an intermediate region in which the dominating factor switches from one case to the other. This region, around $\lambda_c = 0.7$ is a sign of the phase transition.

In order to better characterize the phase transition we can look at the behavior of

the Wilson loops $\langle W_\gamma(\lambda_c)\rangle$. There are various choices for the Wilson loops that we can analyze. We will focus on 9 loops, which are shown in figure 2.3.

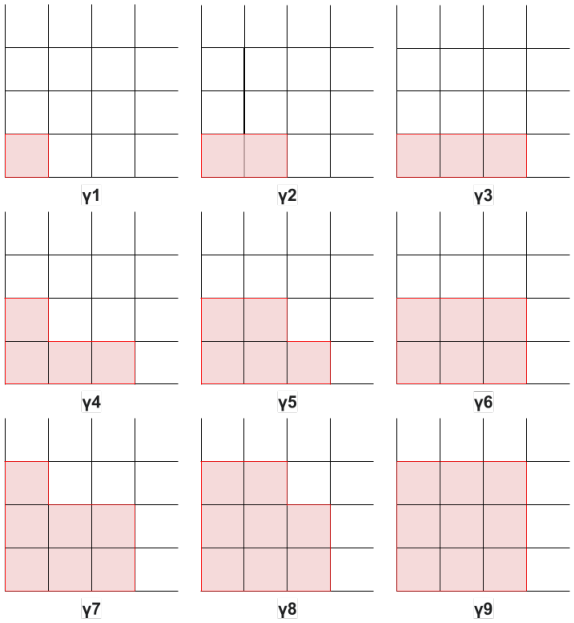

Figure 2.3: The 9 loops we analyze. The loops grow horizontally first and vertically second.

The first analysis we will perform on such quantities is to fix one of the loops and look at its expected value as a function of λ_c. The results are shown in figure 2.4.

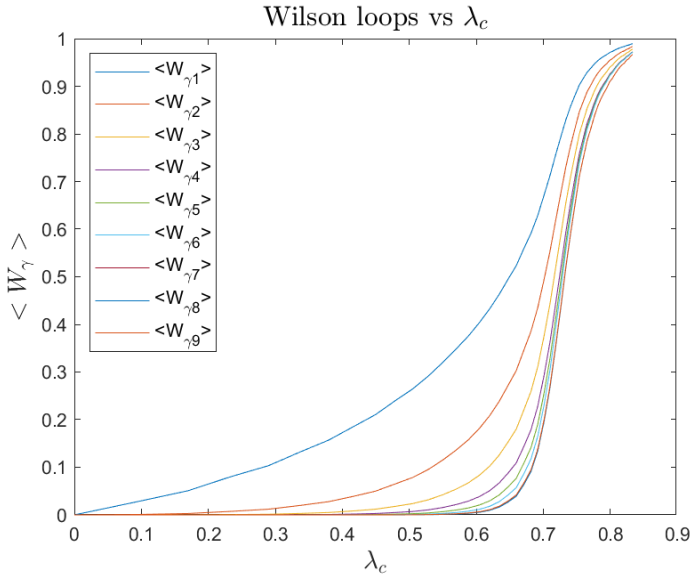

Figure 2.4: Expectation values of the nine Wilson loops we analyzed, as a function of the coupling parameter λ_c

As we can see each Wilson loop has zero expectation value in the purely electric limit. It then grows slowly as the increase in the magnetic contribution to the total Hamiltonian introduces excitations of the Wilson loops expectation values. This increase becomes sharp in the region around $\lambda_c = 0.7$, after which all Wilson loops tend to their limit in the purely magnetic Hamiltonian, which is $\langle W_\gamma(\lambda_c)\rangle = 1$. We can therefore identify three regions: the electric dominated region in which loop excitations are suppressed, indicating a confined phase, the transition region in which the expectation value of Wilson loops rapidly change, and the magnetic dominated region, in which we find loop excitations of any size.
It is interesting to notice how the size of the loop affects its expectation value. We can see from the graph that larger loops always have lower expectation values than their smaller counterparts. This effect is particularly strong in the confined region, with low λ_c, where large excitations are suppressed.
As a consequence large loops show a sharper change in the transition region, and are better indicators of its position. This effect can be understood by the fact that larger loops are dependent on larger regions of the system, and are better equipped to detect the macroscopic changes in the system.

Another useful analysis that we can perform using the Wilson loops is a direct inspection of the area law and perimeter law. The area law is

$$\langle \mathrm{tr}\, \hat{W}_\gamma \rangle_{\lambda_c} = constant \times e^{-\mu(\lambda_c)A[\gamma]} \tag{2.70}$$

and should describe the behavior of the system in the confined phase.
The perimeter law is instead

$$\langle \mathrm{tr}\, \hat{W}_\gamma \rangle_{\lambda_c} = constant \times e^{-\rho(\lambda_c) P[\gamma]} \tag{2.71}$$

and should give a better description in the deconfined phase.
In order to perform this analysis we start by calculating area $A[\gamma]$ and perimeter $P[\gamma]$ of each of the 9 analyzed loops. For the perimeters this is simple. For the areas we need more care, since due to periodic boundary conditions every close loop can be seen as enclosing two different sections of the lattice, with different areas. When dealing with the area law each loop gains two contributes to its expectation values, one for each of the two sections of the lattice it encloses. Since the contribution for the smaller of the two areas dominates the other one, whenever we calculate the area of a loop we consider the smaller of the two possible areas.
Out of the 9 loops we used in our analysis we can see that for $\gamma_1, ...\gamma_8$ the colored area in figure 2.3 is the smaller of the two. For γ_9 the colored area has value 9 while the non colored area has value 7. Therefore we need to consider γ_9 as a loop with area 7.
We can plot the Wilson loops as a function of area and perimeter, obtaining the results in figure 2.5.

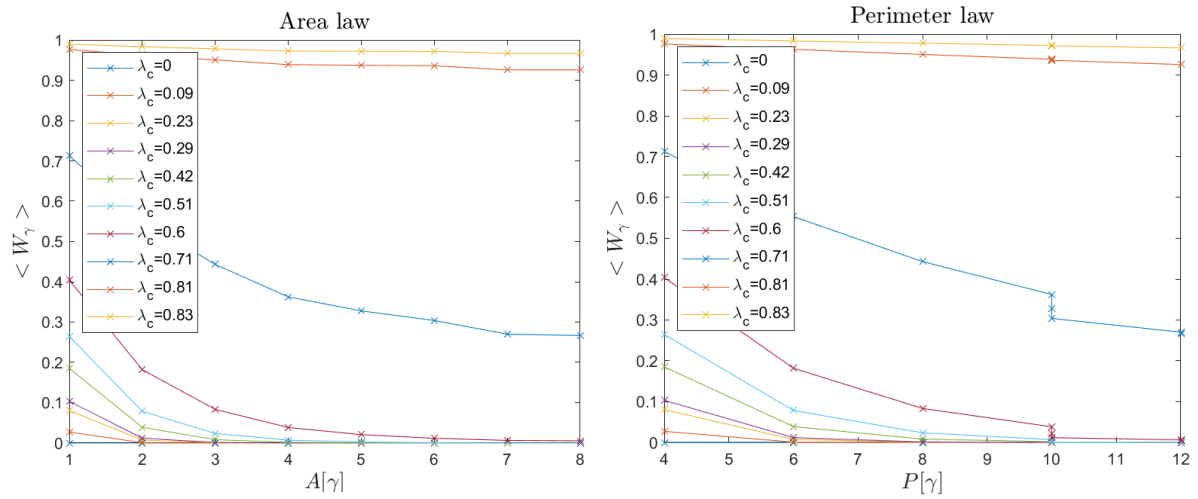

(a) (b)

Figure 2.5: Area law (a) and perimeter law (b) for Wilson loops of varying length at different values of λ_c. The sample values of λ_c are chosen out of the $Ns = 50$ measurements we performed to be evenly spaced across the studied region.

We can recognize two different behaviors in the previous graphs: if λ_c is small we have a rapid decrease in the expectation values of Wilson loops as their size increase,

as can be expected for a confined phase. For large values of λ_c we have instead a slow decrease. For values of λ_c in the transition region we have a rapid change from one case to the other, with intermediate expectation values, as can be seen for $\lambda_c = 0.71$.
Since the expected behavior in at least one of the two cases is an exponential it is interesting to look at the logarithms of the values. This operation cannot be performed with $\lambda_c = 0$, since in that case the expected values of the Wilson loops is $\langle W_\gamma(\lambda_c)\rangle = 0$, for which we cannot take the logarithm. The results are shown in figure 2.6.

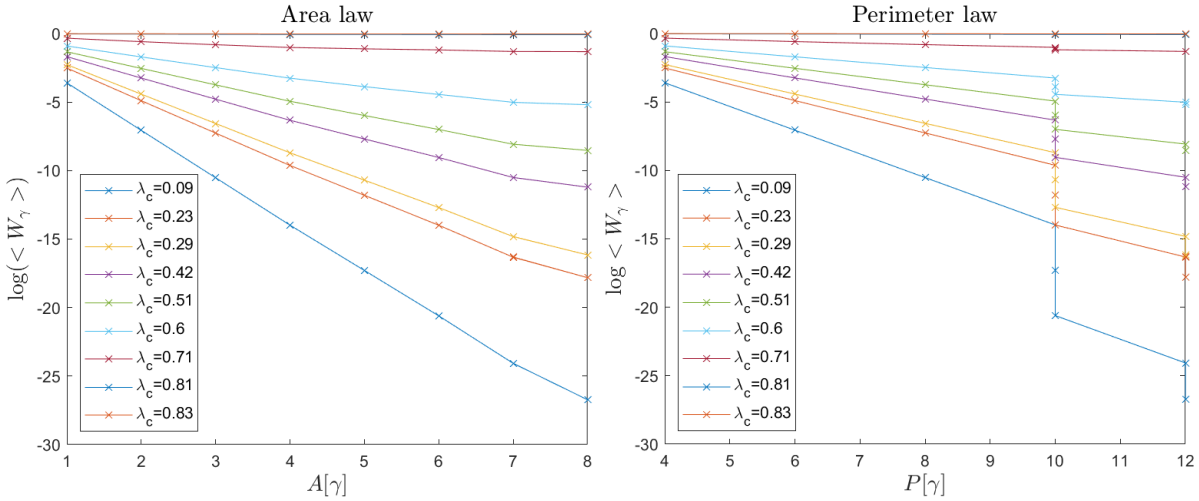

(a) (b)

Figure 2.6: Area law (a) and perimeter law (b) in logarithmic scale for Wilson loops of varying length at different values of λ_c.

In these graphs we can see that for low λ_c the area law assumes almost a linear relation. The exception are the results for the loop with area 8 which show values greater then we expected. This can be understood by the fact that a loop with area 8 in a lattice with $M = 16$ plaquettes gains two equal non-negligible contributions to its expected value, one for each of the two sections with area 8 it encloses, instead of a meaningful and a negligible one like the other loops.
In the perimeter law graph we find a discontinuous behavior. This effected is caused by having multiple loops with the same perimeter, but with different areas. In the confined phase the perimeter law is not followed, therefore this effect can be expected. Nevertheless the same effect is present also for high values of λ_c, even if of a lower magnitude. In that case it can be caused by a finite size effect, due to the small size of our system.

In order to find the parameters of the two laws, μ and ρ, we perform a linear least

square fit using the two following linearized relations:

$$\log \frac{\langle W_\gamma(\lambda_c)\rangle}{\langle W_{\gamma_1}(\lambda_c)\rangle} = -\mu(\lambda_c)\,(A[\gamma] - A[\gamma_1]) \tag{2.72}$$

$$\log \frac{\langle W_\gamma(\lambda_c)\rangle}{\langle W_{\gamma_1}(\lambda_c)\rangle} = -\rho(\lambda_c)\,(P[\gamma] - P[\gamma_1]) \tag{2.73}$$

where we used the measure on the one plaquette Wilson loop to eliminate the dependency on the constants.
The method we used for obtaining the values on which we perform the fit doesn't allow a way to estimate the confidence interval of each point, therefore we assume unitary errors, which translate in the fit procedure as an equal weight for all measures.
For the fits of the area law we don't use the loop γ_8, which would introduce a systematic error due to its double excitation. For the perimeter law we can instead use all the data points.
The results for the two fits are shown in figure 2.7.

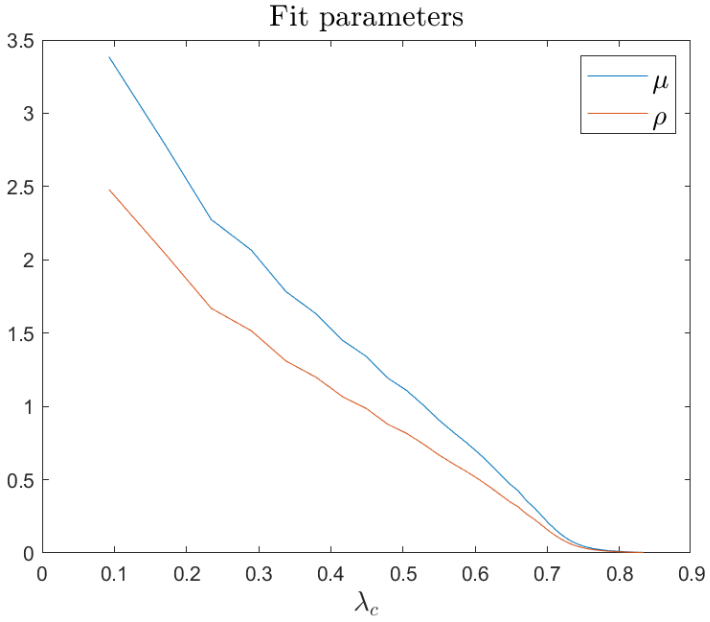

Figure 2.7: Parameter μ of the area law and parameter ρ of the perimeter law, as a function of the parameter λ_c. Results are obtained through a least square fit on the linearized relationship in equations (2.72) and (2.73)

As we can see the values for μ is larger then ρ in the confined phase. They then decrease more rapidly in the transition region and are almost equal thereafter.
It might seem counter-intuitive that the parameter ρ doesn't dominate the other in the

deconfined phase. This effect can be explained by the small size of our system. We can show this by considering what would happen in a larger lattice. For a square loop whose side has length L_x the area is L_x^2, while the perimeter is $4L_x$. The scaling factors in the area and perimeter laws becomes respectively $e^{-\mu L_x^2}$ and $e^{-\rho 4 L_x}$.
Therefore we can expect a surpass of ρ only for loops with $L_x > 4$ where the quadratic term becomes more influential than the coefficient 4. This system would require at least the possibility to measure loops of area 16, which requires at least $M = 32$ plaquettes. This can be attained in a 6x6 or larger lattice.
In order to find which of the two fits better describes the system in the two regions we can look at the χ^2 of the fits. Since we assumed unitary errors the value of the χ^2 is not a reliable parameter for the goodness of the fit. Nevertheless it is well positioned to understand which of the two laws is a better description at a fixed value of λ_c. In order to confront the two results we use the χ^2 normalized with respect to the number of degrees of freedom, which is 7 for the area law fit and 8 for the perimeter law. The results are shown in figure 2.8.

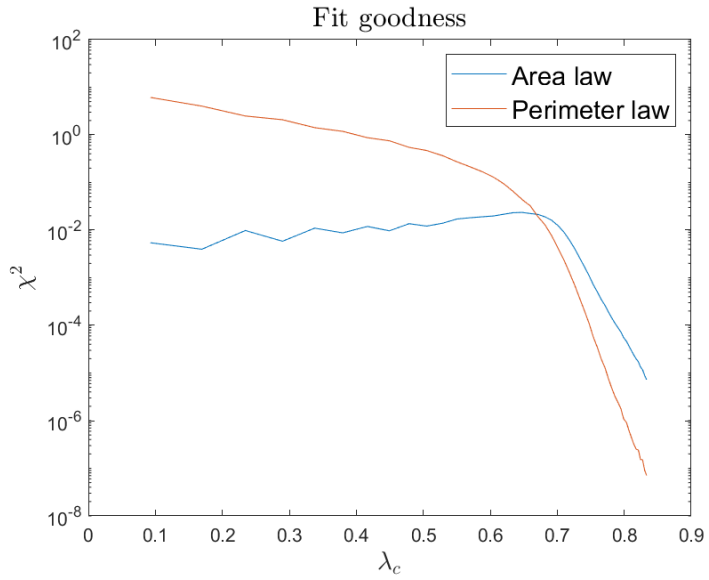

Figure 2.8: Normalized $\chi^2$for the fits with respect to area and perimeter law. Logarithmic scale is used to better represent the data.

As we can see the area law has a smaller χ^2 in the confined region, showing that it is better suited to describe the system where λ_c is small. The perimeter law gives instead a better description in the magnetic dominated region confirming that it corresponds to the deconfined phase.

Taking into account the various considerations in this section we can say that we found a phase transition in the region $\lambda_c \in [0.65, 0.75]$, which is in accordance to previous results obtained from similar methods [8]. We are limited in finding more precise results by the size of the transition region. A larger system would allow to improve on this result, giving a smaller interval.

2.5.2 Results for $\mathbb{Z}_4$

In the $\mathbb{Z}_4$ case each link is mapped into 2 qubits. Since it is more computational intensive we can only simulate up to a 3x3 lattice, which corresponds to a simulation with $2(M-1) = 16$ qubits. The time required for a single run with a system of this size is around 20 minutes depending on the choice of the evolution parameters. A 4x4 lattice simulation can be estimated to to take around 20×2^{14} minutes, which is more than 200 days, underlining the exponential growth in the complexity of the algorithm.
The main difference we incur in using a smaller lattice is that we have a smaller choice of Wilson loops, as can be seen in figure 2.9.

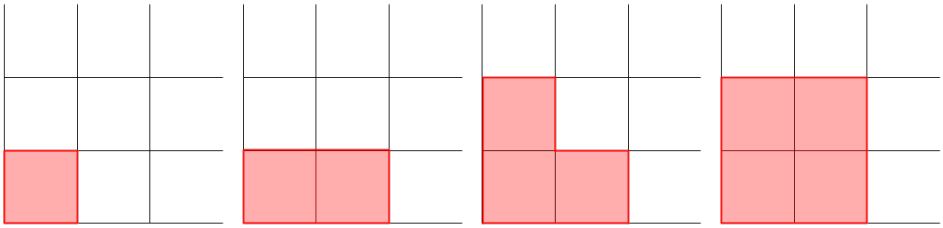

Figure 2.9: The four loops on which we perform the measurements in the 3x3 $\mathbb{Z}_4$ simulations.

The parameters of the simulation are obtained in the same way as for the $\mathbb{Z}_2$ model. We start by imposing $\lambda_{max} = 5$ and $N_s = 50$, and then we run the algorithm multiple times in order to find the best values for Δt and N_{tot}. We obtain $\Delta t = 0.05$ and $N_{tot} = 1000$. These values are the same as the ones we used in the $\mathbb{Z}_2$ simulation. Performing the same calibration on $\mathbb{Z}_4$ lattices of smaller size gives a different set of optimal parameters, showing that this coincidence is probably due to the similar number of qubits needed to perform the simulations, which is 15 in the $\mathbb{Z}_2$ 4x4 case and 16 in the $\mathbb{Z}_4$ 3x3 case.

We start by looking at the ground state energies, both total and divided into the electric and magnetic component. The results are shown in figure 2.10.

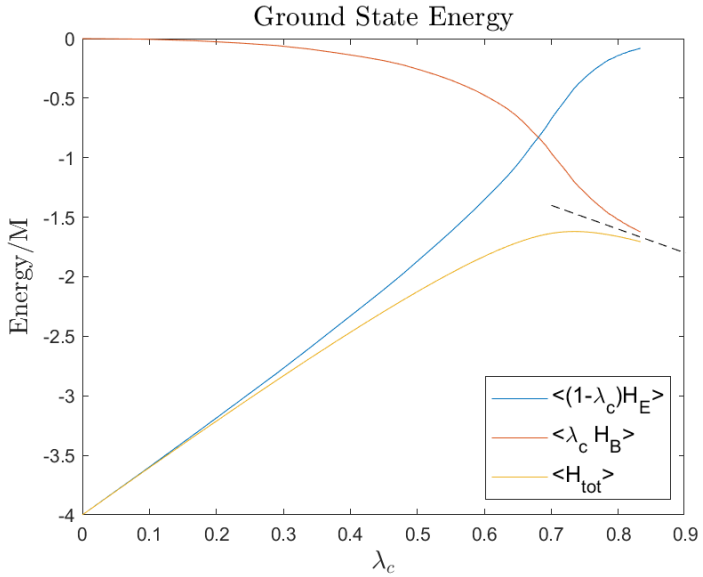

Figure 2.10: Energy measurements in a $\mathbb{Z}_4$ simulation on a 3x3 lattice. We take $N_s = 50$ measurements. All measures are normalized by the size $M = 9$ of the system. The dashed line shows the expected behavior near the magnetic limit.

The expected results are $\langle H_E \rangle / M = -2L/M = -4$ in the case the Hamiltonian is purely electric. Near the magnetic limit we instead expect the system to have energy $\lambda_c \langle H_B \rangle / M = -2\lambda_c$. The observed behavior is in accordance with the predictions, showing that the simulation has been performed with a good enough set of parameters.

We then look at the measured value for the four Wilson loops on which we are able to perform measurements. The results are shown in figure 2.11.

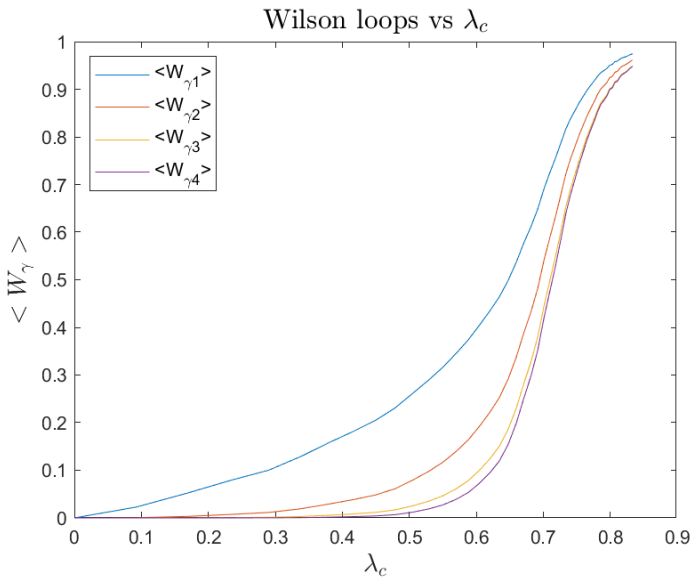

Figure 2.11: Expectation values of the four Wilson loops we analyzed, as a function of the coupling parameter λ_c

Although we don't have access to larger loops, which are better at detecting the phase transition, we can still see how the expectation values of all loops rapidly increase in the region around $\lambda_c = 0.7$, signaling a change in the phase of the system, from one where loops are suppressed, to one where excitations of any size can be found.

We then look at how the expectation values of these loops change as a function of the area and the perimeter of the loops themselves. Since the largest loop has area 4, and the total system has area 9, we can use the colored parts of figure 2.9 in order to calculate the areas $A[\gamma]$ of each loop. The calculation of perimeters $P[\gamma]$ is again straightforward.

We then show the behavior of the Wilson loops expectation value as a function of area and perimeter, which is found in figure 2.12.

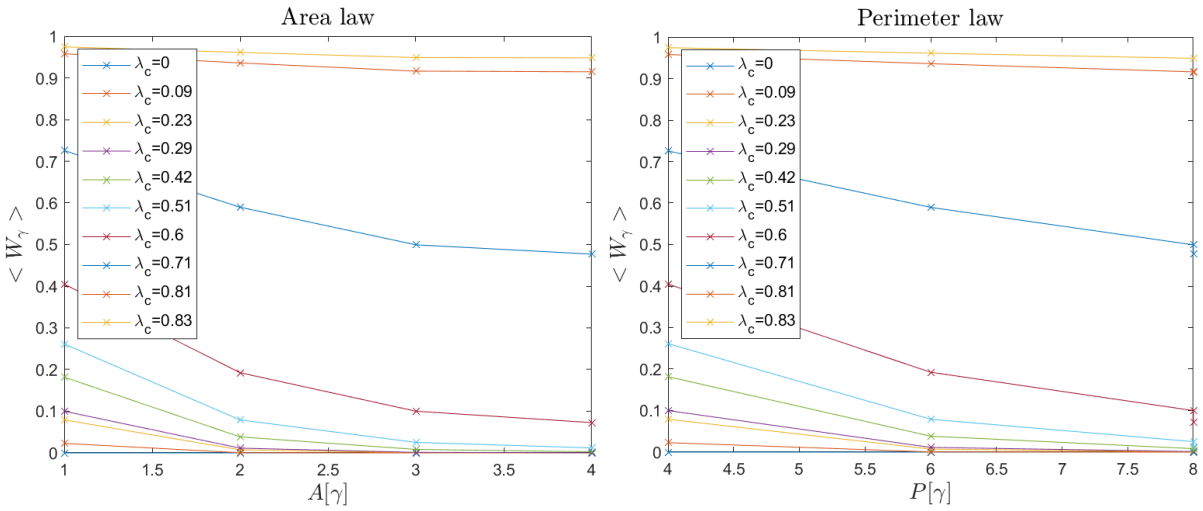

(a) (b)

Figure 2.12: Area law (a) and perimeter law (b) for Wilson loops of varying length at different values of λ_c. The sample values of λ_c are chosen out of the $N_s = 50$ measurements we performed to be evenly spaced across the studied region.

In the figures we can see the different behavior for λ_c small, big or in the intermediate region ($\lambda_c = 0.71$). Since the expected behavior in at least in one of the two phases is an exponential we can look at the graph in the logarithmic scale, which is shown in figure 2.13. We have to omit the case $\lambda_c = 0$, where numerical issues make the logarithm impossible.

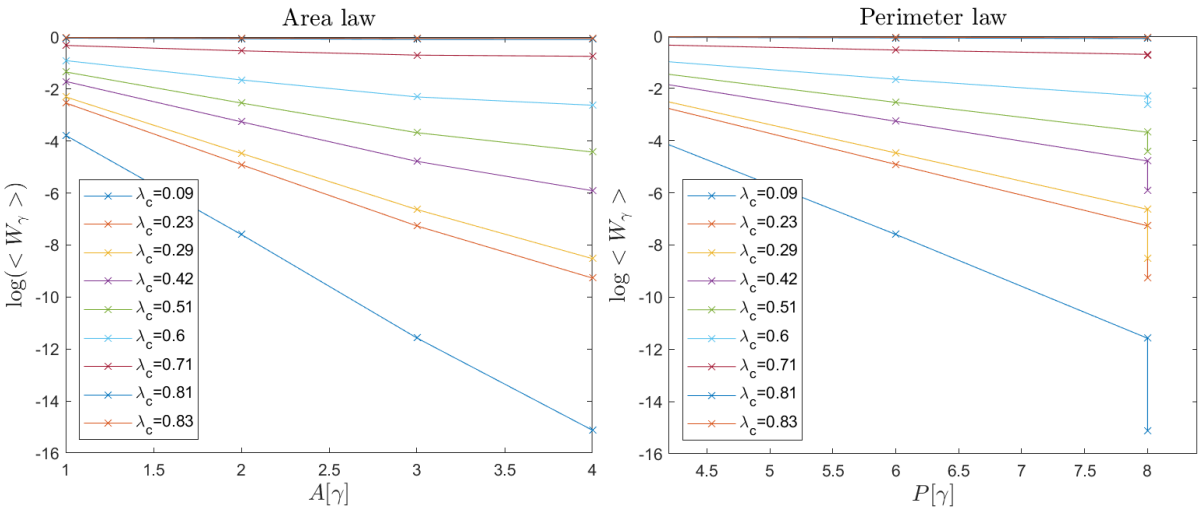

(a) (b)

Figure 2.13: Area law (a) and perimeter law (b) in logarithmic scale for Wilson loops of varying length at different values of λ_c.

The typical step in the perimeter law, caused by two different loops with the same perimeter is observed. The area law shows the expected behavior.

We can then perform the least square linear fit on equations (2.72) and (2.73), in order to obtain the parameters μ and ρ. All loops can be used both for the area and for the perimeter law. The results are shown in figure 2.14.

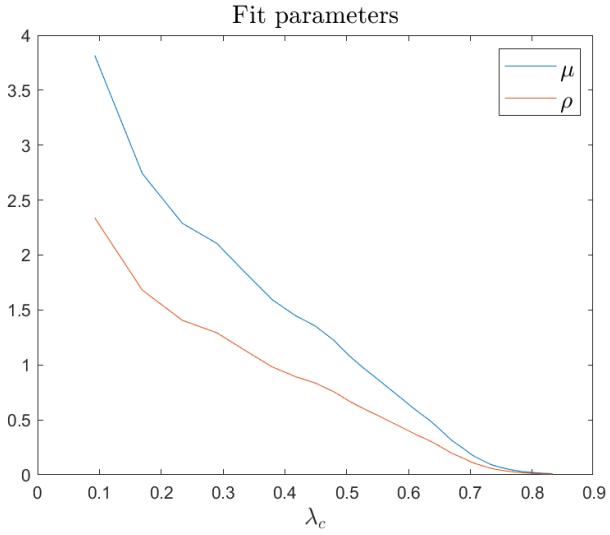

Figure 2.14: Parameter μ of the area law and parameter ρ of the perimeter law, as a function of the parameter λ_c. Results are obtained through a least square fit on an exponential law at each λ_c

In this graph we can see μ larger then ρ in the confined phase, a rapid decrease in both during the transition region, and almost the same value thereafter. The best way to confront the two laws is to look at the χ^2 of the fits. We show the χ^2 normalized by the number of degrees of freedom, which is 3 in both cases. The result is found in figure 2.15.

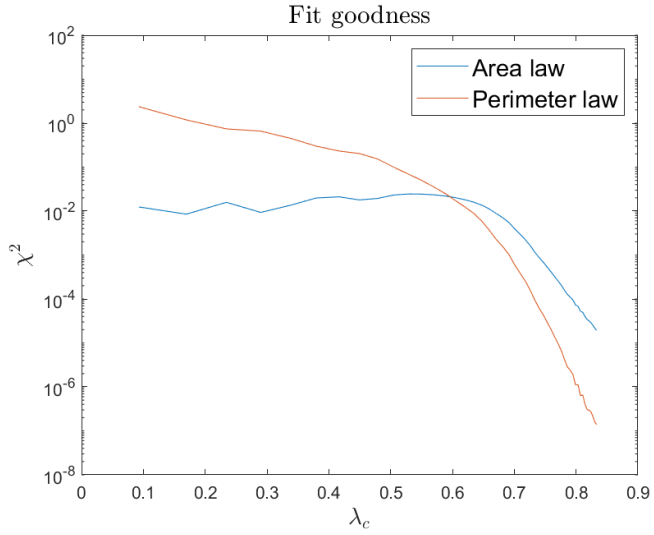

Figure 2.15: Normalized χ^2 for the fits with respect to area and perimeter law. Logarithmic scale is used to better represent the data.

The transition is less defined than in the $\mathbb{Z}_2$ case. Nevertheless we can see that the area law better describes the confined phase, while the perimeter law is better for the description of the deconfined region.

The general behavior of $\mathbb{Z}_4$ theory is almost the same as in the $\mathbb{Z}_2$ theory, with a small difference in the size of the transition region, which can be ascribed to a smaller size of the system. This effect come directly from the larger distance to the thermodynamics's limit, and is enforced by not having access to large Wilson loops, which are better suited to detect the phase transition. Taking into account all the observations of this section we can say that the phase transition is found in the region $\lambda_c \in [0.65, 0.75]$.

Chapter 3

Non-abelian field theory: D4

This section will focus on simulations on Yang-Mills gauge theories with a finite non-abelian symmetry group. The structure of non-abelian finite groups is much deeper that the one of abelian groups, which causes many simplifications we used earlier to fail. In order to examine these effects we will focus on a specific non-abelian group: the dihedral group of order 8, which will be described in the first section. The order of the group is chosen to be a power of 2 for efficient implementation. Working with a specific group allows us to give some explicit examples, which constitute the second section. In the end of this chapter we will discuss ways to implement the circuit and overcome the adversities, and report the results.

3.1 The dihedral group

The dihedral group of order 8, usually referred as D_4[1], is the non-abelian group that describes the symmetries of a square. It contains the simple four rotations, and the four rotations combined with a reflection. It has two generators r and s, in terms of which the presentation of the group is

$$D_4 = \langle r, s \ s.t. \ r^4 = s^2 = (rs)^2 = e \rangle \tag{3.1}$$

The 8 elements can be written as

$$e, r, r^2, r^3, s, rs, r^2s, r^3s \tag{3.2}$$

The identity $(rs)^2 = e$ can be rewritten as a conjugation between the two generators

$$srs^{-1} = r^3 \tag{3.3}$$

[1]This notation is used in geometry; in abstract algebra it is called D_8 instead

From this identity it is possible to calculate all possible conjugations by any element. We find that the group has 5 conjugacy classes:

$$\{e\}, \{r, r^3\}, \{r^2\}, \{s, r^2\}, \{rs, r^3 s\} \tag{3.4}$$

This means that we have 5 irreducible representations. We can number them for j from 0 to 4 where the first is the trivial representation. The characters for each representation can be found in table 3.1.

	$\{e\}$	$\{r, r^3\}$	$\{r^2\}$	$\{s, r^2 s\}$	$\{rs, r^3 s\}$
χ_0	1	1	1	1	1
χ_1	1	-1	1	1	-1
χ_2	1	1	1	-1	-1
χ_3	1	-1	1	-1	1
χ_4	2	0	-2	0	0

Table 3.1: Character table of the D_4 group

As can be seen from the first column of the table the first 4 representations are 1-dimensional. Therefore their characters correspond to the single matrix element of the representation. The representation $j = 4$ is the only 2-dimensional representation, which is the only faithful one. This representation is the one chosen for the eigenvalues of the $\hat{u}$ operators used in the construction of the magnetic term.
The representation $j = 4$ can be written explicitly as:

$$\pi_4(g) = \begin{cases} \begin{pmatrix} i^k & 0 \\ 0 & i^{-k} \end{pmatrix} & \text{if } g = r^k \\ \begin{pmatrix} 0 & i^k \\ i^{-k} & 0 \end{pmatrix} & \text{if } g = r^k s \end{cases} \tag{3.5}$$

meaning that

$$\pi_4(r) = \begin{pmatrix} i & 0 \\ 0 & -i \end{pmatrix} \text{ and } \pi_4(s) = \begin{pmatrix} 0 & 1 \\ 1 & 0 \end{pmatrix} \tag{3.6}$$

Obviously this is not the only explicit representation. An insightful equivalent one is

$$\pi_4(g) = \begin{cases} \begin{pmatrix} \cos\left(\frac{k\pi}{2}\right) & -\sin\left(\frac{k\pi}{2}\right) \\ \sin\left(\frac{k\pi}{2}\right) & \cos\left(\frac{k\pi}{2}\right) \end{pmatrix} & \text{if } g = r^k \\ \begin{pmatrix} \cos\left(\frac{k\pi}{2}\right) & \sin\left(\frac{k\pi}{2}\right) \\ \sin\left(\frac{k\pi}{2}\right) & -\cos\left(\frac{k\pi}{2}\right) \end{pmatrix} & \text{if } g = r^k s \end{cases} \tag{3.7}$$

which is more cumbersome, but shows explicitly that this is a subgroup of the orthogonal group $O(2)$.

The subgroup $N := \{e, r, r^2, r^3\}$, generated by r, is also a subgroup of the special orthonormal group $SO(2)$, and is one of the 2 non-trivial normal subgroups, the other being $\{e, r^2\}$.
Another interesting subgroup is $H := \{e, s\}$, generated by s. Since any element in G can be written uniquely as a product of an element in N and an element in H, we can say that G is a semidirect product of H and N:

$$D_4 = N \rtimes H \tag{3.8}$$

Since $N \simeq \mathbb{Z}_4$, and $H \simeq \mathbb{Z}_2$ we find that the dihedral group can be described as a semidirect product of two cyclic groups:

$$D_4 = \mathbb{Z}_4 \rtimes \mathbb{Z}_2 \tag{3.9}$$

We can brake down the group product operation of D_4 by representing each element of D_4 as couple $(n, h) \in N \times H$. The product becomes

$$(n_1, h_1)(n_2, h_2) = (n_1 \varphi_{h_1}(n_2), h_1 h_2) \tag{3.10}$$

where $\varphi : H \to Aut(N)$ is the group homomorphism given by $\varphi_{h_1}(n_2) = n_2^{h_1}$.

The group algebra of D^4 is an 8-dimensional complex linear space which admits the matrix elements π^j_{mn} as a basis. Each of them is described by a triplets of indices, to which we can associate one index $\bar{\jmath}$ in the condensed notation, according to the conventions in table 3.2. This allow us to cleanly reference all 8 states in the representation basis.

j_{mn}	0_{11}	1_{11}	2_{11}	3_{11}	4_{11}	4_{12}	4_{21}	4_{22}
$\bar{\jmath}$	1	2	3	4	5	6	7	8

Table 3.2: Conventions for the condensed notation in the D_4 group

3.1.1 Dihedral group gauge theory

Since we have chosen a gauge group we can give an explicit description of the Hilbert space, the terms of the Hamiltonian and the gauge conditions.
The single link Hilbert space can be defined in terms of the group basis or the representation basis:

$$|g\rangle \text{ and } |\bar{\jmath}\rangle \tag{3.11}$$

which are connected by the group Fourier transform:

$$|\bar{\jmath}\rangle = \sqrt{\frac{d_j}{|G|}} \sum_g \pi^j_{mn}(g) \, |g\rangle \tag{3.12}$$

The single link electric eigenvalue can be calculated from equation (1.54):

$$f(j) = |\Gamma| - \frac{1}{d_j} \sum_{g \in \Gamma} \chi_j(g) \tag{3.13}$$

where we need to choose Γ as a generating set closed under conjugation and inversion. The set with the smaller number of elements that satisfy this condition is $\Gamma := \{r, r^3, s, r^2 s\}$, which leads to the values for $f(j)$ shown in table 3.3.

j	0	1	2	3	4
$f(j)$	0	4	4	8	4

Table 3.3: Electric single link eigenvalues

The one plaquette Wilson loop operators, which constitutes the magnetic part of the Hamiltonian, can be written in terms of the plaquette operators using equation (1.77):

$$\operatorname{tr} \hat{W}_p = \sum_{g \in G} \chi_4(g) B_p^g \tag{3.14}$$

where $\chi_F = \chi_4$ due to the choice of the representation π_F.
Evaluating this operator on the group basis we obtain:

$$\operatorname{tr} \hat{W}_p \, |g_1, ..., g_L\rangle = \chi_4(g_{\gamma_p}) \, |g_1, ..., g_L\rangle \tag{3.15}$$

where we can see that it has eigenvalue $-2, 0$ or 2, corresponding to the single plaquette energy contribution in the magnetic limit.
The gauge invariant conditions on a given vertex are:

$$G_v(g) \, |phys\rangle = |phys\rangle \, \forall g \quad G_v(g) = L_g(e_1) L_g(e_2) R_g(e_3) R_g(e_4) \tag{3.16}$$

where the four link around the vertex are numbered in the conventional way as in figure 3.1. These conditions are quickly simplified by requiring them to be true only for the two generators, which in this case are r and s.

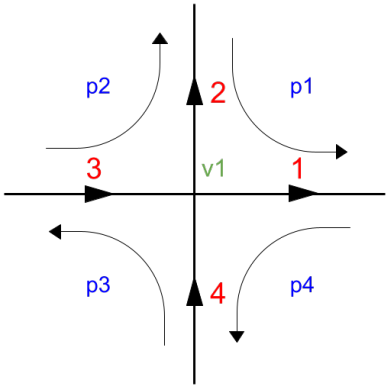

Figure 3.1: Details of a single vertex conventions. In this case the choice of using counterclockwise order in the closed paths gives the position of when to use the adjoint and when not to use it for the representation states on a given link.

The left and right representations are easily given in the representation basis:

$$L_g = \bigoplus_j \pi_j^*(g) \otimes \mathbb{1}_{d_j} \qquad R_g = \bigoplus_j \mathbb{1}_{d_j} \otimes \pi_j(g) \tag{3.17}$$

Using the knowledge of the irreducible representations of the group we can write them explicitly. Before doing so it is useful to make some remarks: there is a noticeable difference in the following analysis in the behavior of states and operators acting based on abelian and non-abelian representations. It is useful to already start to differentiate between the two. In the case of the regulars representation we can separate them by defining

$$L_g^\alpha = \bigoplus_{j\in A} \pi_j^*(g) \qquad L_g^\beta = \bigoplus_{j\in NA} \pi_j^*(g) \otimes \mathbb{1}_{d_j} \tag{3.18}$$

where the direct sum is performed only on the abelian (A) or non-abelian (NA) sector. In the abelian sector all irrep are one dimensional, which means that we can drop the tensor product with the identity.
The total regular representation can be obtained simply as

$$L_g = L_g^\alpha \oplus L_g^\beta \tag{3.19}$$

where each part acts on a different set of states. In particular L_g^α acts on states $|\alpha\rangle = |\bar{\jmath}\rangle$, with $\bar{\jmath} = 1, 2, 3, 4$, which are states in the representation basis which correspond to abelian representations. Meanwhile L_g^β acts on states $|\beta\rangle = |\bar{\jmath}\rangle$, with $\bar{\jmath} = 5, 6, 7, 8$, which correspond to the non-abelian representation.
Through these considerations we can write explicitly the left regular representation of

the generators:

$$L_r^\alpha = \begin{pmatrix} +1 & & & \\ & -1 & & \\ & & +1 & \\ & & & -1 \end{pmatrix} \quad L_r^\beta = \begin{pmatrix} -i & & & \\ & -i & & \\ & & +i & \\ & & & +i \end{pmatrix} \tag{3.20}$$

$$L_s^\alpha = \begin{pmatrix} +1 & & & \\ & +1 & & \\ & & -1 & \\ & & & -1 \end{pmatrix} \quad L_s^\beta = \begin{pmatrix} & & +1 & \\ & & & +1 \\ +1 & & & \\ & +1 & & \end{pmatrix} \tag{3.21}$$

and, following the same conventions, the right regular representation is:

$$R_r^\alpha = \begin{pmatrix} +1 & & & \\ & -1 & & \\ & & +1 & \\ & & & -1 \end{pmatrix} \quad R_r^\beta = \begin{pmatrix} i & & & \\ & -i & & \\ & & +i & \\ & & & -i \end{pmatrix} \tag{3.22}$$

$$R_s^\alpha = \begin{pmatrix} +1 & & & \\ & +1 & & \\ & & -1 & \\ & & & -1 \end{pmatrix} \quad R_s^\beta = \begin{pmatrix} & +1 & & \\ +1 & & & \\ & & & +1 \\ & & +1 & \end{pmatrix} \tag{3.23}$$

Having written the regular representations, which make up the gauge conditions, it is insightful to describe the gauge invariant states on any given vertex. As a starting point we can see that the total Hilbert space on the four links has dimension $|G|^4 = 8^4$. We will show that the gauge conditions reduce the dimension of the space by a factor $|G|$.

Considering invariance under $G(r)$ we see that the eigenvalues are ± 1 in the abelian sector and $\pm i$ in the non abelian sector. Therefore only an even number of abelian links can be connected to a given vertex, otherwise the product would be $\pm i$. We can than distinguish 3 possible cases: 4 abelian links, 2 abelian and 2 non abelian, and 4 non abelian links.

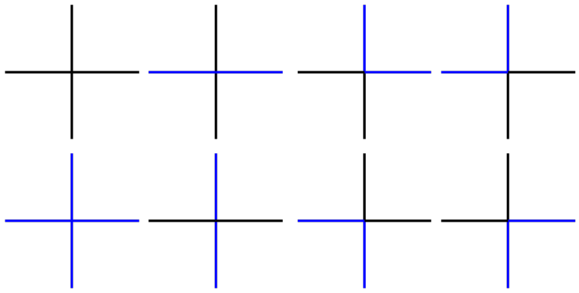

Figure 3.2: In this picture are shown the 8 possible configuration for abelian (in black) and non abelian (in blue) links around a given vertex. The third configuration in the second row is the one chosen out of the six possible for the explicit calculations in the case with two abelian and two non abelian links

In the first case we can arbitrarily choose the states of 3 out of the four links, for example the first three:

$$|\psi\rangle = |\alpha_1\alpha_3\alpha_3 X\rangle \tag{3.24}$$

The fourth state is then uniquely determined, since there is only one state for which $R_r |\alpha_4\rangle = \pm 1 |\alpha_4\rangle$ and $R_s |\alpha_4\rangle = \pm 1 |\alpha_4\rangle$, for each combinations of ± 1, which are determined by the other three states. Therefore this space has a dimension of 64, with 4 choices for each of the first three α.

The second case actually consist of 6 different configurations, which are related to the choice in position of the two abelian and two non abelian links. We give the case for $|\alpha_1\alpha_2\beta_3\beta_4\rangle$ since the other are similar. As before we can choose arbitrarily $\alpha_1\alpha_2$, and then look at the constraint on the non abelian part $|\beta_3\beta_4\rangle$. The best way to develop the calculation is to make the matrix elements of the non-abelian part explicit:

$$|\beta_3\beta_4\rangle = |4_{m_1 n_1} 4_{m_2 n_2}\rangle \tag{3.25}$$

Since $R_g = \mathbb{1} \otimes \pi^4(g)$ in this subspace, m_1 and m_2 are automatically invariant under the action of the gauge operators, and can therefore be chosen arbitrarily (in the case of configurations with the two non-abelian links in a different position we would have the index n_i fixed for each link acted upon by a left representation, instead of index m_i). Once α_1, α_2, m_1 and m_2 are chosen the values of n_1 and n_2 are fixed by the gauge conditions, and must be summed over in accordance to the fact that representation states are not sufficient for the gauge invariant basis. In the end we get that the gauge invariant states can be written as

$$|\alpha_1\alpha_2 4_{an_1} 4_{bn_2}\rangle \pm |\alpha_1\alpha_2 4_{an_1'} 4_{bn_2'}\rangle \tag{3.26}$$

where the sign between the two parts, and the values of n_1, n_1', n_2, n_2' are uniquely determined. Again we have 64 states due to 4 choices for α_1 and α_2 and 2 choices each for a and b.

In the third case we can write explicitly the representation basis and we find that the state can be written as

$$|4_{m_1 a} 4_{m_2 b} 4_{cn_3} 4_{dn_4}\rangle \tag{3.27}$$

where from the same argument as before a, b, c, d are arbitrary. Invariance under $G(r)$ implies that any choice of $m_1 m_2 n_3$ fixes n_4, and invariance under $G(s)$ pairs them up in 4 possible choices, which are shown in table 3.4. Again we have a total of 64 states: 2^4 for each choice of a, b, c, d and 4 for the rest.

$$\begin{array}{l} |4_{1a} 4_{1b} 4_{c1} 4_{d1}\rangle + |4_{2a} 4_{2b} 4_{c2} 4_{d2}\rangle \\ |4_{1a} 4_{1b} 4_{c2} 4_{d2}\rangle + |4_{2a} 4_{2b} 4_{c1} 4_{d1}\rangle \\ |4_{1a} 4_{2b} 4_{c1} 4_{d2}\rangle + |4_{2a} 4_{1b} 4_{c2} 4_{d1}\rangle \\ |4_{1a} 4_{2b} 4_{c2} 4_{d1}\rangle + |4_{2a} 4_{1b} 4_{c1} 4_{d2}\rangle \end{array}$$

Table 3.4: Four choices for fixing the indices n_i and m_i in order to obtain gauge invariant states on a vertex connected to 4 non-abelian links

Since we have 8 configurations with 64 states each the invariant subspace is $|G|^3$-dimensional, as previously stated. The general action of a the invariance condition on a vertex is the reduction of the dimension of a space by a factor $1/|G|$.

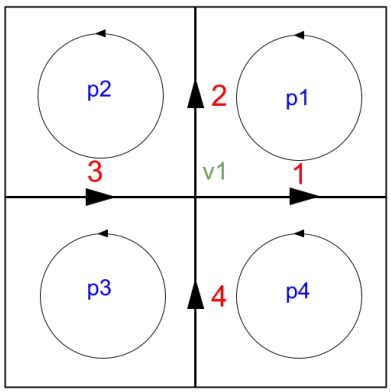

Figure 3.3: Single vertex enclosed by the neighboring links, in order to show the four plaquettes around the vertex in terms of which the state on the vertex can be described.

There is an insightful way to look at these states, based on the plaquette character states. Consider the system in figure 3.3, in which each of the four plaquettes is in a character state χ_j. The state of the system is

$$\sum_{\{g\}} \chi_{j_1}(g_{\gamma_1})\chi_{j_2}(g_{\gamma_2})\chi_{j_3}(g_{\gamma_3})\chi_{j_4}(g_{\gamma_4}) \left|g_1...g_L\right\rangle \tag{3.28}$$

Focusing on the internal links we can write their state as

$$\sum_{\{g\},\{n\}} \pi^{j_1\dagger}_{a_1 n_1}(g_2)\pi^{j_1}_{n_1 b_1}(g_1)\pi^{j_2}_{a_2 n_2}(g_3)\pi^{j_2}_{n_2 b_2}(g_2)\pi^{j_3}_{a_3 n_3}(g_4)\pi^{j_3\dagger}_{n_3 b_3}(g_3)\pi^{j_4\dagger}_{a_4 n_4}(g_1)\pi^{j_4\dagger}_{n_4 b_4}(g_4) \left|g_1 g_2 g_3 g_4\right\rangle \tag{3.29}$$

where the sum is over all g and n, and a and b are the indices on which we sum over in order to complete the plaquette loops. The state on each link is given by 2 contributes, for example link 1 is

$$\sum_{g_1} \pi^{j_1}_{a_1 n_1}(g_1)\pi^{j_4\dagger}_{a_4 n_4}(g_1) \left|g_1\right\rangle \tag{3.30}$$

which can be interpreted in terms of the product algebra, described in appendix A. Using the structure constants defined in equation (A.8) we find:

$$\pi_{\bar{j}_1}\pi_{\bar{j}_2} = \sum_{\bar{j}_3} c^{\bar{j}_3}_{\bar{j}_1\bar{j}_2}\pi_{\bar{j}_3} \tag{3.31}$$

In order to obtain a representation of the structure of the product algebra we can calculate the pairwise product of the matrix elements. For the D_4 group we obtain the structure in table 3.5.

	π_1	π_2	π_3	π_4	π_5	π_6	π_7	π_8
π_1	π_1	π_2	π_3	π_4	π_5	π_6	π_7	π_8
π_2	π_2	π_1	π_4	π_3	π_8	π_7	π_6	π_5
π_3	π_3	π_4	π_1	π_2	π_5	$-\pi_6$	$-\pi_7$	π_8
π_4	π_4	π_3	π_2	π_1	π_8	$-\pi_7$	$-\pi_6$	π_5
π_5	π_5	π_8	π_5	π_8	$\frac{1}{2}(\pi_2+\pi_4)$	0	0	$\frac{1}{2}(\pi_1+\pi_3)$
π_6	π_6	π_7	$-\pi_6$	$-\pi_7$	0	$\frac{1}{2}(\pi_2-\pi_4)$	$\frac{1}{2}(\pi_1-\pi_3)$	0
π_7	π_7	π_6	$-\pi_7$	$-\pi_6$	0	$\frac{1}{2}(\pi_1-\pi_3)$	$\frac{1}{2}(\pi_2-\pi_4)$	0
π_8	π_8	π_5	π_8	π_5	$\frac{1}{2}(\pi_1+\pi_3)$	0	0	$\frac{1}{2}(\pi_2+\pi_4)$

Table 3.5: Structure of the product algebra of the D_4 group. In the first column is $\pi_{\bar{j}_1}$, and in the first row $\pi_{\bar{j}_2}$. Each element of the table corresponds to $\sum_{\bar{j}_3} c^{\bar{j}_3}_{\bar{j}_1\bar{j}_2}\pi_{\bar{j}_3}$.

We find an intresting property in the product algebra of the D_4 group: the product of two abelian or two non-abelian matrix elements is an abelian matrix element, while

the product of one of each type is a non-abelian matrix element. Therefore in order to produce a non abelian state on a link one of the two neighboring plaquette must be in the non-abelian character state χ_4.
We can see this explicitly in the case with link 1 and 2 in an abelian representation and 3 and 4 in the non-abelian. In this situation plaquette 3 must be in the non-abelian character state. We can then use plaquette 2 and 4 to set the abelian state of links 1 and 2. The resulting state is

$$\sum_{n=1}^{2} \sum_{g_1 g_2 g_3 g_4} \pi^{\alpha_2}(g_3)\pi^{\alpha_2}(g_2)\pi^{4}_{an}(g_4)\pi^{4\dagger}_{nb}(g_3)\pi^{\alpha_1\dagger}(g_1)\pi^{\alpha_1\dagger}(g_4)\,|g_1 g_2 g_3 g_4\rangle \tag{3.32}$$

where α_1 is the state of link 1 and α_2 is the state of link 2.

The choice of using plaquettes $2, 3$ and 4 is not unique. For example, the same state as before can be described by setting plaquette 1 with α_1, plaquette 2 in a certain α_3 chosen such that the product between α_1 and α_3 gives α_2 on the second link and plaquette 3 in representation 4. The states on the border of figure 3.3 can be used to find which one is the correct representation.

3.2 Difficulties of the non-abelian case

In this section we will focus on small systems, in order to appreciate the differences between the abelian and non-abelian case.

3.2.1 Two plaquette system

The first appearances of non-trivial behavior can be found in analyzing two neighboring plaquettes, which are shown in figure 3.4. We will show how the one-plaquette basis is no longer enough for the description of the gauge invariant Hilbert space.

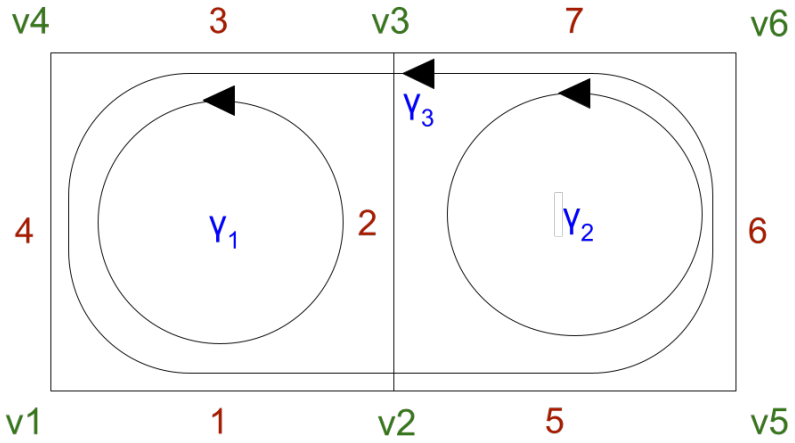

Figure 3.4: Conventions for the two plaquette system, with numbered links and vertices. Three fundamental loops are also shown: γ_1 and γ_2 wrapping around the respective plaquette, and γ_3 wrapping around both plaquettes.

Since the system is small we can find all gauge invariant states explicitly. In doing so we can utilize the knowledge of the single vertex gauge invariant states, which was previously developed. In principle we cannot apply it directly, since by working in a system without periodic boundary condition some vertices are connected only to 2 links (like vertex 1,4,5, and 6) and some have 3 (like vertex 2 and 3). Nevertheless we can consider each of these vertices as a four link vertex where all the links corresponding to missing links are in the trivial state $j = 0$. Since the regular representations act trivially on such states ($L_g |0\rangle = R_g |0\rangle = |0\rangle$) this doesn't affect the conditions on the other links. The condition that the number of non-abelian links connected to a given vertex must be even can be made more precise on the vertices in this system, knowing that the missing links count as abelian. On a vertex connected to two links we can have two configurations: both links are abelian or both links are non-abelian. A vertex connected to 3 links we can have 4 configurations. One in which all links are abelian, and 3 in which we have 2 non-abelian links and one abelian link.
Distinguishing between abelian and non-abelian links leads us to four possible cases for the two plaquette system, which are shown in figure 3.5.

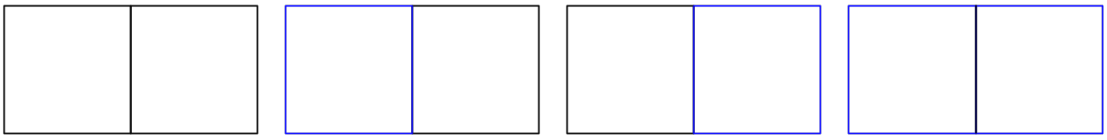

Figure 3.5: Four possible configurations for the abelian states, in black, and the non-abelian states, in blue, for the 2 plaquette system.

In the case of all abelian links there are 16 possible states, which can be written as:

$$|\chi_{\alpha_1}\chi_{\alpha_2}\rangle = \frac{1}{\sqrt{|G|^2}} \sum_{g_1,...,g_7 \in G} \chi_{\alpha_1}(g_{\gamma 1})\chi_{\alpha_2}(g_{\gamma 2})\,|g_1,...,g_7\rangle \tag{3.33}$$

The second and third configuration can be interpreted as one plaquette being in an abelian character one-plaquette state and the other plaquette in a character state connected to the non-abelian representation. Each case contains 4 possible states:

$$|\chi_4\chi_{\alpha_2}\rangle = \frac{1}{\sqrt{|G|^2}} \sum_{g_1,...,g_7 \in G} \chi_4(g_{\gamma 1})\chi_{\alpha_2}(g_{\gamma 2})\,|g_1,...,g_7\rangle \tag{3.34}$$

$$|\chi_{\alpha_1}\chi_4\rangle = \frac{1}{\sqrt{|G|^2}} \sum_{g_1,...,g_7 \in G} \chi_{\alpha_1}(g_{\gamma 1})\chi_4(g_{\gamma 2})\,|g_1,...,g_7\rangle \tag{3.35}$$

The fourth configuration is the most interesting one, since it cannot be represented as a single plaquette state but only by using a multiple plaquette character state. There are four such states:

$$|\chi_4(\gamma_3)\chi_\alpha(\gamma_1)\rangle = \frac{1}{\sqrt{|G|^L}} \sum_{g_1,...,g_7} \chi_4(g_{\gamma 3})\chi_\alpha(g_{\gamma 1})\,|g_1g_2g_3g_4g_5g_6g_7\rangle \tag{3.36}$$

However this is not the unique way to obtain a state with non abelian links on the boundary and a single abelian link in the middle. An alternative way would be to use $|\chi_4(\gamma_3)\chi_\alpha(\gamma_2)\rangle$, using the abelian representation on plaquette 2. The resulting state would have the same abelian state α in the middle link, and a superposition of the four non abelian links on each of the other links. This state is exactly the same as $|\chi_4(\gamma_3)\chi_\alpha(\gamma_1)\rangle$, as can be checked explicitly, providing two different expressions for the same state. It is a similar situation as in the abelian case, where we didn't need to know the state of the M-th plaquette, since it was only producing equivalent expressions of other known states.
In total there are 28 gauge invariant states on a 2 plaquette system. We can check directly that the 28 states we defined are orthonormal.

It is interesting to confront the 28 states we have found with the 25 plaquette character states $|\chi_{j_1}\chi_{j_2}\rangle$ we would obtain if we naively used them as we had in the abelian case. In doing so we find that 24 states are precisely the same. The difference between the two cases lays in the final states, which is the state $|\chi_4\chi_4\rangle$ in the plaquette basis, and the four states $|\chi_4(\gamma_3)\chi_\alpha(\gamma_1)\rangle$ in the explicit description of the gauge invariant space. Some simple calculations shows the relation between these states:

$$|\chi_4\chi_4\rangle = \frac{1}{2}\sum_{\alpha=0}^{3} |\chi_4(\gamma_3)\chi_\alpha(\gamma_1)\rangle \tag{3.37}$$

where we can see that the state on the left is a superposition of the four states on the right.
This means that while the one-plaquette character states are all gauge invariant, they cannot be considered a basis since they are not generators of the gauge invariant subspace. Multiple plaquettes loops are necessary for a complete description.

In section 1.2.5 we warned about an atypical behavior of one-plaquette character states with respect to the single link electric energy, which was given by

$$\langle \chi_{i_1}\chi_{i_2}| \, h_E^2 \, |\chi_{j_1}\chi_{j_2}\rangle = \delta_{i_1,j_1}\delta_{i_2,j_2}\bar{f}(i_1,i_2) \qquad \bar{f}(i,j) = |\Gamma| - \frac{1}{d_i d_j}\sum_{g\in\Gamma}\chi_i^*(g)\chi_j(g) \quad (3.38)$$

The problem appears since the matrix elements make the states looks like they diagonalize the electric operator. Working explicitly in the non-abelian case allows us to show an example of how this is not true.
In order to see this we look at state $|\chi_4\chi_4\rangle$, which can be decomposed as an equal weight sum of $|\chi_4(\gamma_3)\chi_\alpha(\gamma_1)\rangle$. The state of link 2 in each of the latter is determined uniquely by the index alpha, therefore we get:

$$h_E^2 \, |\chi_4(\gamma_3)\chi_\alpha(\gamma_1)\rangle = f(\alpha) \, |\chi_4(\gamma_3)\chi_\alpha(\gamma_1)\rangle \quad (3.39)$$

This means that state $|\chi_4\chi_4\rangle$, being a sum of states with different eigenvalues, is not an eigenstate of the single link Hamiltonian.
In the abelian case the one-plaquette states were a complete basis for the gauge invariant subspace, therefore having diagonal eigenvalues was enough to guarantee the diagonallity of the operator. Instead in the non-abelian case the 28 states are all needed to guarantee a diagonal basis for the single link electric operators.
The reason this is interesting is because if the one-plaquette character base was truly diagonal for all the electric terms we would be able to implement the adiabatic evolution simply by using the matrix elements in equation (3.38). Unfortunately this is not so, and state $|\chi_4\chi_4\rangle$ would be given the wrong evolution by those values.

3.2.2 Periodic boundary conditions

Another issue in the description of gauge invariant states for a non-abelian theory arises when we introduce periodic boundary conditions. In order to show this we can work on two plaquettes with periodic boundary conditions in the horizontal direction, as can be seen in figure 3.6.

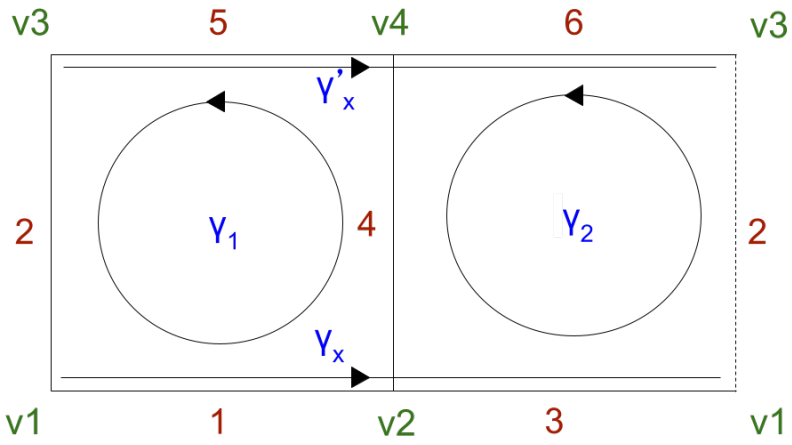

Figure 3.6: Conventions for a two plaquette system with PBC in the horizontal direction. Four important closed loops are shown, two around the plaquettes and two around non-contractible loops. Links and vertices with the same number are identified.

In order to find all the gauge invariant states we can start by looking at all the possible configurations of abelian and non-abelian links. There are 8 possible configurations, which are shown in figure 3.7.

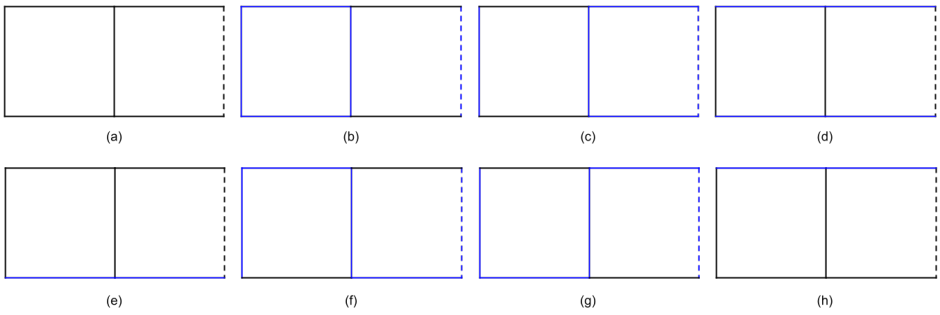

Figure 3.7: Configurations for abelian and non-abelian links for a 2 plaquette system with PBC in one direction.

The simplest configuration is made up of all abelian links, contains 4^3 possible states, and can be described as:

$$|\chi_{\alpha_1}\chi_{\alpha_2}\chi_{\alpha_x}\rangle = \frac{1}{\sqrt{|G|^3}} \sum_{g_1,\ldots,g_7 \in G} \chi_{\alpha_1}(g_{\gamma 1})\chi_{\alpha_2}(g_{\gamma 2})\chi_{\alpha_x}(g_{\gamma x}) \tag{3.40}$$

All other 7 configurations contains 4^2 states, which can be distinguished by the states of the abelian links.
In particular for all cases except configuration (d) we can use an operator χ_4 acting on the non-abelian path to obtain the correct configuration, and then use abelian character operators acting on 2 out of the three loops $\gamma_1, \gamma_2, \gamma_x$ to obtain all the states in that configuration.

For example in configuration (b) the non-abelian path is γ_1, and the two abelian paths we need to use are γ_2, γ_x, since applying an abelian operator on loop γ_1 would leave the state unchanged. We can write these states as:

$$|\chi_4 \chi_{\alpha_2} \chi_{\alpha_x}\rangle = \frac{1}{\sqrt{|G|^3}} \sum_{g_1,\dots,g_7 \in G} \chi_4(g_{\gamma 1}) \chi_{\alpha_2}(g_{\gamma 2}) \chi_{\alpha_x}(g_{\gamma x}) \tag{3.41}$$

In configuration (d) instead we have two non-abelian loops, γ_x and γ'_x. The 4^2 possible states can be identified by the abelian links' states, which in our conventions are link 2 and 4. A problem arises when we try to interpret some of these states as loop states. The position of the non-abelian links implies that in order to construct these states we need to act on the electric vacuum with $\hat{\chi}_4(\gamma_x)$ and $\hat{\chi}_4(\gamma'_x)$. We then need an abelian character's operator in order to set the correct state for the abelian states; looking at $\hat{\chi}_{\alpha_1}(\gamma_1)$ we can see that it acts on both links 2 and 4, setting both of them in state $|\alpha_1\rangle$. Operator $\hat{\chi}_{\alpha_2}(\gamma_2)$ does the same. More generally since any operator connected to a closed loop traverse from the bottom row to the top row an even number of times we are unable to produce a loop representation for any states in which the two abelian links are in two different states.
As an explicit example we can look at the case in which link 2 is in state $\alpha_2 = 0$ and link 4 in state $\alpha_4 = 1$. Applying directly the gauge invariant conditions shows that such state can be represented as

$$|\chi_4(\gamma_x)\chi_4(\gamma'_x)\pi_0(l_2)\pi_1(l_4)\rangle \propto \sum_g \chi_4(g_1 s g_3)\chi_4(g_5 s g_6)\pi_1(g_4)\,|g_1 g_2 g_3 g_4 g_5 g_6\rangle \tag{3.42}$$

In this expression we have inserted explicitly the element s, in order to keep the state invariant on vertices 2 and 4.
The problem of using these expressions is that if we want to completely describe the gauge invariant theory we can no longer use a combination of character operators acting on certain loops, but we need to manually find a good expression for each state.

3.2.3 Generalizing counting

Finding explicit description of the gauge invariant space for larger systems becomes increasingly cumbersome. One step that we can take in this direction is to find a general

way to calculate the number of states in a given lattice.
The quantities we should look at are the number of links L which is related to the size of the total Hilbert space $|G|^L$ and the number of vertices V which gives how many gauge constraint we have to impose.
We also know that for the purely abelian states such constraints are reduced by one, since by the same argument we used in section 2.2.1, now restricted only to the abelian sector, the last constraint is always trivial. It becomes important therefore to calculate how many configurations of abelian and non abelian links are possible.
On each vertex the condition between abelian and non-abelian links reduces to having an even number of each, as we have seen in section 3.1.1. This condition is in direct analogy with the gauge invariant states of an Ising $\mathbb{Z}_2$ gauge model, in which the number of excited states $|1\rangle$ and ground states $|0\rangle$ in the representation basis on each vertex are even. Since the latter is an abelian model with a group of order two the last condition is always trivial. We define $K = L - V + 1$ and find that there are 2^K configurations, of which only one is purely abelian.
For a D_4 group each configuration contains 4^L states, before further constraints. In the purely abelian case such constraints reduce the space to a dimension 4^K, while in all the other $2^K - 1$ configurations we get only 4^{K-1} states, due to the non trivial extra condition. The result is that for any given lattice we have:

$$\#states = 4^K + (2^K - 1)4^{K-1} \tag{3.43}$$

To compare it with the abelian case, where we had $|G|^K$ states we can collect such factor in front, obtaining

$$\#states = |G|^K \left(\frac{1 + 3 \times 2^{-K}}{4} \right) \tag{3.44}$$

where the second term is always less then one, implying a smaller gauge invariant space. We can verify this formula on small systems, as can be seen in table 3.6.

Dimensions	PBC	L	V	K	#states
2x1	no	7	6	2	28
2x1	horiz.	6	4	3	176
2x2	no	12	9	4	1216
2x2	both	8	4	5	8960

Table 3.6: Number of gauge invariant states for a few small systems. A $n \times m$ lattice has n columns and m rows. PBC indicates if periodic boundary conditions are present in the horizontal or vertical direction, or in both.

3.3 Simulation of D_4 gauge theory

We have now seen how some difficulties arise in the description of a Yang-Mills theory with a non-abelian group gauge symmetry. In this section we will focus on the consequences for the simulation of these systems.

3.3.1 Techniques

Similarly to the abelian case we can start by working directly in the gauge invariant space. This allows us to work with the minimal possible number of degrees of freedom, thus producing a small Hilbert space which can be encoded efficiently in any quantum computer. The first issue with this approach is that we can no longer rely only on the one-plaquette basis to generate all gauge invariant states, but we need to also consider all loops around multiple plaquettes. This produces many different representations for some states, and we need to manually eliminate all duplicates. A generating procedure that we used in the previous sections was to first find the configurations of abelian and non-abelian links, and then produce an identifier for every state in each configuration. Nevertheless this procedure is impossible to generalize and require too much manual tuning as soon as the size of the system grows.
Moreover whenever we introduce periodic boundary conditions we can find states that cannot be expressed as combination of loops, and need to be written out explicitly on a case by case basis, elongating this procedure even more.

The only choice we have in order to produce a code which can be generalized to larger lattices is to renounce to the gauge invariant subspace, and work directly on the total Hilbert space, which also contains the non-physical states.
If we use the adiabatic evolution algorithm the state evolves under the Hamiltonian with varying parameters. Being the latter gauge invariant by construction, the state, which starts as the always gauge invariant electric vacuum, will remain invariant during the whole evolution, even if we don't work explicitly in the invariant subspace.

3.3.2 Implementation of the adiabatic algorithm

There are two ways in which we can implement the adiabatic algorithm. The first one is similar to the one we used in the abelian case, mapping the system into a quantum register and using python's qiskit package to reconstruct the evolution through the action of simple gates. The second one instead aims at reproducing the same evolution by writing the unitary matrices and compute the evolution through simple matrix multiplications, and can be implemented efficiently in *Matlab*. With the first technique we construct a quantum circuit, which is then used to build the evolution from which we calculate our results. In the second method we cut out all the encoding procedure necessary to

produce the quantum circuit, and dive at the core of the operations of the simulation, thus producing a more efficient code. Nevertheless it is still interesting to develop all the circuitry, which corresponds to the structure that would be used on a real quantum computer simulation.

3.3.3 The Quantum circuit

Since we now work with the total Hilbert space we can encode each link in a set of qubits. Being the single link Hilbert space of dimension $|G| = 8$, we can map each link into three qubits, associating the states in the representation basis with the computational basis, as can be seen in table 3.7. To describe the whole lattice we need $N_{tot} = 3L$ qubits.

j_{mn}	0_{11}	1_{11}	2_{11}	3_{11}	4_{11}	4_{12}	4_{21}	4_{22}
$\|\psi\rangle$	$\|000\rangle$	$\|001\rangle$	$\|010\rangle$	$\|011\rangle$	$\|100\rangle$	$\|101\rangle$	$\|110\rangle$	$\|111\rangle$

Table 3.7: Conventions for the encoding of single link states.

We can introduce the electric evolution directly on each link of the system, since it is diagonal in the representations basis. For the magnetic part we need instead to first perform a group Fourier transform on each link, in order to go to the group basis. We then need to combine the group elements in order to find the group element that represent each plaquette, on which we can implement the magnetic evolution given by each plaquette Wilson loop.
We can recognize four actions for which we need to give a gate expression: the single link electric evolution, the single plaquette magnetic evolution, the group Fourier transform, and the group operations used to obtain the plaquette state. The first two correspond to a diagonal evolution, and can be easily implemented through control-phase gates. The other two are more complicated and will be analyzed hereafter.

D_4 group Fourier transform. The GFT for group $G = D_4$ can be obtained through the methods derived by M. Püshel [44]. The idea of this algorithm is that if a group G can be written as a semidirect product of a group N and a cyclic group H, and if we know the GFT of N and H, we can combine them in order to obtain the GFT of the total group. Since the H is a cyclic group its GFT is the discrete Fourier transform (DFT). For N we need instead to apply the algorithm recursively, until a group with a known GFT is found.
The core mechanism, by which the algorithm is derived, is obtained by noticing that the GFT of any group is the matrix by which we conjugate the right regular representation in order to obtain the irreducible components of the representation. This idea can be expressed as:

$$\langle g_1|R_g|g_2\rangle = \langle g_1|\bar{\jmath}_1\rangle \langle \bar{\jmath}_1 R_g \bar{\jmath}_2\rangle \langle \bar{\jmath}_2|g_2\rangle \tag{3.45}$$

where $\langle g_1|R_g|g_2\rangle$ is the right regular representation on the group basis, $\langle g_1|\bar{\jmath}_1\rangle$ is GFT, and $\langle \bar{\jmath}_1 R_g \bar{\jmath}_2\rangle = \bigoplus_j (\mathbb{1}_{d_j} \otimes \pi_j(g))$ are the irreducible components. This allows us to draw a parallel between the irreducible representations and the GFT of any group. Extending step by step the irreducible representations of N to the irreducible representations of G is in a one to one correspondence to the steps we need to take in order to extend the GFT of N to the GFT of G.
Writing B as the GFT of G and A as the GFT of N we get the decomposition:

$$B = (\mathbb{1}_p \otimes AP_1M)D(DFT_p \otimes \mathbb{1}_{|N|})CP_2E \tag{3.46}$$

where $p = |H|$, P_1 and P_2 are permutation matrices, DFT_p is the GFT of H, M, D, C are tuning operations, and E is needed to adjust the conventions used in this thesis with the ones in [44].
Due to the implementation methods of the algorithm we also introduce a conventional ordering of the states of the group basis. Since each element of G can be uniquely represented as a couple $(h, n) \in H \times N$, the states $|g\rangle$ can be encoded in the product basis $|h\rangle \otimes |n\rangle$. The order in the tensor product can be understood by looking at equation (3.46), where the GFT of H acts on the first term of the tensor product, while the GFT of N on the second.

In the case of the group D_4 we know that it can be decomposed in the semidirect product

$$D_4 = H \ltimes N \tag{3.47}$$

where $N = \{e, r, r^2, r^3\} \simeq \mathbb{Z}_4$ and $H \simeq \mathbb{Z}_2$ is the cyclic group of order $p = 2$. The GFT of N is therefore QFT_2, the Quantum Fourier transform on 2 qubits, which is already known and we don't need to iterate the algorithm further. The discrete Fourier transform DFT_2 acts instead on length 2 sequences, and can be implemented by QFT_1, the Quantum Fourier transform on a single qubit.
The states of the group basis are encoded into the computational basis in two steps. In the first we assign to each state $|g\rangle$ the state $|h\rangle \otimes |n\rangle$. We can then encode $|h\rangle$ into the one qubit state $|q_2\rangle$, and $|n\rangle$ into the two qubit states $|q_1q_0\rangle$. The final encoding will be in terms of the computational state $|q_2q_1q_0\rangle$, and can be found in table 3.8.

g	e	r	r^2	r^3	s	rs	r^2s	r^3s
$\|\psi\rangle$	$\|000\rangle$	$\|001\rangle$	$\|010\rangle$	$\|011\rangle$	$\|100\rangle$	$\|101\rangle$	$\|110\rangle$	$\|111\rangle$

Table 3.8: Conventions for the encoding of single link states.

Using this basis we can then calculate all the components of formula (3.46) as:

$$p = 2 \tag{3.48}$$

$$|N| = 4 \tag{3.49}$$

$$A = QFT_2 \tag{3.50}$$

$$P_1 = \begin{pmatrix} 1 & 0 & 0 & 0 \\ 0 & 0 & 1 & 0 \\ 0 & 1 & 0 & 0 \\ 0 & 0 & 0 & 1 \end{pmatrix} \tag{3.51}$$

$$M = \mathbb{1}_4 \tag{3.52}$$

$$D = \mathbb{1}_6 \oplus \sigma_x \tag{3.53}$$

$$C = \mathbb{1}_6 \oplus \sigma_z \tag{3.54}$$

$$P_2 = \mathbb{1}_2 \oplus (\sigma_x \otimes \mathbb{1}_2) \oplus \mathbb{1}_2 \tag{3.55}$$

$$E = \mathbb{1}_4 \oplus (H \otimes \mathbb{1}_2) \tag{3.56}$$

Each of these matrices can then be implemented into a gate:

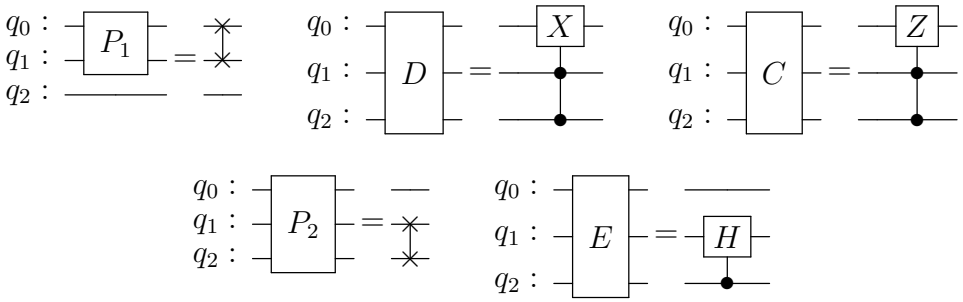

where we used the conventionally defined swap and double controlled gates, whose description is found in the appendix B.

Group operations. Since the group element representing any given plaquette can be given by $g_{\gamma_p} = g_1 g_2 g_3^{-1} g_4^{-1}$, we need two operations. The first one is the inversion operator $INV\,|g\rangle = |g^{-1}\rangle$, the second is the group composition $Pr\,|g_1, g_2\rangle = |g_1, g_1 g_2\rangle$. Under inversion we only need to exchange state to $|r\rangle$ with state $|r^3\rangle$, since all other group elements are their own inverse. This can be performed by the following circuit:

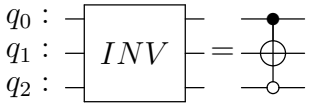

where we used an anti-control gate, described in appendix B.
For the group product we use instead the following expression, already shown in equation (3.10):

$$(n_1, h_1)(n_2, h_2) = (n_1 (n_2)^{h_1}, h_1 h_2) \tag{3.57}$$

A first gate is used to calculate $(n_2)^{h_1}$, and then two summing circuits are implemented, the first for 2 qubits number which allows us to calculate $n_1(n_2)^{h_1}$, and the second one on 1 qubit for $h_1 h_2$. The final circuit is

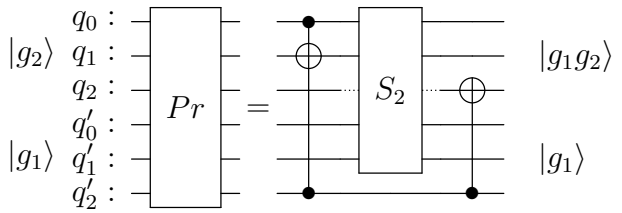

3.3.4 The direct evolution

Although in principle using the unitary matrices directly to calculate the adiabatic evolution is simple, there are some subtleties that can be exploited to obtain a more efficient implementation. Each step of the evolution can be broken down through Trotterization into an electric or magnetic substep, where

$$U_E = e^{-i\Delta t H_E} \qquad U_B = e^{-ig\Delta t H_B} \tag{3.58}$$

If we use the representations basis U_E is diagonal, and contains only $N_{tot} = |G|^L$ non-zero elements. A similar condition holds for H_B in the group basis. A large number of zero-elements is useful because we can use sparse matrices, which require less space and can be multiplied faster. Since we cannot diagonalize both at the same time we need at least one of the two to be expressed in the non-ideal basis. It turns out that implementing U_E in the group basis is the more efficient choice, since every single link evolution can be expressed as

$$GFT e^{-i\Delta t h^l_E} GFT^{-1} \otimes \mathbb{1}_{N_{tot}/|G|} \tag{3.59}$$

which has at most $|G|^{L+1}$ non-zero elements.
Working instead with the magnetic evolution in the electric base, we can separate the single plaquette evolution, which contains up to $|G|^{L+4}$ non-zero elements, and is much more expensive to calculate.
It is important to multiply always a matrix operator directly with the state vector, if possible, since matrix-matrix multiplication is always slower.

3.4 Results

In the D_4 simulations we work with a system whose Hilbert space has dimension $|G|^L$. We can simulate it in reasonable times up to a 2x2 lattice.
The limiting factor is given by the RAM requirements needed in order to save the evolution matrices which give the evolution of the system. The most expensive one is the

single link electric evolution, which has $|G|^{L+1}$ non-zero complex double elements. In a 2x2 lattice, we have $L = 8$ and it occupies a space of $2^{31}B \sim 1GB$, which is manageable. The next size step, which would be the 3x2 lattice, has $L = 12$ and the single link electric evolution operators has 2^{39} non-zero elements, and it occupies $2^{43}B \sim 10TB$, which makes it harder to simulate.

In order to find the simulation parameters we can follow a similar procedure as the one defined in the abelian section. We start by choosing the region that we want to study, which in this case is $\lambda = [0, 5]$. This corresponds to the region in the compactified parameter given by $\lambda_c \in [0, 0.83]$. We then choose the number of measures we want to obtain, which we set to N_s. Δt and N_{tot} are set at low values and then increased until satisfactory results are achieved. We found that the optimal parameters are $\Delta t = 0.03$ and $N_{tot} = 1500$.

The first quantity that we look at is the electric and magnetic energy of the ground state, which is shown in figure 3.8.

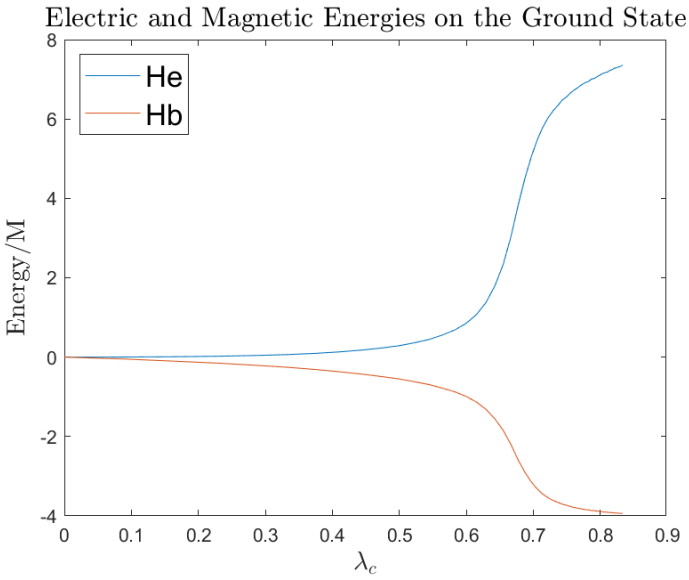

Figure 3.8: Expectation values for the electric and magnetic energy for a D_4 2x2 simulation, normalized by the size $M = 4$ of the system.

We can see that in the electric limit the system is in the electric ground state. With our conventions the single link electric energy is 0, therefore the total electric energy in this limit is also zero. Also the magnetic energy is expected to be zero, since the electric ground state is an equal weight superposition of all possible eigenstates for the one-plaquette Wilson loop operators. In the magnetic limit the magnetic energy receives a

contribute -4 for each plaquette, for a total of -16. Also the electric energy expectation value can be calculated on the magnetic ground state, and is found to be 4 for each link, for a total of 32. The results of the simulation are found to be in accordance with the theoretical predictions, verifying that the choice of parameters is sufficient for obtaining the correct results.
We can also see that there is a transition region around $\lambda_c = 0.7$, where the two energies rapidly change, while in the other regions there are only small changes. Looking at the total energy we find the results shown in figure 3.9

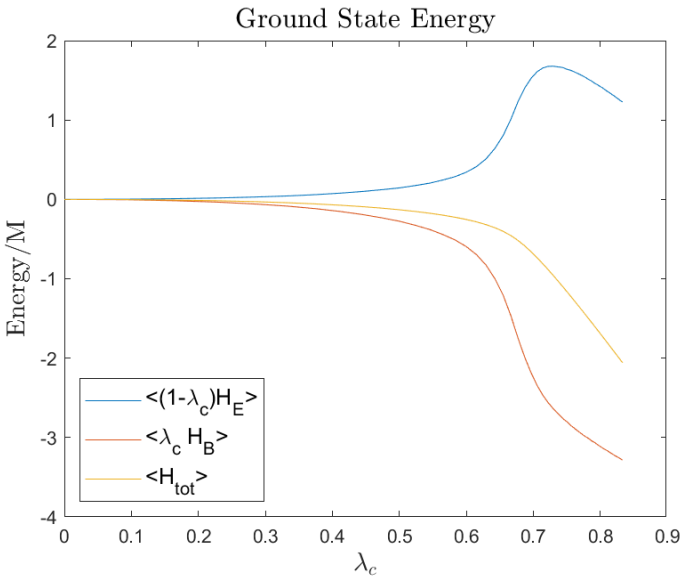

Figure 3.9: Total energy and its electric and magnetic contributes, normalized by the size $M = 4$ of the system.

These results are not visually pleasing, due to the non-zero expectation value of the electric energy on the magnetic ground state, which combines with the factor $(1 - \lambda_c)$ to give the results shown in the picture. In order to obtain better looking results we can take page out of the analysis we performed on the abelian theories, and redefine the electric eigenvalues so that they are centered around zero. This allows better symmetry between the electric and magnetic contribution, without changing the physics of the system. Since the single link electric eigenvalues are centered around the value 4, we can define the new eigenvalues as $\tilde{f}(j) = f(j) - 4$. The results with this new definition are shown in figure 3.10.

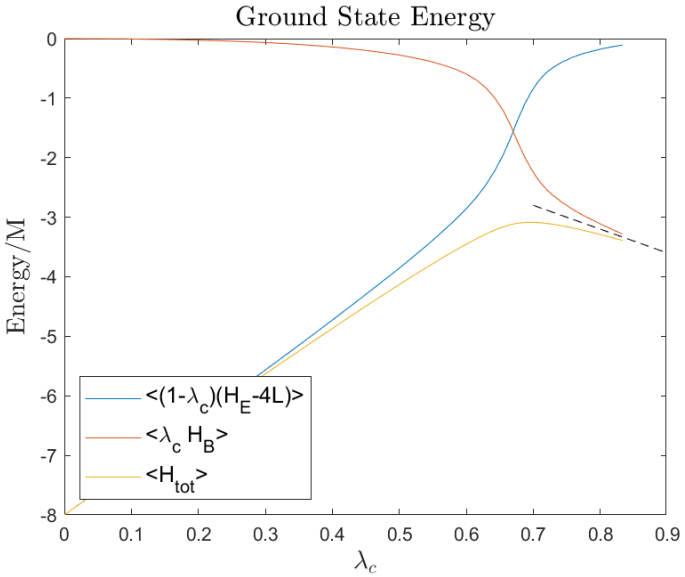

Figure 3.10: Total energy and its electric and magnetic contributes, with the electric eigenvalues shifted to be symmetric around zero.

This graph shows a more familiar behavior in which the electric and magnetic parts dominates one of the two regions of the graph, with a transition region in the middle.

In order to better investigate the nature of the transition we can look at the expectation value of the Wilson loops. In a 2x2 system we have only 1 non-contractible loop, which correspond to the single plaquette. Therefore we cannot study the area and perimeter laws as we did for the abelian case. Nevertheless we can gain an insight in the position of the transition by noticing that the expected value of the one plaquette Wilson loop rapidly changes in the region corresponding to the phase transition, as can be seen in figure 3.11

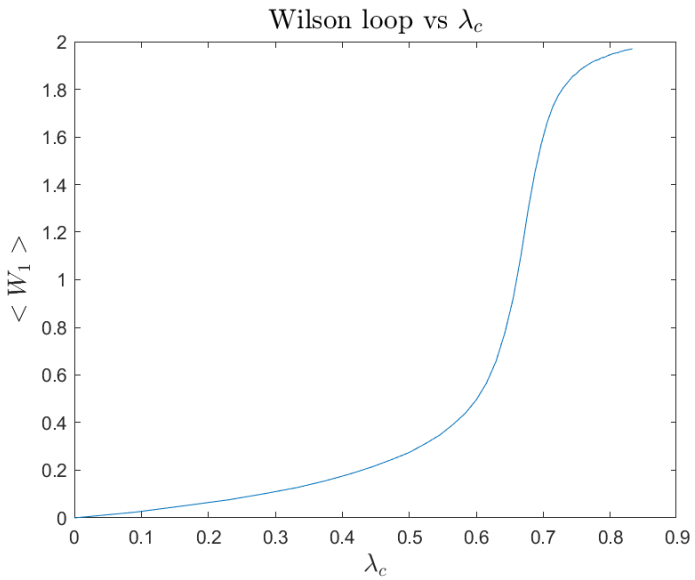

Figure 3.11: Expectation value for a one plaquette Wilson loop, as a function of the parameter λ_c

In this graph we can recognize the confined phase, in which the expectation value of the loop is highly suppressed, and the deconfined phase, in which the Wilson loop reaches a value close to its maximum.
Even with a smaller system the single plaquette shows a sharper transition from one phase to the other than what was observed in the abelian case, meaning that the loops in the confined phase are suppressed to a larger degree. In order to better understand what happens in each phase we would need to investigate the perimeter and area law, which is outside of our present capabilities.
We can nonetheless identify the position of the transition, which happens at $\lambda_c \in [0.65, 0.75]$.

Conclusions and Outlook

In the work of this thesis we have discussed the possibilities for the simulation of a Yang-Mills lattice gauge theory with a finite symmetry group up to a direct implementation for small systems on a classical emulator of a quantum computer, both in the abelian and non-abelian case.
We started from a derivation of the model, showing the connection between the continuous Yang-Mills theory with a continuous symmetry group and the lattice model with a finite group gauge symmetry. Focusing on the general structure of the model we introduced important concepts, such as the character states, and provided useful results regarding the eigenenergies of the two components of the Hamiltonian.
The knowledge developed in the first chapter was applied in the second and third, allowing the implementation of the simulation on the abelian and non-abelian systems.

The main result of this thesis was a complete implementation of a quantum simulation algorithm for both abelian and non-abelian systems. For both cases we were able to show the complete description of the algorithm gate by gate, giving the indications for the possible future implementations on a quantum computer.
In the abelian case we were able to show that the one-plaquette basis forms a complete description of the gauge invariant subspace. We used this result to produce a more efficient encoding of the system on the computational basis. Using plaquette variables instead of link variables in a (2+1)-dimensional system reduces the required number of qubits by half. Due to the relation between quantum computation and its classical emulation this fact provided an exponential speed up in the simulations, which was invested in analyzing larger systems. We were able to perform simulations on a $\mathbb{Z}_2$ 4x4 lattice and on a $\mathbb{Z}_4$ 3x3 lattice, both with periodic boundary conditions. In both cases we identified two phases: a weak coupling deconfined phase and a strong coupling confined phase. The relatively large size of the system we were able to simulate allowed us to analyze the behavior of Wilson loops of different length. We used this data in order to verify the area law and perimeter law. Comparing the two trough a χ^2 goodness fit, we found that the area law better describes the system in the confined phase, while the perimeter law gives a better description in the deconfined phase.
In the case of non-abelian groups we showed how the one-plaquette basis is not sufficient

for the description of the gauge invariant subspace, using examples on small sized systems. We found that this barrier was caused by the emergence of states with multiple plaquette excitations connected to the non-abelian representations of the group, which could not be interpreted as combinations of one-plaquette states like in the abelian case. Nevertheless we successfully developed an algorithm for simulating the non abelian theory D_4 and tested it on a 2x2 periodic lattice. The gate implementation was more complex than in the abelian case. In particular the group operations and the group Fourier transform required more advanced techniques in order to be reduced into smaller substeps, up to the known fundamental gates.
In this algorithm we took the second of the two possible roads in dealing with a constrained quantum mechanical system, forbidding it to evolve into non physical states. In this case this result was achieved by the adiabatic evolution, which acts trough the gauge invariant Hamiltonian.
The results of the simulation were analyzed. Due to the small size of the system we were able to measure only the one plaquette Wilson loop. Nevertheless this was enough to recognize the confined and deconfined phase, and the transition region in-between.

There is still space for improvement in the implementation for the algorithms. A useful step in this direction would be to introduce the evolution with a dynamical Δt. This would allow the algorithm to move faster through the regions of the two phases, while maintaining the computational error small in the rapidly changing transition region. The main issue with this approach is that our algorithm is influenced by two principal errors: the adiabatic approximation and Trotter approximation. A system should be designed in order to keep the changing parameter from improving one of the two but deteriorating the other.
In all our simulations we started from the electric ground state, causing our simulation to be more accurate in the confined phase. Moreover we were unable to reach the magnetic ground state, which would have required an evolution up to a parameter $\lambda = +\infty$. This problem could be solved by starting from the magnetic ground state instead. Checking that in the middle region both methods lead to the same results would be an important confirmation that the adiabatic algorithm works.
In our analysis we confined ourself to the simplest topological sector. A direction in which we could expand the obtained results, would be to analyze the other topological sectors of the theories, looking for different and new phenomena.
Another improvement could be attained by using more powerful computers to simulate larger systems. Nevertheless the exponential scaling of the complexity of the quantum system would quickly limit the size of the system even on powerful supercomputers. Even a the simple description of the state of a 3x3 D_4 system occupies $2^{54}B$, a space larger than the RAM of a supercomputer. True progress will be possible only with real quantum computers, which at the present time are still in development.
A direct implementation on a quantum computer could be made possible by trying dif-

ferent algorithms, better suited for the noisy small scale systems of the present era. Classical emulation of this algorithms could be useful to predict the expected results, and could be verified by comparing them against the result of our thesis.

Going beyond the model we analyzed, an important step would be the generalization of the system, in order to include fermionic matter, allowing the study of interesting dynamical phenomena. It would also allow to perform the simulation in regions with a non-zero chemical potential, justifying the original reason for the implementation of gauge theory simulations on a quantum computer.

Appendices

Appendix A

Finite Groups: Representations and algebra

In this section are gathered some important results regarding finite groups, their representations, and the group algebra, which are used through the thesis. We will refrain from giving proofs, which can be found in [56].
Let's start with some basic definitions. For any group G the *order* $|G|$ is the number of elements in the group.
Two elements g_1, g_2 of G are called *conjugate* if there exist $h \in G$ such that $g_1 = hg_2h^{-1}$. Being conjugate is an equivalence relation, the resulting set is the set of conjugacy classes $\tilde{G}$

A.1 Finite groups representation

Definition 1 *The representation of a group G is a couple (V, ρ) where V is a complex vector space and ρ is a linear map $\rho : G \to GL(V)$ which preserve the group structure. The degree d of a representation is the dimension of the space V.*

A representation is called *unitary* if $\rho(g)^{-1} = \rho(g)^\dagger \ \forall g$. In the case of finite groups it's possible to redefine any hermitian product on V in a way that all finite representations are unitary. To do so we start from any hermitian product $\langle , \rangle_0$ on V. Then we define:

$$\langle x, y \rangle = \frac{1}{|G|} \sum_{g \in G} \langle \rho(g)x, \rho(g)y \rangle_0 \tag{A.1}$$

These new product is hermitian, and it can be shown with some simple calculations that the representation ρ is unitary with respect to it.
A representation is called *irreducible* if it does not contain any non-trivial invariant subspaces. An *invariant subspace* is a subspace L of V which is closed under the action of

the representation: $\rho(g)x \in x \ \forall x \in L$.
Two representations ρ_1, ρ_2 are said to be *equivalent* if there exist a vector space isomorphism $A : V_1 \to V_2$ such that $A\rho_1(g) = \rho_2(g)A \ \forall g$.
A representation is called *reducible* if it is equivalent to a direct sum of irreducible representations.
We are now ready to give the first important results:

Theorem 1 *All unitary representation are reducible*

Corollary 1.1 *All finite representations are reducible*

This means that instead of studying all possible representations of a given group we only need to describe the irreducible representations, which will be referred as π_j to distinguish them from the general representations ρ. For a finite group G, by $\hat{G}$ we denote the set of isomorphism classes of the irreducible representations of G.

A.2 The Group Algebra

Definition 2 *The Group algebra $\mathbb{C}[G]$ is the set of all functions $f : G \to \mathbb{C}$*

In the case of finite groups this space corresponds to the space $\mathbb{C}^{|G|}$ or equivalently the Hilbert space $L_2(G)$.
There are 3 important structures on the group

- The hermitian product $\langle f_1, f_2 \rangle = \sum_{g \in G} f_1^*(g) f_2(g)$
- The function product $(f_1 f_2)(g) := f_1(g) f_2(g)$ which produces a $\mathbb{C}$-algebra structure on the space.
- The convolution $f_1 \star f_2(g) := \frac{1}{|G|} \sum_{h \in G} f_1(gh^{-1}) f_2(h)$ which gives another $\mathbb{C}$-algebra structure on the space.

A orthonormal basis of the space is given by the set e_h defined such that $e_h(g) = \delta(h, g)$. Any other functional can be written as $f = \sum_g f_g e_g$, where:

$$f_g = \langle e_g, f \rangle = f(g) \tag{A.2}$$

As with all binary linear operations, once a basis is chosen it is possible to calculate the *structure constants* of the operation on that basis. For the two algebras we have introduced the structures constants are respectively

- $\langle e_g, e_h e_k \rangle = \delta(g, h)\delta(g, k)$
- $\langle e_g, e_h \star e_k \rangle = \delta(g, hk)$

In order to introduce the Dirac formalism we can simply associate e_g with $|g\rangle$. In this formalism an arbitrary state can be represented by $|f\rangle = \sum_g f_g |g\rangle$.

Let's now look at an important subspace of the group algebra

Definition 3 *A class function on a group G is a function which is constant on conjugate classes; that is,* $f(g) = f(hgh^{-1}) for all g, h \in G$.

Since both binary operations are closed on the set of class function, such set is a subalgebra of the group algebra. The dimension of the space is equal to the number of conjugacy classes of the set $C(G)$.

A.3 Character theory

Definition 4 *We define the character of a representation* (V, ρ) *to be the map* $\chi : G \to \mathbb{C}$, *where* $\chi(g) = Tr(\rho(g)) \ \forall g \in G$

Characters can be used to find all irreducible representations of a given group, thanks to the following result.

Theorem 2 *The characters of all the elements of the quotient group of irreducible representation* $\hat{G}$ *form an orthonormal basis for the space H of class functions on G with respect to the Hermitian inner product* $(|) = \frac{1}{|G|} \langle , \rangle$

Corollary 2.1 *For a finite group there are as many irrep as the number of conjugacy classes* $|C(G)|$.

Corollary 2.2 *Given an arbitrary character* χ *of a representation* ρ *and a irreducible character* χ_j *then* $(\chi|\chi_j) = n_j$, *where* n_j *is the number of times the representation j appears in the decomposition of* ρ

If we collect the values for all irreducible characters on all conjugacy classes of G we obtain the *character table*, which is a square table useful to collect information about the representations. Since

$$\sum_g \chi_i^*(g)\chi_j(g) = |G|\delta_{ij} \tag{A.3}$$

$$\sum_j \chi_j^*(g)\chi_j(h) = \begin{cases} \frac{|G|}{|C(g)|} & \text{if } g \sim h \\ 0 & \text{otherwise} \end{cases} \tag{A.4}$$

Where $C(g)$ is the conjugacy class of g. These relations means that both the columns and the rows of the character table are orthogonal.

Calculating the orthogonality relation for the identity element e, we get the useful relation:

$$\sum_j d_j^2 = |G| \tag{A.5}$$

Which imply that a finite group has a finite number of irreducible representations, each with a finite dimension.

A.4 Representation basis and Group Fourier transform

Connecting representation theory with the group algebra we notice that given an irreducible representation (V_j, π_j), all the *matrix elements* π^j_{mn} are elements of $L_2(G)$. Moreover it is possible to show that these functions are orthogonal:

$$\left\langle \pi^{j_1}_{m_1 n_1}, \pi^{j_2}_{m_2 n_2} \right\rangle = \frac{|G|}{d_{j_1}} \delta(j_1, j_2)\delta(m_1, m_2)\delta(n_1, n_2) \tag{A.6}$$

This property, together with the fact that $|G| = \sum_j d_j^2$ shows that the matrix elements form a basis of $L_2(G)$. After normalization we get the elements of the new basis to be:

$$|j_{mn}\rangle = \sqrt{\frac{d_j}{|G|}} \sum_{g \in G} \pi^j_{mn}(g) \, |g\rangle \tag{A.7}$$

This basis is known as the *representation basis*, which will be sometimes written in the condensed notation $|\bar{j}\rangle$, where we make a one to one identification between the triplet j, m, n and $\bar{j}$.
The transformation from the group basis to the representation basis is known as the *group Fourier transform*(GFT).
It can be seen as a generalization of the quantum Fourier transform, which correspond to the group Fourier transform for $G = \mathbb{Z}_n$.

Since the matrix elements are a basis of the Hilbert space we can calculate the structure constants of the two algebras with respect to them.

$$\langle \pi_{\bar{j}_1}, \pi_{\bar{j}_2} \pi_{\bar{j}_3} \rangle = c^{\bar{j}_1}_{\bar{j}_2 \bar{j}_3} \tag{A.8}$$

$$\langle \pi_{\bar{j}_1}, \pi_{\bar{j}_2} \star \pi_{\bar{j}_3} \rangle = C^{\bar{j}_1}_{\bar{j}_2 \bar{j}_3} \tag{A.9}$$

Appendix B

Quantum gates

In this chapter we introduce the quantum gates used in the description of the circuits used in the thesis. In the first section we will show the circuit and matrix expression for various fundamental gates, while in the second we will focus on two more complex gates, used in the implementation of the sum and difference operation.

B.1 Fundamental quantum gates

There are many gates commonly used in quantum computing. In order to give the proper matrix expression we will need to define a conventional order for the computational states. Following typical quantum computing conventions each computational state is mapped into a binary number. The qubit corresponding to the least significant figure is assigned the index 0, and all the other qubits are subsequently named. As a result a n-qubit states can be written as

$$|q_{n-1}, ..., q_0\rangle \tag{B.1}$$

The binary number it represent can be written as

$$N = \sum_{k=0}^{n-1} q_k 2^k \tag{B.2}$$

All states are then put in increasing order based on the number N they represent, from 0 to $2^n - 1$.

The three simplest gates are the ones associated with the three Pauli matrices. They act on a single qubit and take the matrix form:

$$\sigma_x = \begin{pmatrix} 0 & 1 \\ 1 & 0 \end{pmatrix} \quad \sigma_y = \begin{pmatrix} 0 & -i \\ i & 0 \end{pmatrix} \quad \sigma_z = \begin{pmatrix} 1 & 0 \\ 0 & -1 \end{pmatrix} \tag{B.3}$$

In a quantum circuit they are represented by

$$q_0 : \boxed{X} \qquad q_0 : \boxed{Y} \qquad q_0 : \boxed{Z}$$

The X gate is also known as the NOT gate, since when acting on the computational state $|0\rangle$ gives as an output state $|1\rangle$, and vice versa, mimicking the action of the NOT boolean operation in classical computing.
Another set of important one qubits gates are the three rotations, related to the three Pauli matrices:

$$R_i(\theta) = \exp\left(-i\sigma_i \frac{\theta}{2}\right) \quad i = x, y, z \tag{B.4}$$

They are implemented on a circuit by the following gate

$$q_0 : \boxed{R_i(\theta)}$$

On two qubits the most important gate is the controlled-NOT gate, abbreviated as $CNOT$ gate. This gate applies the NOT gate only if the state in the control qubit is in state $|1\rangle$. It has the matrix representation

$$CNOT = \begin{pmatrix} 1 & 0 & 0 & 0 \\ 0 & 1 & 0 & 0 \\ 0 & 0 & 0 & 1 \\ 0 & 0 & 1 & 0 \end{pmatrix} \tag{B.5}$$

and is implemented in the quantum circuit by

$$\begin{array}{l} q_0 : \\ q_1 : \end{array} \quad \begin{array}{c} \oplus \\ \bullet \end{array}$$

where the dot represents the control qubit, while the $\oplus$ symbol represents the NOT operation, and is equivalent to the X gate.
A generalization of the $CNOT$ gate is the controlled-U gate where the NOT gate is substituted with a more general unitary operation U. This gate has matrix representation

$$C\text{-}U = \begin{pmatrix} \mathbb{1}_2 & 0 \\ 0 & U \end{pmatrix} \tag{B.6}$$

and circuit representation

$$\begin{array}{l} q_0 : \\ q_1 : \end{array} \quad \begin{array}{c} \boxed{U} \\ \bullet \end{array}$$

The controlled operation U can also act on multiple qubits. A gate similar to the controlled gate is the anti-controlled gate, in which the controlled operation is performed

only if the controlling qubit is in state $|0\rangle$. In the case the controlled operation is NOT it has the matrix representation

$$\begin{pmatrix} 0 & 1 & 0 & 0 \\ 1 & 0 & 0 & 0 \\ 0 & 0 & 1 & 0 \\ 0 & 0 & 0 & 1 \end{pmatrix} \tag{B.7}$$

and is introduced in the circuit formalism by an empty dot:

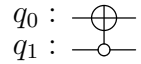

Another useful 2 qubit gate is the $SWAP$ gate, in which the state of the two qubits is exchanged. It is represented by the matrix

$$SWAP = \begin{pmatrix} 1 & 0 & 0 & 0 \\ 0 & 0 & 1 & 0 \\ 0 & 1 & 0 & 0 \\ 0 & 0 & 0 & 1 \end{pmatrix} \tag{B.8}$$

and the circuit

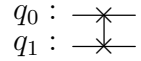

On three qubits an important gate is the Toffoli gate, also known as the controlled-controlled-NOT gate. It performs the NOT operation only if both the controlled qubits are in the $|1\rangle$ state. It has matrix representation

$$\begin{pmatrix} 1 & & & & & & & \\ & 1 & & & & & & \\ & & 1 & & & & & \\ & & & 1 & & & & \\ & & & & 1 & & & \\ & & & & & 1 & & \\ & & & & & & 0 & 1 \\ & & & & & & 1 & 0 \end{pmatrix} \tag{B.9}$$

where all spaces correspond to zeroes. Its circuit representation is

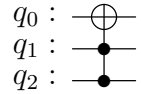

One generalization of the Toffoli can be obtained by using more general U gate instead of the NOT gate. Another generalization substitutes one or both of the control qubits with anti-control qubits. The matrix and circuit representations of these gates can be easily found.

B.2 Sum and difference gates

In this section we will follow the procedure described by T. Draper[12], in order to figure out the correct expression for the summing and subtracting circuits. The main advantage of using this algorithm is that it doesn't need any ancillary qubits in order to perform the computation. Since one operation is the inverse of the other we need only to show the summing circuit; the subtracting circuit can then be obtained by inverting the previous gate by gate.
If we want to add M numbers we need M sets of n qubits, where n is the number of qubits in which each addend is encoded. Using larger n allows us to sum bigger numbers. All sums are performed modulo 2^n.
In the algorithm a set of qubits is chosen as the target set, in which the end result of the operation will be stored. All other sets are left unchanged.
The circuit can be divided in three parts: in the first a quantum Fourier transform is used on the target qubits, in the second a set of gates, which we denote as CZ (generalized control z) is used to adjust the phase on each qubit of the first set based on the state of the other sets, and in the end an Inverse Quantum Fourier transform is applied on the first set, in order to produce the correct result.

In the $\mathbb{Z}_2$ case we sum 1 digit numbers. The 1 qubit Fourier and Inverse Quantum Fourier transform is the Hadamard gate H. The CZ gate reduces to the 2 qubit control z gate. Therefore to sum 2 numbers we have

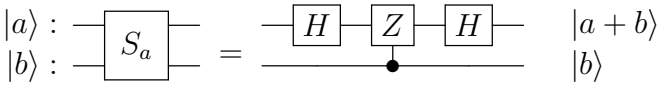

where the subscript in S_a identify the qubit on which the final sum is stored. If we want to sum over 3 or more numbers we need to include a CZ from all the addends to the target qubit:

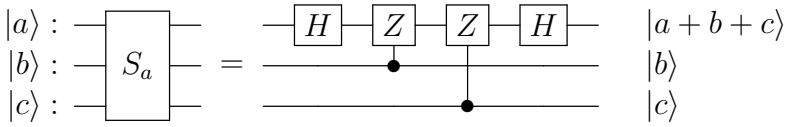

In the $\mathbb{Z}_4$ case we are interested in the sum of two digits number. Each CZ gate can be expressed as 3 control phase gates, where the phase gate P_k is a 1 qubit gate whose matrix representation is:

$$P_k = \begin{pmatrix} 1 & 0 \\ 0 & e^{\frac{i2\pi}{2^k}} \end{pmatrix}$$

The sum between two numbers is

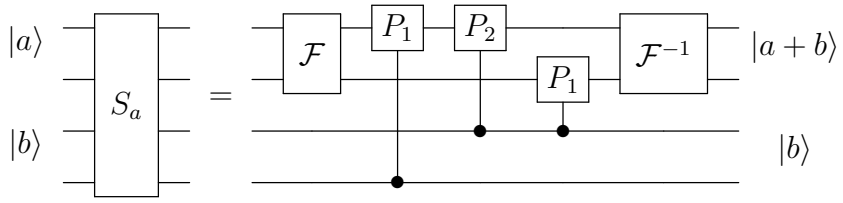

while the sum between three or more numbers can be performed by repeating the three gates that compose the CZ gate for each other addend:

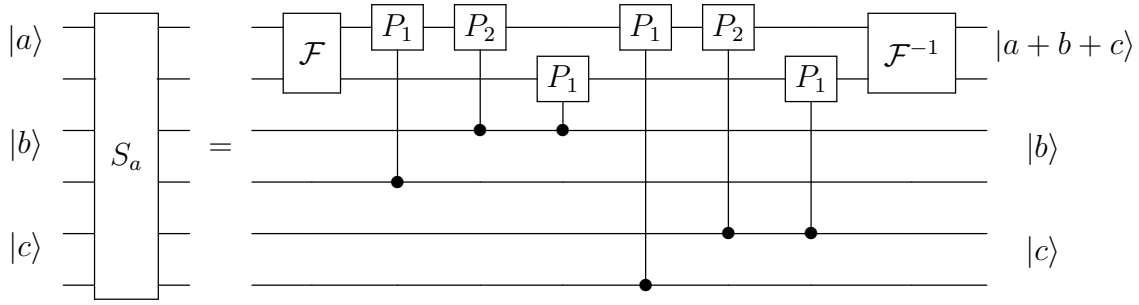

Bibliography

[1] Gert Aarts. Introductory lectures on lattice qcd at nonzero baryon number. *Journal of Physics: Conference Series*, 706:022004, Apr 2016.

[2] E. M. Alfsen. A simplified constructive proof of the existence and uniqueness of haar measure. *Mathematica Scandinavica*, 12:106–116, Dec. 1963.

[3] Mari Carmen Bañuls, Rainer Blatt, Jacopo Catani, Alessio Celi, Juan Ignacio Cirac, Marcello Dalmonte, Leonardo Fallani, Karl Jansen, Maciej Lewenstein, Simone Montangero, and et al. Simulating lattice gauge theories within quantum technologies. *The European Physical Journal D*, 74(8), Aug 2020.

[4] Michael Creutz. *Quarks, gluons and lattices*. Cambridge Monographs on Mathematical Physics. Cambridge Univ. Press, Jun 1985.

[5] Michael Creutz. Lattice gauge theory: A retrospective. *Nuclear Physics B-Proceedings Supplements*, 94(1-3):219–226, 2001.

[6] Andrew Cross. The ibm q experience and qiskit open-source quantum computing software. In *APS March Meeting Abstracts*, volume 2018, pages L58–003, 2018.

[7] Shawn X. Cui, Dawei Ding, Xizhi Han, Geoffrey Penington, Daniel Ranard, Brandon C. Rayhaun, and Zhou Shangnan. Kitaev's quantum double model as an error correcting code. *Quantum*, 4:331, Sep 2020.

[8] Xiaopeng Cui, Yu Shi, and Ji-Chong Yang. Circuit-based digital adiabatic quantum simulation and pseudoquantum simulation as new approaches to lattice gauge theory. *Journal of High Energy Physics*, 2020(8):1–35, 2020.

[9] Zohreh Davoudi, Mohammad Hafezi, Christopher Monroe, Guido Pagano, Alireza Seif, and Andrew Shaw. Towards analog quantum simulations of lattice gauge theories with trapped ions. *Phys. Rev. Research*, 2:023015, Apr 2020.

[10] Mark Wild de Propitius and F Alexander Bais. Discrete gauge theories. In *Particles and fields*. Springer, 1999.

[11] Robbert Dijkgraaf, Vincent Pasquier, and Philippe Roche. Quasi hope algebras, group cohomology and orbifold models. *Nuclear Physics B-Proceedings Supplements*, 18(2), 1991.

[12] Thomas G Draper. Addition on a quantum computer. *arXiv preprint quant-ph/0008033*, 2000.

[13] Vladimir Gershonovich Drinfeld. Quantum groups. *Zapiski Nauchnykh Seminarov POMI*, 155, 1986.

[14] D.Tong. "gauge theory". Available: `http://www.damtp.cam.ac.uk/user/tong/gaugetheory.html`, 2018. (accessed in September 2021)[online].

[15] S. Elitzur. Impossibility of spontaneously breaking local symmetries. *Phys. Rev. D*, 12:3978–3982, Dec 1975.

[16] Richard P Feynman. Simulating physics with computers. In *Feynman and computation*, pages 133–153. CRC Press, 2018.

[17] Eduardo Fradkin. *Field Theories of Condensed Matter Physics*. Cambridge University Press, 2nd edition, 2013.

[18] Jean Gallier and Jocelyn Quaintance. *Correction to: Differential Geometry and Lie Groups*, pages C1–C1. Springer International Publishing, Cham, 2020.

[19] Christof Gattringer and Christian Lang. *Quantum chromodynamics on the lattice: an introductory presentation*, volume 788. Springer Science & Business Media, 2009.

[20] Christof Gattringer and Kurt Langfeld. Approaches to the sign problem in lattice field theory. *International Journal of Modern Physics A*, 31(22):1643007, 2016.

[21] Brian C. Hall. *Lie Groups, Lie Algebras, and Representations*, pages 333–366. Springer New York, New York, NY, 2013.

[22] P. Hauke, D. Marcos, M. Dalmonte, and P. Zoller. Quantum simulation of a lattice schwinger model in a chain of trapped ions. *Phys. Rev. X*, 3:041018, Nov 2013.

[23] Gordon James, Martin W Liebeck, and Martin Liebeck. *Representations and characters of groups*. Cambridge University Press, 2001.

[24] Juan Pablo Ibieta Jimenez. Gauge and matter fields on a lattice: Generalizing kitaev's toric code model. Master's thesis, Instituto de Física, University of São Paulo, 2015.

[25] A Yu Kitaev. Quantum computations: algorithms and error correction. *Russian Mathematical Surveys*, 52(6):1191–1249, dec 1997.

[26] John Kogut and Leonard Susskind. Hamiltonian formulation of wilson's lattice gauge theories. *Phys. Rev. D*, 11:395–408, Jan 1975.

[27] Hans Kurzweil and Bernd Stellmacher. *The theory of finite groups: an introduction*, volume 1. Springer, 2004.

[28] Robert G. Leigh, Djordje Minic, and Alexandr Yelnikov. Glueball spectrum of pure yang-mills theory in $2+1$ dimensions. *Phys. Rev. D*, 76:065018, Sep 2007.

[29] N. Ligterink, N. Walet, and R. Bishop. Toward a many-body treatment of hamiltonian lattice su(n) gauge theory. *Annals of Physics*, 284:215–262, 2000.

[30] Luca Lumia. Digital quantum simulations of yang-mills lattice gauge theories. Master's thesis, Università di Bologna, 2020.

[31] Shahn Majid. *Foundations of quantum group theory*. Cambridge university press, 2000.

[32] Alessandro Mariani. Finite-group yang-mills lattice gauge theories in the hamiltonian formalism. Master's thesis, Università di Bologna, 2020.

[33] Esteban A. Martinez, Christine A. Muschik, Philipp Schindler, Daniel Nigg, Alexander Erhard, Markus Heyl, Philipp Hauke, Marcello Dalmonte, Thomas Monz, Peter Zoller, and et al. Real-time dynamics of lattice gauge theories with a few-qubit quantum computer. *Nature*, 534(7608):516–519, Jun 2016.

[34] Jarrod R McClean, Jonathan Romero, Ryan Babbush, and Alán Aspuru-Guzik. The theory of variational hybrid quantum-classical algorithms. *New Journal of Physics*, 18(2):023023, feb 2016.

[35] C. Monroe, W. C. Campbell, L.-M. Duan, Z.-X. Gong, A. V. Gorshkov, P. W. Hess, R. Islam, K. Kim, N. M. Linke, G. Pagano, P. Richerme, C. Senko, and N. Y. Yao. Programmable quantum simulations of spin systems with trapped ions. *Rev. Mod. Phys.*, 93:025001, Apr 2021.

[36] I. Montvay and G. Munster. *Quantum fields on a lattice*. Cambridge Monographs on Mathematical Physics. Cambridge University Press, 3 1997.

[37] H.B. Nielsen and M. Ninomiya. A no-go theorem for regularizing chiral fermions. *Physics Letters B*, 105(2):219–223, 1981.

[38] Michael A Nielsen and Isaac Chuang. Quantum computation and quantum information, 2002.

[39] Simone Notarnicola, Mario Collura, and Simone Montangero. Real-time-dynamics quantum simulation of (1+1)-dimensional lattice qed with rydberg atoms. *Physical Review Research*, 2(1), Mar 2020.

[40] Simone Notarnicola, Elisa Ercolessi, Paolo Facchi, Giuseppe Marmo, Saverio Pascazio, and Francesco V Pepe. Discrete abelian gauge theories for quantum simulations of qed. *Journal of Physics A: Mathematical and Theoretical*, 48(30):30FT01, Jul 2015.

[41] Danny Paulson, Luca Dellantonio, Jan F Haase, Alessio Celi, Angus Kan, Andrew Jena, Christian Kokail, Rick van Bijnen, Karl Jansen, Peter Zoller, et al. Towards simulating 2d effects in lattice gauge theories on a quantum computer. *arXiv preprint arXiv:2008.09252*, 2020.

[42] Michael E Peskin. *An introduction to quantum field theory*. CRC press, 2018.

[43] John Preskill. Quantum computing in the nisq era and beyond. *Quantum*, 2:79, Aug 2018.

[44] Markus Püschel, Martin Rötteler, and Thomas Beth. Fast quantum fourier transforms for a class of non-abelian groups. In *International Symposium on Applied Algebra, Algebraic Algorithms, and Error-Correcting Codes*, pages 148–159. Springer, 1999.

[45] H. Reinhardt, G. Burgio, D. Campagnari, E. Ebadati, J. Heffner, M. Quandt, P. Vastag, and H. Vogt. Hamiltonian approach to qcd in coulomb gauge - a survey of recent results, 2017.

[46] U.-J. Wiese S. Chandrasekharan. An introduction to chiral symmetry on the lattice. *Progress in Particle and Nuclear Physics*, 53(2):373–418, Oct 2004.

[47] Jean-Pierre Serre. *Linear representations of finite groups*, volume 42. Springer, 1977.

[48] Barry Simon. Representations of finite and compact groups. 1995.

[49] Federica M. Surace, Paolo P. Mazza, Giuliano Giudici, Alessio Lerose, Andrea Gambassi, and Marcello Dalmonte. Lattice gauge theories and string dynamics in rydberg atom quantum simulators. *Physical Review X*, 10(2), May 2020.

[50] Andreas Trabesinger. Quantum simulation. *Nature Physics*, 8(4):263–263, Apr 2012.

[51] Xiao-Gang Wen. Topological orders in rigid states. *International Journal of Modern Physics B*, 4(02):239–271, 1990.

[52] Kenneth G Wilson. Confinement of quarks. *Physical review D*, 10(8):2445, 1974.

[53] Edward Witten. Quantum field theory and the jones polynomial. *Communications in Mathematical Physics*, 121(3):351–399, 1989.

[54] C. N. Yang and R. L. Mills. Conservation of isotopic spin and isotopic gauge invariance. *Phys. Rev.*, 96:191–195, Oct 1954.

[55] Bei Zeng, Xie Chen, Duan-Lu Zhou, and Xiao-Gang Wen. Quantum information meets quantum matter – from quantum entanglement to topological phase in many-body systems, 2018.

[56] A. Zimmerman. Representation theory of finite groups and burnside's theorem. 2015.